Time-Dependent Electron Localization Function

Diplomarbeit by
Tobias Burnus
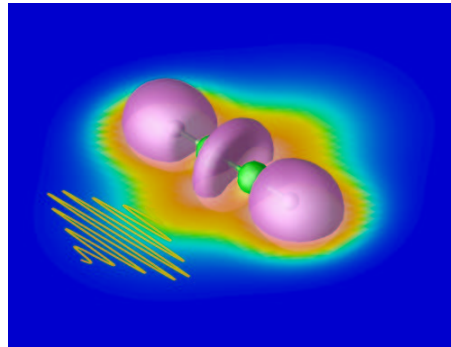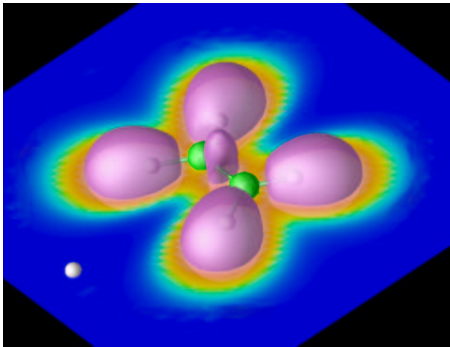
Adviser:
Prof. Dr. E. K. U. Groß

Fachbereich Physik
Freie Universität Berlin

2004
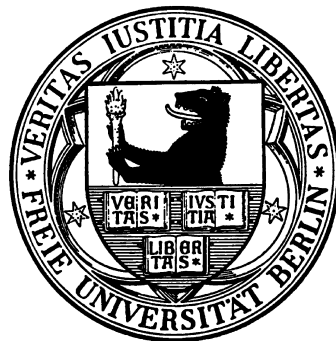
Time-Dependent Electron Localization Function

Tobias Burnus

The electron localization function ELF, which is crafted to reveal chemical bonds and their properties, has been generalized to the time-dependent regime. This allows the time-resolved visualization of the formation, modulation and breaking of bonds and gives thus insight into the dynamics of excited electrons. This has been illustrated by the π–π^* transition of ethyne induced by a laser field, and by the destruction of bonds and the formation of lone-pairs in a scattering process of a proton with ethene. In the second part, an optimal control algorithm is used to determine an optimized laser pulse of a HOMO–LUMO transition of the diatomic molecule lithium fluoride.

Title page: *ELF images showing a proton on collision course with the left carbon of ethene (left) and ethyne (right) in a laser field polarized along the molecular axis.*

Typeset using ConTeXt in Latin Modern and Computer Modern 12pt. The ELF and density images and movies have been created using OpenDX.

Dedication:
For my parents

We haven't got the money, so we've got to think!

<div align="right">— Ernest Rutherford, 1871–1937</div>

Preface

A physics professor, teaching quantum mechanics, once said that one is not allowed to ask where the electrons are during the transition between two states. But nevertheless: How does a chemical bond such as a triple bond break? One knows from chemisty or molecular physics courses that there are bonding and anti-bonding states. But what happens exactly at which time. We know that the breaking of bonds happens on a time-scale of hundreds of attoseconds, which is the time-scale of the electrons. With the advance of attosecond spectroscopy, one might even be able two answer some of these questions experimentally.

For tackling this problem, we describe the system using the density-functional theory which enables us to calculate molecules with many electrons and propagate such a system in time. We therefore give a short introduction into this theory in chapter 1, which is necessarily short and incomplete.

Before we can ask how a chemical bond breaks, we need to know what actually defines a bond. This is not as simple as it seems, in the real world the atom does not know about orbitals which have been used to visualize and to understand the concept of a bond. The orbitals that stem from calculations, however, can be lineary combined or may be delocalized over several atoms. Using the density does not help much, either: The only maxima of the density are located at the nuclei and while there is density between bond atoms, it is hard to classify or even only to visualize the chemical bonds. The solution is to make use of the localizability of the electrons instead of utilizing the density directly. This does the the so-called electron localization function (ELF) which we cover in chapter 2. Up to now, the ELF had only been used for static systems or for those which can be described adiabatically. We have devised a version which can be utilized for time-dependent systems. This TDELF has then be used to scrutinize the effects of a strong laser (electric field) on ethyne and for scattering of fast protons by ethene. We were able to see how a transition from the π bonding to the π^* anti-bonding state was building up, bonds were breaking and re-forming, and lone-pairs emerging.

Preparing a certain state, such as the π^* anti-bonding state, can be tricky if the exact transition energy is unknown or, in other cases, intermediate states exists. One possibility to create a tailored laser is provided by the various optimal control theories. We look at a functional based on optimal control theory in chapter 3. Since doing optimal control for a larger molecule requires a lot of book-keeping and computational resources, we started with a simpler example: The HOMO–LUMO

transition of a cylinder-symmetric diatomic molecule. Using a such tailored laser, we achieved a population transfer of over eighty per cent from HOMO to LUMO in lithium fluoride.

The final part of this thesis, chapter 4, contains conclusions and aspects which need further investigation.

Throughout the thesis, two kind of units are used: the SI units and the atomic units (see appendix D for the conversion factor). Using the former, the numbers can easily be compared with experimental results. On the other hand, atomic units drop a lot of constants and the numerical results of atomic calculations can usually be written without exponentials. This makes atomic units ideal for both numerics and lengthy calculations. I hope that I found the right balance between these two common unit systems.

Acknowledgement

While it has become a custom to write an acknowledgment and it is often only a mere item on the list of the things which are part of a thesis, for me it has not lost its original meaning since I know that I would not have reached this point and finished the thesis without the help and support of various people. Regarding this diploma thesis I would like to express my special thanks to the following people.

I feel deeply indebted to my adviser Professor Eberhard 'Hardy' K. U. Groß. I am grateful for his encouragement and support, the discussion we had and the impulses he gave me. While he was not always reachable, especially in the second half of the year when he was a guest at the University of Cambridge, he managed to be always available when needed. In addition, this proved to be an efficient way to stimulate the productive intra-group communication which otherwise might be not as intensive. Without him I would not have attended a summer school in Sweden, where I not only learnt a lot about DFT and could present my results but met new friends. Especially enjoyable were his group dinner meetings, where he sometimes even played the piano.

I have benefitted from Miguel Marques who introduced me to `octopus` and helped me with all problems I had with it. His Fortran style as used in `octopus` influenced mine to the better. I also gained a lot from his experience especially in calculating larger systems and he helped me to tackle some analytical problems.

Jan Werschnik is the expert of our group in optimal control and was therefore of tremendous help during the second part of the thesis, though as an office mate he he had to answer tons of little and not so little questions throughout the the whole year. I am especially grateful for his and Stephan Kurth's help as I got stuck with the bondary conditions of the discretized matrix, where they kindly spend much of

their spare time to crack this problem. Especially during this phase we had vivid and constructive discussions.

I would like to thank Nicole Helbig, who always lend an sympathetic ear to me. She also helped me with some mathematical problems and was the driving force behind our group ice skatings. Furthermore, she, Stephan and Jan volenteered to give introductionary lectures about DFT just for us two *Diplomanden*.

Thanks also to Heiko Appel who is a real treasure trove regarding articles, furthermore he helped me finding and choosing the right numerical methods. I would like to thank Angelica Zacarias who found a cylindrical diatomic molecule and did the Gaussian calculations. Finally, I want to express my thanks to the whole group who created a pleasant atmosphere; I really enjoyed that year.

There are two further persons whom I would like to thank – my parents. They have supported and encouraged me, and where there when I needed them.

Contents

Contents

viii

A new scientific truth does not triumph by convincing its opponents and making them see the light, but rather because its opponents eventually die, and a new generation grows up that is familiar with it.   — Max Planck, 1858–1947

1 Density functional theory

While traditional many-particle wave-function methods perform well for a wide range of systems, they come to their limits for non-symmetric or periodic systems with many (chemically active) electrons. That is because the numerical effort to calculate and store multi-particle wave functions grows exponentially with the number of electrons. Therefore, these methods can currently only be applied to systems with about ten chemically active electrons [1]. A solution to this exponential wall is density-functional theory (DFT). Several introductory texts on DFT can be found in the literature. Among them are Kohn's Nobel lecture [1], the lecture notes by Perdew and Kurth [2], Burke's *ABC of DFT* [3], or Taylor and Heinonen's DFT chapter in [4]. For time-dependent DFT, the TD-Review by Groß *et al.* [5] provides a clear and in-depth introduction.

This chapter provides a short overview of the theory but is not meant to give a complete and self-contained account about all aspects. The next section covers the Hohenberg–Kohn theorem, which proves that every observable can be written as a unique functional of the electron density. The Kohn–Sham theory, described in section 1.2, states that the density of an interacting system can be obtained using an effective single particle potential. This is then generalized to the time-dependent regime by the Runge–Groß theorem in section 1.3. The numerical effort can be further reduced by pseudopotentials described in section 1.4.

1.1 The Hohenberg–Kohn theorem

A quantum system of N particles can be completely described[1] by its Hamiltonian $H = T + V + W$. The Hamilton operator consists of the kinetic part

$$T = -\frac{\hbar^2}{2m} \sum_{i=1}^{N} \nabla_i^2, \tag{1.1}$$

the interaction W, which – for the case of Coulomb interactions between electrons – has the form

---

[1] In this thesis we completely neglect effects which can only be described by quantum electrodynamics (QED).

$$W = \frac{1}{4\pi\varepsilon_0} \sum_{\substack{i,j=1 \\ i<j}}^{N} \frac{e^2}{|\boldsymbol{r}_i - \boldsymbol{r}_j|} = \frac{1}{2}\frac{1}{4\pi\varepsilon_0} \sum_{\substack{i,j=1 \\ i\neq j}}^{N} \frac{e^2}{|\boldsymbol{r}_i - \boldsymbol{r}_j|}, \tag{1.2}$$

and of the so-called external potential V, which contains for instance the potential created by the nuclei.

The ground-state wave function Ψ_0, obtained by solving the static Schrödinger equation

$$H\Psi_i = E_i\Psi_i, \tag{1.3}$$

can be used to calculate the ground-state electron density

$$n(\boldsymbol{r}) = N \sum_{\sigma_1,\dots,\sigma_N} \int \mathrm{d}^3 r_2 \cdots \int \mathrm{d}^3 r_N \, |\Psi_0(\boldsymbol{r}\sigma_1, x_2, \dots, x_N)|^2, \tag{1.4}$$

where x_i is a short hand for spatial and spin variables. Hohenberg and Kohn have shown [6] that one can also take the reverse route: the ground-state density determines the external potential (and thus the Hamiltonian) which in turn can be used to obtain the wave functions. Or mathematically rigorous: The ground-state density $n(\boldsymbol{r})$ of a bound system of interacting electrons in some external potential V determines the potential uniquely (up to a purely additive constant).[2] The implication of this theorem is that we can in principle determine any observable and all eigenfunctions Ψ_i (including excited states) from the ground-state density.

Note that the Hohenberg–Kohn theorem assumes non-degenerate ground states, a version for degenerate ground states exists.

We first show by reductio ad absurdum that different potentials lead to different wave functions. Be V and V' two potentials which differ by more than an additive constant and Ψ_0 and Ψ_0' be their associated ground-state wave functions. The Schrödinger equations for Ψ_0 and Ψ_0' are

$$H|\Psi_0\rangle = (T + W + V)|\Psi_0\rangle = E_0|\Psi_0\rangle \tag{1.5}$$
$$H'|\Psi_0'\rangle = (T + W + V')|\Psi_0'\rangle = E_0'|\Psi_0'\rangle, \tag{1.6}$$

where E_0 and E_0' are the respective ground-state energies. Suppose now that Ψ_0 and Ψ_0' are the same. We can then substract Eq. (1.6) from Eq. (1.5) to obtain

$$(V - V')|\Psi_0\rangle = (E - E')|\Psi_0\rangle. \tag{1.7}$$

---

[2] Starting from the density, one might ask whether any well-behaved, positive function $n(\boldsymbol{r})$ is a possible ground-state density to some potential V, i.e. whether n is V-representable. While this is indeed not the case, this issue has so far not imposed any limits on practical applications [1].

But $E - E'$ is a real number, so that means that the two potentials differ at most by a constant which is a contradiction to our hypothesis. We have thus shown that if $V \neq V'$ then $\Psi_0 \neq \Psi_0'$. We now look at the relation ship between the density and the wave function. Be n the ground-state density in the potential V with its corresponding ground-state wave function Ψ. Then the total energy is

$$E = \langle \Psi | H | \Psi \rangle = \langle \Psi | (T + W) | \Psi \rangle + \int V(\boldsymbol{r}) n(\boldsymbol{r}) \, \mathrm{d}^3 r. \tag{1.8}$$

Be V' another potential which differs from V by more than an additive constant and Ψ' be its associated wave function, which yields the same density n as Ψ does. The Rayleigh–Ritz minimal principle states that

$$E < \langle \Psi' | H | \Psi' \rangle = \langle \Psi' | (T + W) | \Psi' \rangle + \int V(\boldsymbol{r}) n(\boldsymbol{r}) \, \mathrm{d}^3 r$$
$$= E' + \int \big(V(\boldsymbol{r}) - V'(\boldsymbol{r}) \big) n(\boldsymbol{r}) \, \mathrm{d}^3 r, \tag{1.9}$$

where we have used that $n' \equiv n$ by assumption. Analogously we find for E',

$$E' < E + \int \big(V'(\boldsymbol{r}) - V(\boldsymbol{r}) \big) n(\boldsymbol{r}) \, \mathrm{d}^3 r. \tag{1.10}$$

Adding Eq. (1.9) and Eq. (1.10), gives

$$E + E' < E + E' + \int \big(V(\boldsymbol{r}) - V'(\boldsymbol{r}) + V'(\boldsymbol{r}) - V(\boldsymbol{r}) \big) n(\boldsymbol{r}) \, \mathrm{d}^3 r = E + E'. \tag{1.11}$$

This is a contradiction to the assumption that both Ψ and Ψ' have the same ground-state density. We have thus established that two different, non-degenerate ground states lead to different ground-state densities. We further know that different potentials lead to different wave functions. Therefore, we proved that knowing the ground-state density $n(\boldsymbol{r})$ of a system is sufficient to construct the external potential (if n is V-representable).

There is also an important variational principle associated with the Hohenberg–Kohn theorem. We know that the electronic ground-state energy can be obtained by making use of the Rayleigh–Ritz principle,

$$E = \min_{\tilde{\Psi} \in \{\tilde{\Psi}\}} \langle \tilde{\Psi} | H | \tilde{\Psi} \rangle, \tag{1.12}$$

where $\{\tilde{\Psi}\}$ is the set of all normalized, antisymmetric N-particle wave functions. Hohenberg and Kohn showed that the Rayleigh–Ritz principle can also be applied to the energy functional,

$$E[n] = \langle \Psi_0[n]|(T + W + V)|\Psi_0[n] \rangle = F_{\text{HK}}[n] + \int V(\boldsymbol{r})n(\boldsymbol{r})\,\mathrm{d}^3 r, \qquad (1.13)$$

where Ψ_0 is the ground-state wave function and

$$F_{\text{HK}}[n] = \langle \Psi_0[n]|(T[n] + W[n])|\Psi_0[n] \rangle. \qquad (1.14)$$

The ground-state energy can be found by varying the density, i.e.

$$E = \min_{\tilde{n} \in \tilde{N}} \left(F_{\text{HK}}[\tilde{n}] + \int \tilde{n}(\boldsymbol{r})V(\boldsymbol{r})\,\mathrm{d}^3 \boldsymbol{r} \right), \qquad (1.15)$$

where $\tilde{N}$ is the set of all V-representable trial densities. In other words, the minimum of this functional can only be reached with the ground-state density corresponding to the potential $V(\boldsymbol{r})$. In this case the value of the functional is the ground-state energy.

Note that the functional $F_{\text{HK}}[n]$ is a universal functional. By this we mean that it is the same functional of the density $n(\boldsymbol{r})$ for *all* N-particle systems, which have the same kind of interaction (e.g. Coulomb). Especially, it is independent of the external potential V. Therefore, we need to approximate it only once and can then apply it to all systems.

1.2 The Kohn–Sham formalism

While the Hohenberg–Kohn theorem establishes that we may use the density alone to find the ground-state energy of an N-electron problem, it does not provide us with any useful computational scheme. This is accomplished by the Kohn–Sham (KS) formalism [7]. The idea is to use an auxiliary, non-interacting system and to find an external potential V_{KS} such that this non-interacting system has the same electron density as the real, interacting system. This density can then be used in the energy functional (Eq. (1.13)). The ground-state of the Kohn–Sham system is given by a Slater determinant of the N lowest, single-particle states of the Hamiltonian which contains V_{KS}. While this provides us with a route for calculations, there is a drawback. The potential V_{KS} depends on the electron density (see below). Therefore, the potential has to be found iteratively in a self-consistent way.

Let us start with the non-interacting N-particle system described by the external potential V_{KS}. The Hamiltonian of the system is given by

$$H = T + V_{\text{KS}}. \qquad (1.16)$$

The ground-state density of this system has the form

$$n(\boldsymbol{r}) = \sum_{i=1}^{N} |\phi_i(\boldsymbol{r})|^2, \tag{1.17}$$

where the N single-particle orbitals ϕ_i in Eq. (1.17) satisfy the Schrödinger equation

$$\left(-\frac{\hbar^2}{2m} \nabla^2 + v_{\mathrm{KS}}(\boldsymbol{r}) \right) \phi_i(\boldsymbol{r}) = \varepsilon_i \phi_i(\boldsymbol{r}), \tag{1.18}$$

and have the N lowest eigenenergies ε_i. The total energy of the ground-state of the non-interacting system is therefore

$$E_{\mathrm{KS}} = \sum_{i=1}^{N} \varepsilon_i. \tag{1.19}$$

Note that the value of this energy does not correspond to the ground-state energy of the interacting system. According to the Hohenberg–Kohn theorem, it exists a unique energy functional

$$E_{\mathrm{KS}}[n] = T_{\mathrm{KS}}[n] + \int V_{\mathrm{KS}}(\boldsymbol{r}) n(\boldsymbol{r}) \, \mathrm{d}^3 r. \tag{1.20}$$

We note that $T_{\mathrm{KS}}[n]$ is the kinetic energy functional of the non-interacting system and it is therefore different from the functional $T[n]$ in Eq. (1.14). In order to solve the interacting system, we need to find a form of V_{KS}, so that the ground-state densities of the non-interacting and the interacting system are the same. Since we are really interested in the interacting system, we rewrite Eq. (1.13) as

$$E[n] = T[n] + W[n] + \int n(\boldsymbol{r}) V(\boldsymbol{r}) \, \mathrm{d}^3 r \tag{1.21}$$

$$= T_{\mathrm{KS}}[n] + \frac{1}{4\pi\varepsilon_0} \frac{e^2}{2} \int \int \frac{n(\boldsymbol{r}) n(\boldsymbol{r}')}{|r - r'|} \, \mathrm{d}^3 r \, \mathrm{d}^3 r' + \int n(\boldsymbol{r}) V(\boldsymbol{r}) \, \mathrm{d}^3 r + E_{\mathrm{xc}}[n].$$

Here, the second term is the direct, or Hartree, term and the last term is the so-called exchange-correlation (xc) energy functional, defined as

$$E_{\mathrm{xc}}[n] = F_{\mathrm{HK}}[n] - \frac{1}{4\pi\varepsilon_0} \frac{e^2}{2} \int \int \frac{n(\boldsymbol{r}) n(\boldsymbol{r}')}{|r - r'|} \, \mathrm{d}^3 r \, \mathrm{d}^3 r' - T_{\mathrm{KS}}[n]. \tag{1.22}$$

With this formalism at hand, one only needs to develop reasonable approximations for E_{xc}, which contain the electron–electron interaction beyond the Hartree term

and the difference in the kinetic energy functionals $T[n] - T_{\mathrm{KS}}[n]$. Since the ground-state density n minimizes the functional $E[n]$, we obtain by varying Eq. (1.21) in terms of the density,[3]

$$\frac{\delta E[n]}{\delta n(\boldsymbol{r})} = \frac{\delta T_{\mathrm{KS}}[n]}{\delta n(\boldsymbol{r})} + \frac{1}{4\pi\varepsilon_0}e^2 \int \frac{n(\boldsymbol{r}')}{|r - r'|}\,\mathrm{d}^3 r' + V(\boldsymbol{r}) + v_{\mathrm{xc}}[n](\boldsymbol{r}) = 0, \qquad (1.23)$$

where we defined the exchange-correlation potential as

$$v_{\mathrm{xc}}[n](\boldsymbol{r}) := \frac{\delta E_{\mathrm{xc}}[n]}{\delta n(\boldsymbol{r})}. \qquad (1.24)$$

Analogously, for the auxiliary system we obtain from Eq. (1.20)

$$\frac{\delta T_{\mathrm{KS}}[n]}{\delta n(\boldsymbol{r})} + V_{\mathrm{KS}}(\boldsymbol{r}) = 0. \qquad (1.25)$$

Subtracting Eq. (1.23) from Eq. (1.25), we see that the effective, or Kohn–Sham, potential has to satisfy

$$V_{\mathrm{KS}}(\boldsymbol{r}) = V(\boldsymbol{r}) + \frac{1}{4\pi\varepsilon_0}e^2 \int \frac{n(\boldsymbol{r}')}{|r - r'|}\,\mathrm{d}^3 r' + v_{\mathrm{xc}}(\boldsymbol{r}). \qquad (1.26)$$

Now we could start implementing the self-consistent Kohn–Sham scheme. Note that this formalism is in principle exact, supposing that we find the exact exchange-correlation potential v_{xc}. Solving a Kohn–Sham system with single-particle orbitals is feasible even for systems with a few hundred electrons (cf. [1, 4]). Formally, the Kohn–Sham equations look similar to the self-consistent Hartree equations, the only difference is the exchange-correlation potential. Neither ϕ_i nor ε_i have any known, directly observable meaning, except that the ϕ_i yield (in principle) the true ground-state density and that the magnitude of the highest occupied ε_i, relative to the vacuum, equals the ionization energy [8].

One famous approximation for the exchange-correlation energy is the local density approximation (LDA) by Kohn and Sham [7].

$$E_{\mathrm{xc}}^{\mathrm{LDA}}[n] := \int n(\boldsymbol{r})\varepsilon_{\mathrm{uni}}(n(\boldsymbol{r}))\,\mathrm{d}^3 r, \qquad (1.27)$$

where $\varepsilon_{\mathrm{uni}}$ denotes the exchange-correlation energy per particle of a uniform electron gas with the density n. $\varepsilon_{\mathrm{uni}}(n)$ can be obtained using quantum Monte Carlo calculations [9].

----

[3] Note though that 'the KS scheme does *not* follow from the variational principle. [...] The KS scheme follows from the basic 1-1 mapping (applied to non-interacting particles) and the assumption of non-interacting V-representability.' [5]

1.3   Time-dependent DFT – the Runge–Groß theorem

The time-dependent density-functional theory (TDDFT) extends the stationary DFT in a way that not only makes time-dependent phenomena available to computation, but it also provides a natural way to calculate excitations of a system. For static systems, we have seen how the Hohenberg–Kohn theorem establishes a one-to-one correspondence between the external potential and the density. We now look at systems, where the external potential V depends explicitly on time. We start with the time-dependent Schrödinger equation

$$i\hbar\partial_t\Psi(t) = H(t)\Psi(t). \tag{1.28}$$

For the theorem, a fixed initial state

$$\Psi(t_0) = \Psi_0 \tag{1.29}$$

is required, which is not required to be an eigenstate of the initial Hamiltonian. While the kinetic part T and the electron–electron interaction W remain unchanged compared to static DFT, the potential V becomes time-dependent

$$V(t) = \sum_{i=1}^{N} v(\boldsymbol{r}_i, t). \tag{1.30}$$

The theorem by Runge and Gross [10] now states: If the potentials V and V' (both Taylor expandable around t_0) differ by more than a purely time-dependent but spatially uniform function, i. e.

$$V(\boldsymbol{r}, t) \neq V'(\boldsymbol{r}, t) + c(t), \tag{1.31}$$

then the densities $n(\boldsymbol{r}, t)$ and $n'(\boldsymbol{r}, t)$, evolving from the common initial state Ψ_0 under the influence of the two potentials, are different. For the proof, both potentials are Taylor expanded in time. Then a $k \in \mathbb{N}$ exists so that the difference beween the k-th Taylor coefficients is not constant, i. e. the difference is $\boldsymbol{r}$ dependent. The proof [5, 10] shows next that under these circumstances the current densities become different and then that the densities are different.

For any given time-dependent density n (and initial state Ψ_0) the external potential can be determined uniquely up to an additive purely time-dependent function; and this potential uniquely determines the wave function, up to a purely time-dependent phase. This phase cancels if we calculate the expectation value of any quantum mechanical operator $O[n](t) = \langle\Psi[n](t)|O(t)|\Psi[n](t)\rangle$. Thus any observable is a unique functional of the time-dependent density and of the initial state Ψ_0.

Once the Runge–Groß theorem is established, one can continue and derive the Kohn–Sham equations [5, 10]. The density of the interacting system can be obtained from

$$n(\boldsymbol{r}, t) = \sum_{i=1}^{N} |\phi_i(\boldsymbol{r}, t)|^2 \tag{1.32}$$

with the orbitals ϕ_i satisfying the time-dependent Kohn–Sham equation

$$i\partial_t \phi_i(\boldsymbol{r}, t) = \left(-\frac{\hbar^2}{2m} \nabla^2 + v_{\text{KS}}[n](\boldsymbol{r}, t) \right) \phi_i(\boldsymbol{r}, t). \tag{1.33}$$

The Kohn–Sham, or single-particle, potential can be written as

$$v_{\text{KS}}[n](\boldsymbol{r}, t) = V(\boldsymbol{r}, t) + \frac{e^2}{4\pi\varepsilon_0} \int \frac{n(\boldsymbol{r}', t)}{|r - r'|} \, \mathrm{d}^3 r + v_{\text{xc}}[n](\boldsymbol{r}, t) \tag{1.34}$$

where $V(\boldsymbol{r}, t)$ is the time-dependent external field.

1.4 Pseudo potentials

Chemical reactions and excitations with energies below X-ray wavelengths hardly affect closed inner shells. Therefore, the many-particle Schrödinger equation can be simplified to a great extent by dividing the electrons into two groups: valence and inner core electrons. Since the inner core electrons are strongly bound, the chemical properties are almost completely determined by the valence electrons. Formally, one can create an effective interaction of the valence electrons with the ionic core, which consists of the nuclei and the inner core electrons. This pseudopotential approximates the potential felt by the valence electrons. The main advantage of pseudopotentials is the reduced numerical effort. This is the case since one has to consider only the valence orbitals. In addition, the problems with the $1/r$ potential (Coulomb singularity for $r \to 0$) is eliminated. Therefore, a wider grid is viable. The tutorial by Nogueira *et al.* [11] and Pickett's article [12] are good primers on pseudopotentials. In the following, a brief summary of the important properties and downsides is given.

Modern pseudopotentials (PP) are obtained by inverting the Schrödinger equation for a given reference electronic configuration and forcing the pseudo wave function to coincide with the all-electron valence wave function beyond a certain distance r_l. The pseudo wave functions are also forced to have the same norm as the all-electron wave functions. This can be written as

$$R_l^{\mathrm{PP}}(r) = R_{nl}^{\mathrm{AE}}(r), \quad \text{if } r > r_l,$$

$$\int_0^{r_l} r^2 |R_l^{\mathrm{PP}}(r)| \, \mathrm{d}r = \int_0^{r_l} r^2 |R_{nl}^{\mathrm{AE}}(r)| \, \mathrm{d}r, \quad \text{if } r < r_l, \tag{1.35}$$

where $R_l(r)$ is the radial part of the wave function with angular momentum l. AE denotes the all-electron wave function and the index n the valence level. Note that the distance r_l, beyond which the all-electron and the pseudo wave function are equal, depends on the angular momentum l. Moreover, pseudo wave functions shall not have nodal surfaces and the pseudo energy eigenvalues $\varepsilon_l^{\mathrm{PP}}$ should match the all-electron valence eigenvalues $\varepsilon_{nl}^{\mathrm{AE}}$. Potentials constructed in this way are called norm conserving, and are semi-local potentials that depend on the energies of the reference electronic levels $\varepsilon_l^{\mathrm{AE}}$. Unfortunately, pseudopotentials may introduce new, non-physical states (so called ghost states) into the calculation, so care must be taken while generating the pseudopotential.

The choice of the cut-off radii establishes only the region where the pseudo and the all-electron wave function coincide. They can thus be considered as a measure of the quality of the pseudopotential. Their smallest possible value is determined by the location of the outermost nodal surface of the all-electron wave functions. For cut-off radii close to this minimum, the pseudopotential is very realistic and strong; for large r_l, the potential is smooth, almost independent of angular momentum, but not very realistic. Since the pseudopotentials have no nodal surface and are smooth, much fewer grid points are needed near the core and thus uniform grids are feasible.

octopus [13], which has been used for the ELF calculations in this work (see section 2) and for obtaining a Kohn–Sham potential (optimal control, section 3), supports the Hartwigsen–Goedecker–Hutter (HGH) [14] and the Troullier–Martins (TM) [15] pseudopotentials. The HGH pseudopotentials are norm-conserving, dual-space Gaussian pseudopotentials. The coefficients for all elements between H and Rn can be found in [14]. Troullier and Martins defined the pseudo wave functions as

$$R_l^{\mathrm{PP}}(r) := \begin{cases} R_{nl}^{\mathrm{AE}}(r), & \text{if } r > r_l \\ r^l \mathrm{e}^{p(r)}, & \text{if } r < r_l \end{cases}, \tag{1.36}$$

where

$$p(r) = c_0 + c_2 r^2 + c_4 r^4 + c_6 r^6 + c_8 r^8 + c_{10} r^{10} + c_{12} r^{12}. \tag{1.37}$$

The coefficients of $p(r)$ are adjusted by imposing norm conservation, the continuity of the pseudo wave functions and their first derivative at $r = r_l$. Furthermore, it is required that the screened pseudopotential has zero curvature at the origin.

What I cannot create, I do not understand.

— Richard Phillips Feynman, 1918–88

2 The time-dependent electron localization function

The electron localization function (ELF) is used to classify and visualize chemical bonds. In the next section, an introduction into the description of chemical bonds and the usefulness of the ELF is given. Afterwards, we look at the definition of the static ELF, constructed by Becke and Edgecombe, in section 2.2. Next, in section 2.3 we derive a time-dependent generalization of the ELF. This TDELF is then used to visualize the $\pi-\pi^*$ transition of ethyne in a strong laser pulse and the breaking and formation of bonds in a scattering process of a proton with ethene in section 2.4. Finally, the conclusions of this chapter can be found in section 2.5.

2.1 Introduction

Already in the chemistry classes of secondary schools chemical bonds are introduced. The concept of a bond presented there and also in the undergraduate courses is reasonable clear and comprehensive; they are typically defined [16] as:

> **chemical bond.** A strong force of attraction holding atoms together in a molecule or crystal. Typically chemical bonds have energies of about 1000 kJ· mol^{-1} and are distinguished from the much weaker forces between molecules ([. . .] van der Waals' forces). There are various types. *Ionic* (or *electrovalent*) bonds can be formed by transfer of electrons. [. . .] *Covalent* bonds are formed by sharing of valence electrons rather than by transfer. [. . .] A particular type of covalent bond is one in which one of the atoms supplies both the electrons. These are known as *coordinate* (*semipolar* or *dative*) bonds [. . .]. Covalent or coordinate bonds in which one pair of electrons is shared are electron-pair bonds and are known as single bonds. Atoms can also share two pairs of electrons to form double bonds or three pairs in triple bonds.

The idea of a bond is thus the sharing of electrons of neighbouring atoms whose orbitals overlap. This is the classical Lewis picture of bonding [17]. Transforming this concept into a mathematically rigorous scheme for classifying chemical bonds turns out to be astonishingly difficult. While using orbitals works well for small systems, this becomes cumbersome for larger systems. Especially, since the one-electron wave functions that stem from Hartree–Fock or density-functional theory calculations are generally quite delocalized over several atoms and do not represent

a unique bond. In addition, Hartree–Fock orbitals are ambiguous with regard to unitary transformations among the occupied orbitals. The total energy does not change under such transformations. Kohn–Sham orbitals are ambiguous only if they are degenerate.

In the density, which contains all observable information, the bonds and their nature are only barely visible; features like lone pairs are especially hidden. Moreover, the density plots differ from the classical Lewis picture, where the charge is accumulated in the mid of covalent-bond atoms. Density plots show no local maxima in the bond region between the nuclei. There are basically two approaches which are nowadays used to classify chemical bonds: The Laplacian of the density $-\nabla^2 n$ introduced by Bader in 1984 [18] and the electron localization function constructed by Becke and Edgecombe in 1990 [19]. Both methods show essential similarities in their structure. (For a comparison of the two, see Bader's article [20].) The Laplacian of the electron density seems to be superior for partial pairing of electrons as in acid–base reactions, while the ELF is more useful for comparing bonds [20]. In the following we focus on the ELF which is widely used in chemistry [21].

The ELF is a functional of the density and the orbitals, designed to visualize the bonding properties. It was originally used for electronic shells of atoms, where it shows all shells (while other methods like the Laplacian of the density $-\nabla^2 n$ fail to show more than five shells), and for covalent bonds [19]. Subsequently, it has been used to analyze lone pairs, hydrogen bonds [22], surfaces [23], ionic and metallic bonds [23], and solids [23–25]. In addition, the ELF has the nice property of being rather insensitive to the method used to calculate the wave functions of the system: Hartree–Fock, density-functional theory or even extended Hückel methods yield quantitatively similar results [23]. The ELF can also be constructed from experimentally measured electron densities using X-ray data [25], utilizing an approximate functional for the dependence of the kinetic energy density on the electron density.

The (static) ELF as constructed by Becke and Edgecombe can only be used to study systems in their ground state. Extending it to the time-dependent regime opens the possibility to study the creation, breaking or changing of bonds [26]. Examples of these include scattering processes (see section 2.4.2) and the excitation by a laser (see section 2.4.1), where a wealth of non-linear phenomena such as multi-photon ionization or high-harmonic generation can occur. Such phenomena happen on a time-scale of few femtoseconds, which can be examined using ulta-short laser pulses [27–29].

2.2 The static electron localization function

The (static) electron localization function, developed by Becke and Edgecombe [19], is a descriptor of chemical bonding based on the Pauli exclusion principle. The correlation between the ELF and chemical bonding is a topological and not an energetic one, i.e. the ELF represent the organization of chemical bonding in real space [21, 30]. The local maxima of the function define localization attractors, which can be attributed to bonds, lone pairs, atomic shells and other elements of chemical bonding [21]. The resulting isosurfaces of the ELF densities tend to conform to the classical Lewis picture of bonding.

In Slater determinant formulation[4], the probability of finding two particles with the same spin, located at $\boldsymbol{r}$ and $\boldsymbol{r}'$, is

$$D_\sigma(\boldsymbol{r}, \boldsymbol{r}') = n_\sigma(\boldsymbol{r})n_\sigma(\boldsymbol{r}') - \left|n_\sigma(\boldsymbol{r}, \boldsymbol{r}')\right|^2, \tag{2.1}$$

where $D_\sigma(\boldsymbol{r}, \boldsymbol{r}')$ is the same-spin pair probability and $n_\sigma(\boldsymbol{r})$ is the σ-spin single-particle density matrix,

$$n_\sigma(\boldsymbol{r}, \boldsymbol{r}') = \sum_{i=1}^{N_\sigma} \phi_{i\sigma}^*(\boldsymbol{r})\phi_{i\sigma}(\boldsymbol{r}'). \tag{2.2}$$

The probability to find an electron at $\boldsymbol{r}'$, knowing with certainty that a like-spin reference electron is at $\boldsymbol{r}$, is given by the conditional pair probability

$$P_\sigma(\boldsymbol{r}, \boldsymbol{r}') = n_\sigma(\boldsymbol{r}') - \frac{|n_\sigma(\boldsymbol{r}, \boldsymbol{r}')|^2}{n_\sigma(\boldsymbol{r})}, \tag{2.3}$$

which is invariant with respect to unitary transformations. Since only the local, short-range behaviour is of interest, the spherically averaged conditional pair probability p_σ is Taylor expanded. We obtain

$$p_\sigma(\boldsymbol{r}, s) = \frac{1}{3} \left(\sum_{i=1}^{N_\sigma} |\nabla\phi_{i\sigma}|^2 - \frac{1}{4}\frac{|\nabla n_\sigma|^2}{n_\sigma} \right) s^2 + O(s^3), \tag{2.4}$$

where $(\boldsymbol{r}, s)$ denotes the spherical average on a shell of the radius s around the reference point $\boldsymbol{r}$. In the Taylor expansion, the first s-independent term vanishes due to the Pauli principle, also the term linear in s vanishes (see section 2.3.1 or [31]). We define τ_σ as the positive-definite kinetic energy density

---

[4] This means, the wave function is written as determinant of single-particle wave functions; this single-particle picture encompasses the Kohn–Sham and Hartree–Fock formalism.

$$\tau_\sigma = \sum_{i=1}^{N_\sigma} |\nabla \phi_{i\sigma}|^2. \tag{2.5}$$

and can now write the s^2 coefficient of Eq. (2.4) as

$$C_\sigma(\boldsymbol{r}) := \tau_\sigma - \frac{1}{4} \frac{|\nabla n_\sigma|^2}{n_\sigma}. \tag{2.6}$$

This function, evaluated at the reference point, contains information about the electron localization. The smaller the probability of finding a second like-spin electron near $\boldsymbol{r}$, the higher localized is this reference electron. C_σ is not bounded from above, and approaches zero for strongly localized systems.

Becke and Edgecombe defined [19] the electron localization function as

$$\text{ELF} = \frac{1}{1 + \left(C_\sigma(r)\right)^2 / \left(C_\sigma^{\text{uni}}(r)\right)^2}, \tag{2.7}$$

where C_σ^{uni} denotes the kinetic energy density of the uniform electron gas

$$C_\sigma^{\text{uni}}(\boldsymbol{r}) = \frac{3}{5} (6\pi^2)^{2/3} n_\sigma^{5/3}(\boldsymbol{r}) =: \tau_\sigma^{\text{uni}}(\boldsymbol{r}). \tag{2.8}$$

Contrary to C_σ, the ELF is restricted to values between zero and one. A value of 1 stands for perfect localization and $1/2$ for the complete delocalization (uniform electron gas).

Since this derivation [19] of the ELF assumes that the $\phi_{i\sigma}$ are real, Eq. (2.6) is only valid for the static case, where the $\phi_{i\sigma}$ can be chosen to be real. In the next section, we derive a C_σ and thus an ELF without this restriction.

2.3   Derivation of the time-dependent ELF

In this section, we generalize the static electron localization function to complex wave functions, which is required for a time-dependent treatment. We follow essentially the steps by Becke and Edgecombe [19], but do not assume Hartree–Fock, i. e. Slater determinant, wave functions from the start (cf. [32]).

The reduced single-particle density matrix is defined as

$$n_\sigma(\boldsymbol{r}, \boldsymbol{r}', t) = N_\sigma \sum_{\sigma_2 \cdots \sigma_N} \int \mathrm{d}^3 r_2 \cdots \int \mathrm{d}^3 r_N \ \Psi^*(\boldsymbol{r}\sigma, \boldsymbol{r}_2\sigma_2, \dots, \boldsymbol{r}_N\sigma_N, t)$$
$$\times \Psi(\boldsymbol{r}'\sigma, \boldsymbol{r}_2\sigma_2, \dots, \boldsymbol{r}_N\sigma_N, t), \tag{2.9}$$

where Ψ is an N-electron wave function. For $\boldsymbol{r} = \boldsymbol{r}'$, it is known as spin density

$$n_\sigma(\boldsymbol{r}, t) := n_\sigma(\boldsymbol{r}, \boldsymbol{r}, t). \tag{2.10}$$

Eq. (2.10) gives the probability of finding a particle with spin σ at $\boldsymbol{r}$ and is normalized to the particle number N_σ. For the ELF we need the spin-diagonal ($\sigma_1 = \sigma_2$) of the reduced two-particle density matrix

$$D_{\sigma_1\sigma_2}(\boldsymbol{r}_1, \boldsymbol{r}_2, t) = N(N-1) \sum_{\sigma_3\cdots\sigma_N} \int \mathrm{d}^3 r_3 \cdots \int \mathrm{d}^3 r_N \, |\Psi(\boldsymbol{r}_1\sigma_1, \boldsymbol{r}_2\sigma_2, \ldots, \boldsymbol{r}_N\sigma_N, t)|^2, \tag{2.11}$$

which describes the probability of finding an electron with spin σ_1 at $\boldsymbol{r}_1$ and another electron at $\boldsymbol{r}_2$ with spin σ_2. For $\sigma_1 = \sigma_2$, it is known as the same-spin pair probability. Central for the electron localization function is the so-called *conditional pair probability*. It is defined analogously to the static case as

$$P_\sigma(\boldsymbol{r}, \boldsymbol{r}', t) := \frac{D_{\sigma\sigma}(\boldsymbol{r}, \boldsymbol{r}', t)}{n_\sigma(\boldsymbol{r}, t)} \tag{2.12}$$

and gives the probability of finding an electron with spin σ at $\boldsymbol{r}'$ at time t knowing with *certainty* that another electron with the *same spin* is at $\boldsymbol{r}$ at that time.

2.3.1   Spherical average and Taylor expansion of $P_\sigma(\boldsymbol{r}, \boldsymbol{r} + \boldsymbol{s}, t)$

Since we are only interested in the probability of finding an electron in the vicinity of $\boldsymbol{r}$, we substitute $\boldsymbol{r}'$ by $\boldsymbol{r} + \boldsymbol{s}$ and do a spherical average of the Taylor expansion in s for small s, $s := |\boldsymbol{s}|$.

Expanding the wave function in terms of $\boldsymbol{s}$ (in the second argument) gives

$$\Psi(\boldsymbol{r}\sigma, (\boldsymbol{r}+\boldsymbol{s})\sigma, \ldots, \boldsymbol{r}_N\sigma_N, t) = \Psi(\boldsymbol{r}\sigma, (\boldsymbol{r}+\boldsymbol{s})\sigma, \ldots, \boldsymbol{r}_N\sigma_N, t)\big|_{s=0}$$
$$+ \sum_{i=1}^{3} s_i \left.\frac{\partial\Psi}{\partial s_i}\right|_{s_i=0} + O(s^2). \tag{2.13}$$

The first term surely vanishes since two electrons with the same spin cannot be at the same location (Pauli exclusion principle). Thus we get

$$|\Psi|^2 \propto \sum_{i,k=1}^{3} s_i s_k c_{ik} + O(s^3), \tag{2.14}$$

where c_{ik} contains the factors and the $\boldsymbol{s}$-independent derivative of Ψ and Ψ^*. $\boldsymbol{s}$ can be written in spherical coordinates as $\boldsymbol{s} = (s_1, s_2, s_3)^{\mathrm{T}} = s\,(\cos\phi_s\sin\theta_s, \sin\phi_s\sin\theta_s, \cos\theta_s)^{\mathrm{T}}$. Doing the spherical average of Eq. (2.14) leads to

$$\langle |\Psi|^2 \rangle_{\text{sph.av.}} \propto \sum_{i=1}^{3} c_{ii} \int s_i s_i \, d\Omega + \sum_{\substack{i,k=1 \\ i \neq k}}^{3} c_{ik} \int s_i s_k \, d\Omega + O(s^3). \tag{2.15}$$

Evaluating the integrals gives

$$\langle s_i s_j \rangle_{\text{sph.av.}} := \frac{1}{4\pi} \int s_i s_j \, d\Omega = 0, \quad i \neq j \tag{2.16}$$

and

$$\langle s_i^2 \rangle_{\text{sph.av.}} = \frac{1}{3} s^2, \tag{2.17}$$

and thus $\langle |\Psi|^2 \rangle_{\text{sph.av.}} \dot{\propto} s^2$. We define p_σ as the spherical average of P_σ

$$p_\sigma(\boldsymbol{r}, s, t) := \langle P_\sigma(\boldsymbol{r}, \boldsymbol{r} + \boldsymbol{s}, t) \rangle_{\text{sph.av.}}. \tag{2.18}$$

and do a Taylor expansion

$$
\begin{aligned}
&p_\sigma(\boldsymbol{r}, s) \\
&= \frac{1}{n_\sigma(\boldsymbol{r}, t)} N(N-1) \sum_{\sigma_3, \dots, \sigma_N} \int d^3 r_3 \cdots \int d^3 r_N \, \langle |\Psi|^2 \rangle_{\text{sph.av.}} \\
&\doteq \frac{1}{n_\sigma(\boldsymbol{r}, t)} N(N-1) \sum_{\sigma_3, \dots, \sigma_N} \int d^3 r_3 \cdots \int d^3 r_N \, \frac{s^2}{3} \sum_{i=1}^{3} \left(\frac{\partial}{\partial s_i} \Psi^* \right)_{s=0} \left(\frac{\partial}{\partial s_i} \Psi \right)_{s=0}.
\end{aligned}
\tag{2.19}
$$

Since $\Psi|_{\boldsymbol{s}=0} = 0$ and hence

$$2 \sum_{i=1}^{3} \partial_{s_i} \Psi^* \partial_{s_i} \Psi \bigg|_{\boldsymbol{s}=0} = \nabla_{\boldsymbol{s}}^2 |\Psi|^2 \bigg|_{\boldsymbol{s}=0} = \nabla_{\boldsymbol{r}'}^2 |\Psi(r\sigma, r'\sigma, \dots)|^2 \bigg|_{\boldsymbol{r}=\boldsymbol{r}'}, \tag{2.20}$$

Eq. (2.19) can be simplified to

$$p_\sigma(\boldsymbol{r}, s, t) = \frac{1}{3} s^2 \left(\frac{1}{2} \frac{\nabla_{\boldsymbol{r}'}^2 D_\sigma(\boldsymbol{r}, \boldsymbol{r}', t)}{n_\sigma(\boldsymbol{r}, t)} \right) \bigg|_{\boldsymbol{r}=\boldsymbol{r}'} + O(s^3) \equiv \frac{1}{3} s^2 C_\sigma(\boldsymbol{r}, t) + O(s^3). \tag{2.21}$$

The term in the bracket

$$\boxed{C_\sigma = \frac{1}{2} \frac{\nabla_{\boldsymbol{r}'}^2 D_\sigma(\boldsymbol{r}, \boldsymbol{r}', t)}{n_\sigma(\boldsymbol{r}, t)} \bigg|_{\boldsymbol{r}=\boldsymbol{r}'},}$$
$$\tag{2.22}$$

is a measure of the electron localization (cf. section 2.2). A small value of $C_\sigma(r)$ denotes a small probability of finding another electron near $\boldsymbol{r}$. Thus there is a high electron localization at $\boldsymbol{r}$ which repels other like-spin electrons. In order to use C_σ

in density-functional calculations, we need to express D_σ and $n_\sigma(\boldsymbol{r}', \boldsymbol{r}, t)$ in terms of single-particle wave functions, which we do in the next sections.

2.3.2   Derivation of D_σ in the single-particle picture

We now evaluate D_σ and n_σ using Slater determinant wave functions. In the following, π and μ denote permutations, π_i and μ_i the i-th component of a given permutation (i.e. $\pi = (\pi_1, \dots, \pi_N)$), and $\mathrm{sgn}\,\pi$ the sign of the permutation π. With these definitions, a determinantal wave function containing $N = N_\sigma$ orbitals, $\Phi_{i\sigma} = \Phi_i$, is given by

$$
\Psi^{\mathrm{det}}(\boldsymbol{r}_1, \dots, \boldsymbol{r}_N, t) = \frac{1}{\sqrt{N!}} \det\{\phi_i(\boldsymbol{r}_j, t)\} = \frac{1}{\sqrt{N!}}
\begin{vmatrix}
\phi_1(\boldsymbol{r}_1, t) & \cdots & \phi_1(\boldsymbol{r}_N, t) \\
\vdots & \ddots & \vdots \\
\phi_N(\boldsymbol{r}_1, t) & \cdots & \phi_N(\boldsymbol{r}_N, t)
\end{vmatrix}
$$

$$
= \frac{1}{\sqrt{N!}} \sum_\pi \mathrm{sgn}\,\pi\, \phi_1(\boldsymbol{r}_{\pi_1}, t) \cdots \phi_N(\boldsymbol{r}_{\pi_N}, t).
$$

(2.23)

By definition, the following identities are true: $(\mathrm{sgn}\,\pi)^2 = 1$ and

$$
\int \phi_i^*(\boldsymbol{r}, t)\phi_j(\boldsymbol{r}, t)\, \mathrm{d}^3 r = \delta_{ij}.
$$

(2.24)

We now insert the Slater determinant wave function into the single-particle density matrix Eq. (2.9) and obtain

$$
n_\sigma(\boldsymbol{r}, \boldsymbol{r}', t)
$$
$$
= \frac{N}{N!} \int \mathrm{d}^3 r_2 \cdots \int \mathrm{d}^3 r_N \sum_{\pi,\mu} \mathrm{sgn}\,\pi\, \mathrm{sgn}\,\mu\, \phi_{\pi_1}^*(\boldsymbol{r}_1, t)\phi_{\mu_1}(\boldsymbol{r}_1, t), \cdots \phi_{\pi_N}^*(\boldsymbol{r}_N, t)\phi_{\mu_N}(\boldsymbol{r}_N, t)
$$
$$
= \frac{N}{N!} \sum_{\pi,\mu} \mathrm{sgn}\,\pi\, \mathrm{sgn}\,\mu\, \phi_{\pi_1}^*(\boldsymbol{r}', t)\phi_{\mu_1}(\boldsymbol{r}, t) \underbrace{\left(\int \mathrm{d}^3 r_2\, \phi_{\pi_2}^*(\boldsymbol{r}_2, t)\phi_{\mu_2}(\boldsymbol{r}_2, t) \right)}_{\delta_{\pi_2 \mu_2}} \cdots
$$
$$
\times \underbrace{\left(\int \mathrm{d}^3 r_N\, \phi_{\pi_N}^*(\boldsymbol{r}_N, t)\phi_{\mu_N}(\boldsymbol{r}_N, t) \right)}_{\delta_{\pi_N \mu_N}}.
$$

(2.25)

We therefore know that all terms with $\pi_i \neq \mu_i$, $i = 2, \dots, N$ vanish, and due to the definition of permutations, π_1 and μ_1 have to be identical. Thus $\pi = \mu$, $\mathrm{sgn}\,\pi = \mathrm{sgn}\,\mu$, and Eq. (2.25) simplifies to

$$n_\sigma(\boldsymbol{r}, \boldsymbol{r}', t) = \frac{N}{N!} \underbrace{\sum_\pi \phi^*_{\pi_1}(\boldsymbol{r}', t) \phi_{\mu_1}(\boldsymbol{r}, t) \prod_{i=2}^N \delta_{\pi_i \pi_i}}_{N! \text{ terms}}$$

$$= \frac{N}{N!}(N-1)! \underbrace{\sum_{l=1}^N \phi^*_l(\boldsymbol{r}', t) \phi_l(\boldsymbol{r}, t)}_{N \text{ terms}} = \sum_{l=1}^N \phi^*_l(\boldsymbol{r}', t) \phi_l(\boldsymbol{r}, t).$$

(2.26)

Following an analogous route for D_σ, we obtain

$$D_\sigma(\boldsymbol{r}, \boldsymbol{r}', t) = \frac{N(N-1)}{N!} \sum_{\pi,\mu} \mathrm{sgn}\,\pi\,\mathrm{sgn}\,\mu\, \phi^*_{\pi_1}(\boldsymbol{r}', t) \phi_{\mu_1}(\boldsymbol{r}, t) \phi^*_{\pi_2}(\boldsymbol{r}', t) \phi_{\mu_2}(\boldsymbol{r}, t)$$

$$\cdot \prod_{i=3}^N \underbrace{\int \mathrm{d}^3 r_i\, \phi^*_{\pi_i}(\boldsymbol{r}'_i, t) \phi_{\mu_i}(\boldsymbol{r}_i, t)}_{\delta_{\pi_i \mu_i}}.$$

(2.27)

There are only two types of permutations which contribute to this sum. They are: $\pi_1 = \mu_1$, $\pi_2 = \mu_2$ (with $\mathrm{sgn}\,\pi\,\mathrm{sgn}\,\mu = 1$) and $\pi_1 = \mu_2$, $\pi_2 = \mu_1$ (with $\mathrm{sgn}\,\pi\,\mathrm{sgn}\,\mu = -1$). Thus Eq. (2.27) simplifies to

$$D_\sigma(\boldsymbol{r}, \boldsymbol{r}', t) = \frac{N(N-1)}{N!} \left(\sum_\pi |\phi_{\pi_1}(\boldsymbol{r}_1, t)|^2 |\phi_{\pi_2}(\boldsymbol{r}_2, t)|^2 \prod_{i=3}^N \delta_{\pi_i \pi_i} \right)$$

$$- \frac{N(N-1)}{N!} \left(\sum_\pi \phi^*_{\pi_1}(\boldsymbol{r}_1, t) \phi_{\pi_2}(\boldsymbol{r}_1, t) \phi^*_{\pi_2}(\boldsymbol{r}_2, t) \phi_{\pi_1}(\boldsymbol{r}_2, t) \prod_{i=3}^N \delta_{\pi_i \pi_i} \right).$$

(2.28)

Each sum has $N!$ terms, and we know that

$$n_\sigma(\boldsymbol{r}, t) n_\sigma(\boldsymbol{r}', t) = \left(\sum_{i=1}^N |\phi_i(\boldsymbol{r}, t)|^2 \right) \left(\sum_{j=1}^N |\phi_j(\boldsymbol{r}', t)|^2 \right) = \sum_{\substack{i,j=1 \\ i \neq j}}^N |\phi_i(\boldsymbol{r}, t)|^2 |\phi_j(\boldsymbol{r}', t)|^2,$$

(2.29)

where $i \neq j$ comes from the Pauli exclusion principle. The sum in Eq. (2.29) therefore has $N(N-1)$ terms and the first term of Eq. (2.28) simplifies to

$$D_\sigma(\boldsymbol{r}, \boldsymbol{r}', t) = n_\sigma(\boldsymbol{r}, t) n_\sigma(\boldsymbol{r}', t) + (\text{second term}).$$

(2.30)

We further know that

$$\left(n_\sigma(\boldsymbol{r}, \boldsymbol{r}', t)\right)^* \left(n_\sigma(\boldsymbol{r}, \boldsymbol{r}', t)\right) = \sum_{\substack{i,j=1 \\ i \neq j}} \phi_j^*(\boldsymbol{r}, t)\phi_i(\boldsymbol{r}, t)\phi_i^*(\boldsymbol{r}, t)\phi_j(\boldsymbol{r}, t) \tag{2.31}$$

has $N(N-1)$ terms which yields as final result of the derivation

$$D_\sigma(\boldsymbol{r}, \boldsymbol{r}', t) = n_\sigma(\boldsymbol{r}, t)n_\sigma(\boldsymbol{r}', t) - |n_\sigma(\boldsymbol{r}, \boldsymbol{r}', t)|^2. \tag{2.32}$$

This is the same-spin pair probability in the single-particle picture. It gives the probability of finding two particles with the same spin, located at $\boldsymbol{r}$ and $\boldsymbol{r}'$.

2.3.3 Calculation of C_σ

We now calculate C_σ (see Eq. (2.22)),

$$C_\sigma(\boldsymbol{r}, t) = \frac{1}{2}\nabla_{\boldsymbol{r}'}^2 \frac{D_\sigma(\boldsymbol{r}', \boldsymbol{r}, t)}{n_\sigma(\boldsymbol{r}, t)}\bigg|_{\boldsymbol{r}'=\boldsymbol{r}} \tag{2.33}$$

using the single-particle formulation of n_σ Eq. (2.26) and D_σ Eq. (2.32). In the following, $\phi_{i\sigma}$ denotes the single-particle wave function and $n_{i\sigma} := |\phi_{i\sigma}|^2$.

Inserting D_σ from Eq. (2.32) gives

$$C_\sigma(\boldsymbol{r}, t) = \frac{1}{2}\nabla_{\boldsymbol{r}'}^2 n_\sigma(\boldsymbol{r}', t)\big|_{\boldsymbol{r}'=\boldsymbol{r}} - \frac{1}{2}\nabla_{\boldsymbol{r}'}^2 \frac{|n_\sigma(\boldsymbol{r}', \boldsymbol{r}, t)|^2}{n_\sigma(\boldsymbol{r}, t)}\bigg|_{\boldsymbol{r}'=\boldsymbol{r}} \tag{2.34}$$

The second term can be simplified as shown in appendix A, using this result we obtain

$$\begin{aligned} C_\sigma(\boldsymbol{r}, t) &= \frac{1}{2}\left(\nabla^2 n_\sigma(\boldsymbol{r}', t)\big|_{\boldsymbol{r}'=\boldsymbol{r}} - \nabla_{\boldsymbol{r}'}^2 \frac{|n_\sigma(\boldsymbol{r}', \boldsymbol{r}, t)|^2}{n_\sigma(\boldsymbol{r}, t)}\bigg|_{\boldsymbol{r}'=\boldsymbol{r}}\right) \\ &= \frac{1}{2}\bigg(\underbrace{\nabla^2 n_\sigma(\boldsymbol{r}', t) - \nabla^2 n_\sigma(\boldsymbol{r}, t)}_{=0} - \frac{1}{2}\frac{\left(\nabla n_\sigma(\boldsymbol{r}, t)\right)^2}{n_\sigma(\boldsymbol{r}, t)} - 2\frac{j_\sigma^2(\boldsymbol{r}, t)}{n_\sigma(\boldsymbol{r}, t)} \\ &\quad + 2\sum_{i=1}^{N_\sigma} \frac{j_{i\sigma}^2(\boldsymbol{r}, t)}{n_{i\sigma}(\boldsymbol{r}, t)} + \frac{1}{2}\sum_{i=1}^{N_\sigma} \frac{\left(\nabla n_{i\sigma}(\boldsymbol{r}, t)\right)^2}{n_{i\sigma}^{1/2}(\boldsymbol{r}, t)}\bigg), \end{aligned} \tag{2.35}$$

where j_σ denotes the absolute value of the current density, $j_\sigma^2/n = (\nabla\alpha)^2 n$. This can be rewritten by introducing

$$\tau_\sigma = \sum_{i=1}^{N_\sigma} |\nabla\phi_{i\sigma}(\boldsymbol{r}, t)|^2 = \sum_{i=1}^{N_\sigma} \left(\frac{1}{4}\frac{\left(\nabla n_{i\sigma}(\boldsymbol{r}, t)\right)^2}{n_{i\sigma}(\boldsymbol{r}, t)} + \frac{\left(j_{i\sigma}(\boldsymbol{r}, t)\right)^2}{n_{i\sigma}(\boldsymbol{r}, t)}\right) \tag{2.36}$$

which represents the kinetic energy of a system of N_σ non-interacting electrons, described by the single-particle orbitals $\phi_{i\sigma}$. The final result is thus

$$C_\sigma(\boldsymbol{r}, t) = \tau_\sigma - \frac{1}{4} \frac{\left(\nabla n_\sigma(\boldsymbol{r}, t)\right)^2}{n_\sigma(\boldsymbol{r}, t)} - \frac{j_\sigma^2(\boldsymbol{r}, t)}{n_\sigma(\boldsymbol{r}, t)}.$$

(2.37)

C_σ is a measure of the electron localization and ranges from zero (perfect localization) to infinity. The main difference to the ground-state C_σ Eq. (2.6) is the appearance of the term proportional to j^2. The existence of this term can be made plausible for a system with one electron (per spin channel): here, D_σ has to vanish by definition. If we evaluate τ_σ for $N_\sigma = 0$, the second and the third term of Eq. (2.37) appear. Section A.2 of the appendix contains an alternative derivation for a simplified, two electron case, which gives the same result.

The electron localization function itself is defined as before (cf. Eq. (2.7))

$$\mathrm{ELF} = \frac{1}{1 + \left(C_\sigma(r, t)\right)^2 / \left(C_\sigma^{\mathrm{uni}}(r)\right)^2}.$$

(2.38)

where C_σ^{uni} denotes the kinetic energy density of the uniform gas,

$$C_\sigma^{\mathrm{uni}}(\boldsymbol{r}) = \frac{3}{5} (6\pi^2)^{2/3} n_\sigma^{5/3}(\boldsymbol{r}) =: \tau_\sigma^{\mathrm{uni}}(\boldsymbol{r}).$$

(2.39)

The ELF returns values between zero and one. One stands for perfect localization and 1/2 for complete delocalization (uniform electron gas). (Note that only the ELF not C_σ 'shows all the exciting structuring in direct space that makes ELF such a valuable tool.' [21]). For systems with only one electron per spin channel (such as H_2 or parahelium) the ELF is meaningless since it is constant and equal to one.

As already stated above there is (counter-intuitively) no direct relation between the electron density (the probability of finding an electron at point $\boldsymbol{r}$) and the ELF (the electron localization), in fact the density can be high when the ELF is low.

2.3.4 Comparison with the static ELF

For static problems, one can choose the wave function to be real, then $\alpha \equiv 0$ and thus $j \equiv 0$, in addition $n(\boldsymbol{r}, t) \to n(\boldsymbol{r})$. Therefore,

$$C_\sigma(\boldsymbol{r}) = \tau_\sigma - \frac{1}{4} \frac{\left(\nabla n_\sigma(\boldsymbol{r})\right)^2}{n_\sigma(\boldsymbol{r})}, \quad \tau_\sigma = \sum_{i=1}^{N_\sigma} |\nabla \phi_{i\sigma}(\boldsymbol{r})|^2 = \sum_{i=1}^{N_\sigma} \frac{1}{4} \frac{\left(\nabla n_{i\sigma}(\boldsymbol{r})\right)^2}{n_{i\sigma}(\boldsymbol{r})}.$$

(2.40)

This is exactly the same result which Becke and Edgecombe have obtained Eq. (2.6).

2.4 Application of the TDELF

We shall now illustrate the time-dependent electron localization function by two examples: The excitation of ethyne in a laser pulse and the scattering of a proton with ethene (FIG. 2.1). Supplementary information such as the movies of the ELF and the density and more examples can be found at `http://www.net-b.de/~burnus/thesis/`.

$$H — C ≡ C — H$$

(a) Ethyne (acetylene)   (b) Ethene (etylene)
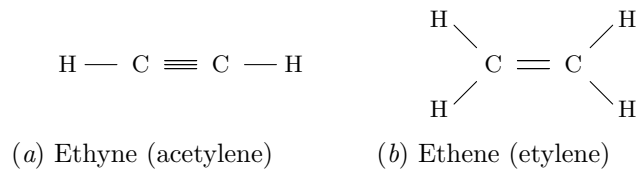
Fig. 2.1 Structure of used molecules.

All calculations have been performed in the framework of time-dependent density-functional theory using the real-space, real-time program `octopus` [13] with a Troullier–Martins pseudopotential (cf. section 1.4). The motion of the cores is treated classically. There exists a kind of colour standard for ELF plots [23] which we follow (see colourbar in FIG. 2.3). The isosurfaces and the contourlines are drawn at ELF = 0.8.

2.4.1 Excitation of molecules
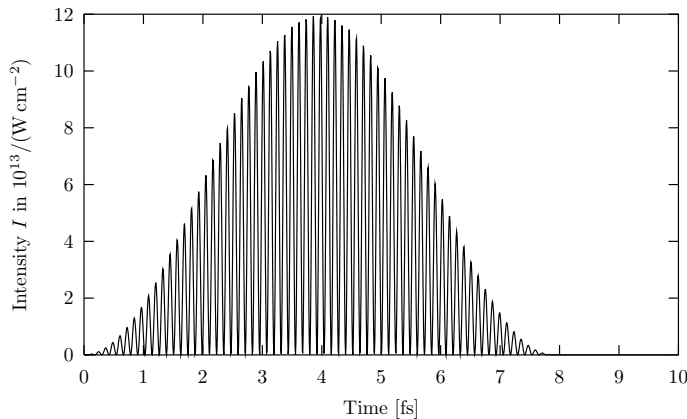
Fig. 2.2 Intensity of the laser, used to excite ethyne. The laser has a frequency of 17.15 eV$/h$ ($\lambda = 72.3$ nm) and a maximal intensity of $I_0 = 1.19 \times 10^{14}$ W $\cdot$ cm^{-2}.

We used a strong laser to excite ethyne (acetylene, FIG. 2.1a) and observed the reaction of the electron system, especially of the triple bond. The laser is polarized along the molecular axis (see right image on the title page). The system has been

excited using the following laser frequencies: (i) $\nu = 17.15$ eV$/h = 4146$ THz, $\lambda = 72.3$ nm, (ii) $\nu = 13.35$ eV$/h = 3010$ THz, $\lambda = 99.6$ nm and (iii) $\nu = 9.55$ eV$/h = 2309$ THz, $\lambda = 129.8$ nm. The intensity of the laser was chosen to be either $E_0 = 3$ eV$/$Å, $I_0 = 1.19 \times 10^{14}$ W$\cdot$cm^{-2} or $E_0 = 0.5$ eV$/$Å, $I_0 = 3.318 \times 10^{13}$ W$\cdot$cm^{-2}. Since the resulting ELF movies show essentially the same features, only the results using a laser with $\nu = 17.15$ eV$/h$, $E_0 = 3$ eV$/$Å (FIG. 2.2) are shown.

Calculation settings: We used a spherical mesh with radius $r = 8.2$ Å and $\Delta = 0.15$ Å as spacing. The bond lengths (cf. [33]) are $d(\mathsf{H–C}) = 1.06$ Å and $d(\mathsf{C–C}) = 0.6612$ Å. Absorbing boundaries with a mask of width 1.0 Å were used. The calculation was done using the local-density approximation for exchange and Perdew and Zunger's parametrization of the correlation part [34].

For time-evolution the Suzuki–Trotter method [35] was used with a time-step of $\Delta t = 0.0008\,\hbar/$eV $= 0.53 \times 10^{-18}$ s for $T = 20\,\hbar/$eV $= 13.2$ fs. The laser had the frequency $\nu = 17.15$ eV$/h = 4146$ THz and the wavelength $\lambda = 72.3$ nm, a maximal amplitude of $E_0 = 3$ eV$/$Å and therefore a maximal intensity of $I_0 = 1.19 \times 10^{14}$ W$\cdot$cm^{-2}. The laser had a cosine envelope and was turned on from $t = 0$ to $T_{\text{laser}} = 12\,\hbar/$eV $= 7.9$ fs, reaching its maximal intensity at $t = 6\,\hbar/$eV $= 3.9$ fs.
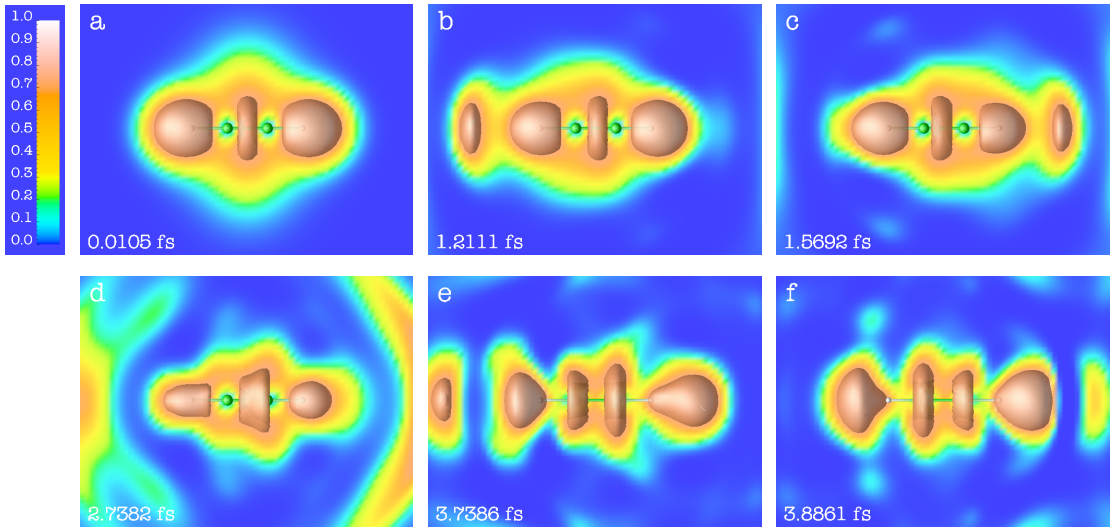
Fig. 2.3 Snapshots of the time-dependent ELF for the excitation of ethyne (acetylene) by a 17.15 eV ($\lambda = 72.3$ nm) laser pulse. The pulse had a total length of 7 fs, a maximal intensity of 1.2×10^{14} W cm^{-2}, and was polarized along the molecular axis. Ionization and the transition from the bonding π to the anti-bonding π^* are clearly visible.

FIG. 2.3 depicts snapshots of the ELF of acetylene in form of slabs through a plane of the molecule. At the beginning (FIG. 2.3a) the system is in the ground state and the ELF visualizes these features: The torus between the carbon atoms, which is typical

for triple bonds (in the Lewis picture, they are formed by the two π orbitals), and the blobs around the hydrogen atoms (cf. [23]). As the intensity of the laser (FIG. 2.2) increases, the system starts to oscillate and then ionizes (FIG. 2.3*b,c*). Note that the ionized charge leaves the system in fairly localized packets (the blob on the left in *b* and on the right in *c*). The central torus then starts to widen (FIG. 2.6*d*) until it breaks into two tori centered around the two carbon atoms (FIG. 2.3*e,f*). This can be interpreted as a transition from the π bonding to the π^* non-bonding state. The system then remains in this excited state for some time after the laser has been switched off.
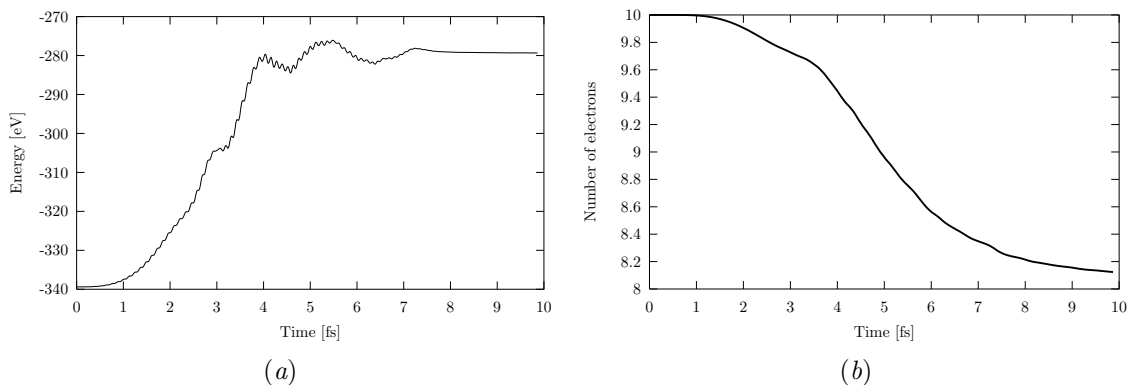
Fig. 2.4   Ethyne excited by a laser. (*a*) Total energy of the electron system which shows that about 60 eV are absorbed. (*b*) Number of electrons in the system, about 1.8 electrons are lost due to ionization.

The molecule absorbs about 60 eV of energy due to the laser (FIG. 2.4*a*) and looses 1.8 electrons through ionization (this has to be interpreted statistically; FIG. 2.4*b*). The absorption spectra (FIG. 2.5*b*) of ethyne, using a laser with $\nu = 17.15$ eV/h, shows a strong absorption at 16.5 eV/h below the laser frequency and a smaller peak at $\nu = 18.5$ eV/h which matches the calculated excitation energies (FIG. 2.5*a*). Note that the absorption spectra could be a bit distorted due to the ionization.

2.4.2   Proton scattering

In the second type of application, a fast (i. e. non-thermic), but still non-relativistic proton ($E_{kin} = 2$ keV, $v = 1.02 \times 10^5$ m/s) is sent against an ethene (etylene) molecule. The proton is scattered by one of the carbon atoms (FIG. 2.6). The initial configuration is shown in FIG. 2.6*a*. While the proton approaches the carbon, it accumulates some charge around it (FIG. 2.6*b*). It then scatters and leaves the system (FIG. 2.6*c*), taking some charge (about 0.2*e*) with it, i. e. in about every fifth scattering process a hydrogen atom forms. The ethene molecule is thus excited and the molecule starts to disintegrate. In panels *d,e* the leftmost carbon has already broken the two bonds with the hydrogens (that will later form a H_2 molecule (left)
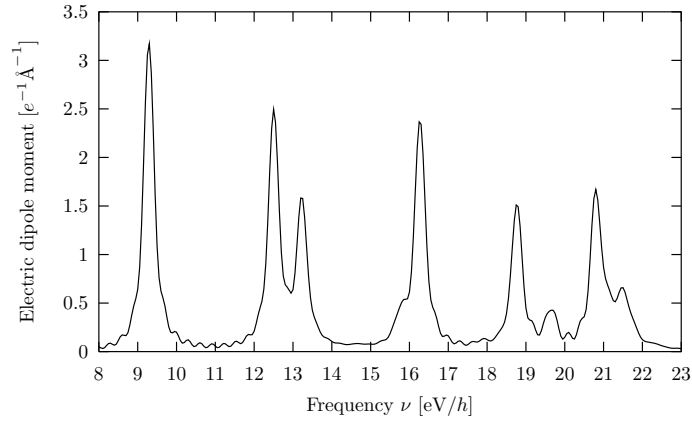
(a)
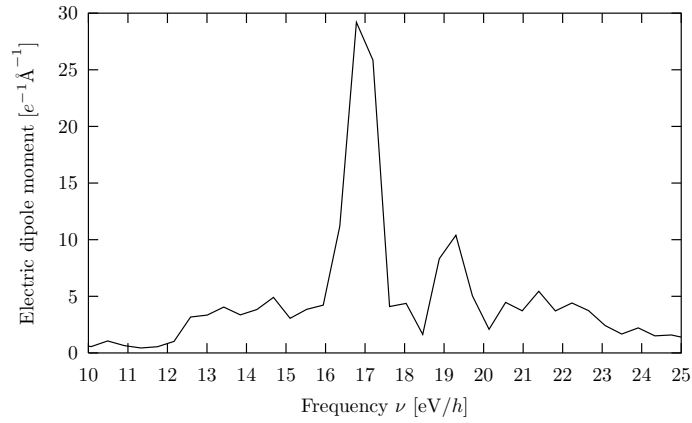
(b)

Fig. 2.5 (a) Excitation energies of ethyne. (b) The absorptions
when excited using a laser with $\nu = 17.15$ eV$/h$.

and two CH molecules (middle and right). Finally, the rightmost CH molecule breaks, yielding a carbon and a hydrogen atom. The ELF shows how the double bond between the carbons is distorted, breaks and lone pairs form. The breaking of the CH bond and the formation of a lone pair can be seen in panel (d).

The electronic system absorbs a bit less than 30 eV (FIG. 2.8a). The peak around 7 fs is due to numerical errors in the time propagation when the proton comes close to the carbon nucleus. Because of the rapid change of protonic momentum at this point in time, a much finer time step is needed to prevent this error. In total, about two electron charges get ionized (FIG. 2.8b). During the first 1.5 fs, the time the proton is in the box, about 0.2 electron charges are lost, mainly as electron cloud around the proton. Towards the end of the simulation, electrons are also absorbed because the nuclei are close to boundaries of the box.
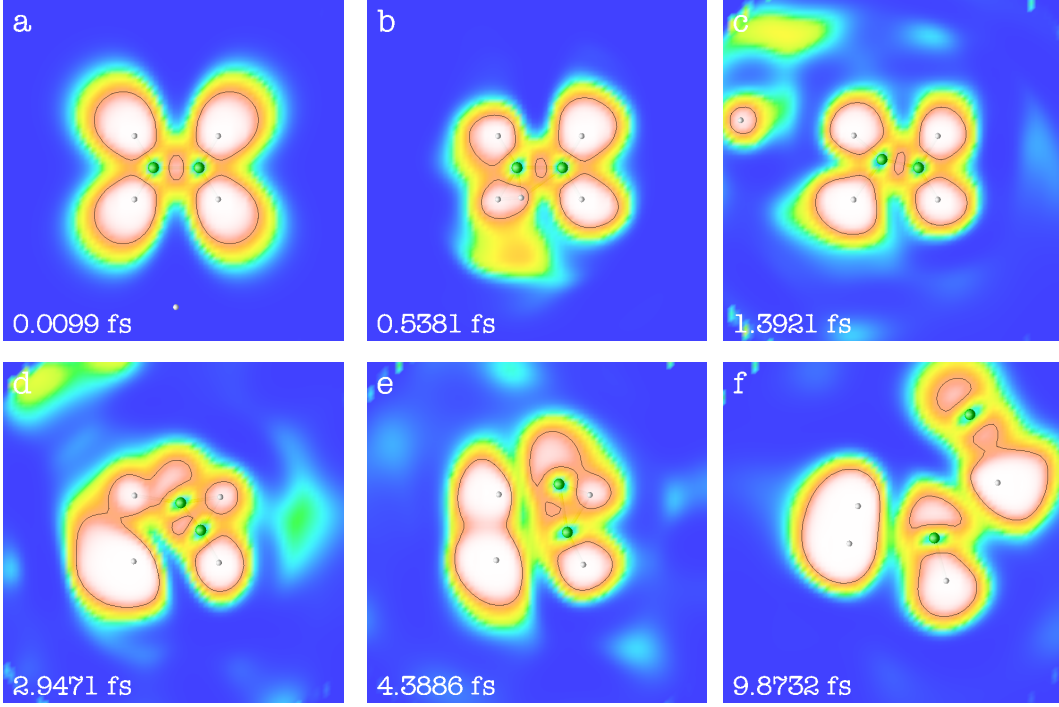
Fig. 2.6 Snapshots of the time-dependent ELF for the scattering of a fast, non-relativistic proton ($E_{\mathrm{kin}} = 2\,\mathrm{keV}$, white dot in the mid bottom of *a*) by ethene (etylene). The molecule breaks in several pieces. During this fragmentation process, the breaking of bonds and the subsequent creation of lone pairs becomes clearly visible.

If one carefully examines the moment when the proton hits the carbon (FIG. 2.7), one observes that even before the proton hits the carbon, ionization occurs (FIG. 2.7*a*). This blob of localized electrons leaves the system downwards, roughly into the direction of the approaching proton. Shortly after, another blob leaves the system (FIG. 2.7*b,c*) this time upwards. This is quite surprising since it seems as if the proton repels the electrons while it attracts them in reality. We believe that this phenomon is due to an overshooting of the electron oscillation between the approaching proton and the ethene.

Calculation settings: We used a spherical mesh with a radius $r = 7$ Å and $\Delta = 0.14$ Å as spacing. The used bond lengths are $d(\mathsf{C\text{–}C}) = 1.339$ Å and $d(\mathsf{C\text{–}H}) = 1.085$ Å. The angle between the hydrogen atoms was $\angle(\mathsf{H\text{–}C\text{–}H}) = 117.8°$. Absorbing boundaries with a mask of the width of 0.5 Å were used. The calculation was done using the local-density approximation for exchange and Perdew and Zunger's parametrization of the correlation part [34].

For the time-evolution the Suzuki–Trotter method [35] was used with a timestep of $\Delta t = 0.0005\,\hbar/\mathrm{eV} = 0.33 \times 10^{-18}$ s for $T = 150\,\hbar/\mathrm{eV} = 9.8$ fs. The ion movement used Newton dynamics with the velocity Verlet algorithm. The

(a) (b) (c)
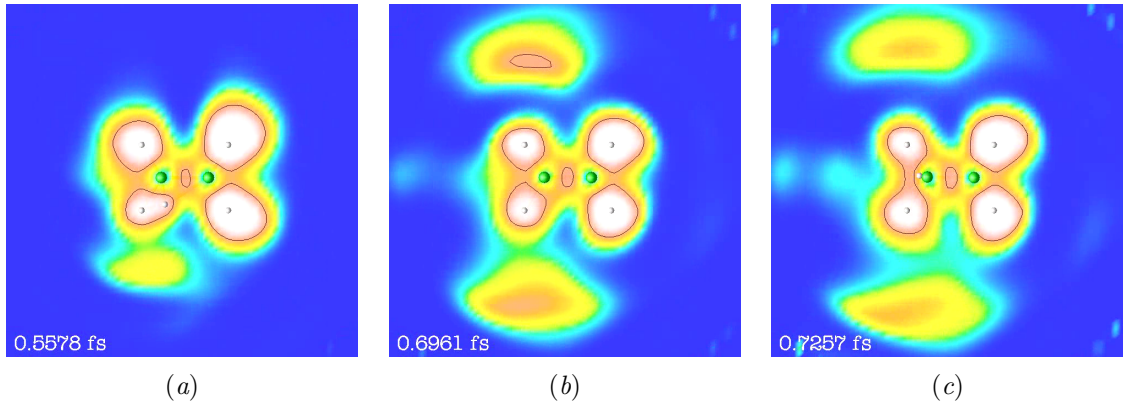
Fig. 2.7 Ionisation details scattering of a proton by ethene. (*a*) Even before the proton scatters, ionization occurs which is roughly directed downwards, in the direction of the proton. Soon after (*b, c*) one can also see ionization in the opposite direction.

(a) (b)
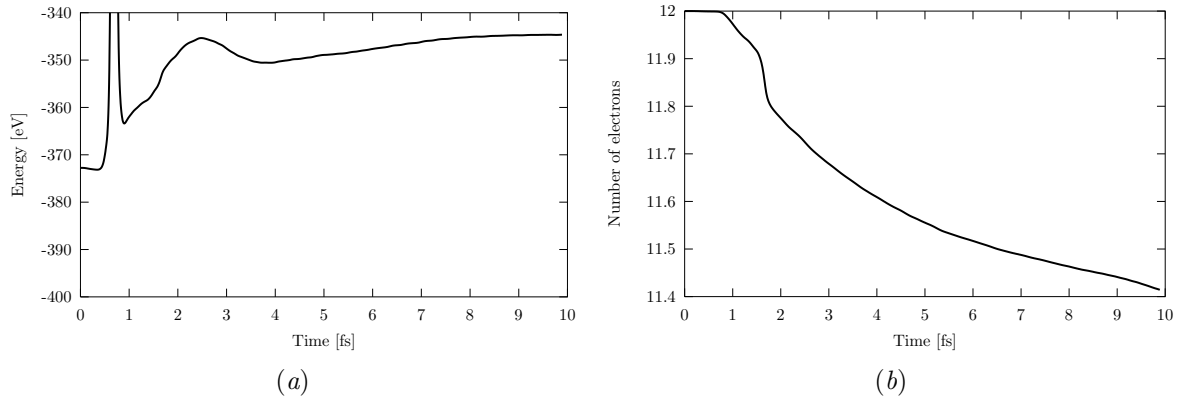
Fig. 2.8 Proton scattering by carbon. (*a*) The total energy of the electronic system is shown. The peak around 7 fs is due to numerical errors when the proton is close to the carbon. The proton transfers about 20 eV to the system. (*b*) Number of electrons in the box (using pseudo-potentials), the drop by about 0.2 in the first 2 fs is mostly due to the charge picked up by the proton; the drop by another 0.4 is mostly caused by ionization.

scattering proton was initially in the middle, 4 Å below the C–C axis of the molecule and had an initial velocity of 4.67×10^{-10} eV$/\hbar = 0.709 \times 10^{6}$ m/s.

2.5 Conclusions

These examples illustrate the wealth information which can be obtained from the time-dependent electron localization function by simply looking at it. It visualizes the $\pi–\pi^*$ transitions, the breaking and forming of bonds, the creation of lone pairs. The time-dependent ELF is expected to be a valuable tool in the analysis of other physical processes as well, such as creation and decay of collective excitations or

the scattering of electrons by atoms and molecules. The key feature is the time-resolved observation of the formation, modulation and creation of chemical bonds, thus providing a visual understanding of the dynamics of excited electrons.

It is more important to have beauty in one's equations than to have them fit experiment ... It seems that if one is working from the point of view of getting beauty in one's equations, and if one has a really sound insight, one is on a sure line of progress. If there is not complete agreement between the results of one's work and experiment, one should not allow oneself to be too discouraged, because the discrepancy may well be due to minor features that are not properly taken into account and that will get cleared up with further developments of the theory.

— Paul Dirac, 1902–84

3 Optimal control

We are interested in maximizing the transfer of population to a particular molecular state, such as the π^* state as depicted in the previous chapter (section 2.4.1). This state optimization can be used not only to stimulate chemical reactions, but also to trigger molecular switches. In this chapter, we concentrate on the HOMO–LUMO transition of lithium fluoride, which bears some of the hallmarks needed for transport. After a short introduction, we describe the used algorithm in section 3.2, which is based on the idea to maximize a suitable functional. In section 3.3 we look at the actual implementation of this algorithm for molecules having cylindrical symmetry. This encompasses the discretization and the time-propagation. Section 3.4 contains the results obtained for lithium fluoride and section 3.5 contains the conclusion and an outlook.

3.1 Introduction

In subjects reaching from mathematics, engineering and physics to chemistry and economics optimal control theories (OCT) are used. In physics, such theories are applied to prepare quantum bits (qbits), align and orient molecules, select reaction pathways, increase the yield of chemical reactions or to control molecular transport. Several optimal control techniques are used [36], among them are genetic alogrithms, feedback-control of experimental systems [37–38], and *ab-initio,* functional based methods [39–40]. Coming from a density-functional theory background, we focus on the last method in this chapter.

3.2 Algorithm

Since we want to use a laser for optimal control, we assume that the Hamilton operator is of the following form

$$H = T + V - \epsilon\mu =: H_0 - \epsilon\mu, \tag{3.1}$$

where $\epsilon = \epsilon(t)$ denotes the electrical field and μ the dipole operator, which can be written as

$$\mu = \sum_{i=1}^{N} e\boldsymbol{r}_i. \tag{3.2}$$

Note that the dipole approximation is only valid if the system of regard is small compared to the wavelength. Then the field is approximately constant in space.

The idea is that a tailored laser takes the system from the initial state Ψ_i to the final state Φ_f within a given time T. In other words, the overlap $|\langle\Psi_i(T)|\Phi_f\rangle|^2$ has to be maximized. In order to reduce ionization, the energy of the laser should be as small as possible, i.e. the energy density (energy per area)

$$E = c\varepsilon_0 \frac{1}{2} \int_0^T |\epsilon(t)|^2 \,\mathrm{d}t, \tag{3.3}$$

has to to be minimized. Here, c denotes the speed of the light and ε_0 the electric constant. Summarizing, we want to find a laser field which maximizes the overlap of the propagated wave function with a given final state and minimizes the applied laser energy. This can achieved by maximizing the following functional

$$J = |\langle\Psi_i(T)|\Phi_f\rangle|^2 - \alpha \int_0^T |\varepsilon(t)|^2 \,\mathrm{d}t, \tag{3.4}$$

where α is a Lagrange multiplier which controls the importance of the energy minimization. Therefore, it is known as penalty factor. A wide range of values of α are sensible, depending on the system. In order to make the second term dimensionless, $1/\alpha$ has the unit of a squared electric field ($\mathrm{V}^2 \cdot \mathrm{m}^{-2}$) times the unit of time (s), in atomic units α has therefore the unit $e^2 a_0^2/\hbar E_\mathrm{h}$.

In order to tackle the problem of maximizing J, we subtract a carefully chosen zero. Since Ψ_i is a wave function, it fulfils the Schrödinger equation

$$\mathrm{i}\hbar\partial_t\Psi_i = H\Psi_i$$
$$\Leftrightarrow (-H + \mathrm{i}\hbar\partial_t)\Psi_i = 0$$
$$\Leftrightarrow \left(\frac{\mathrm{i}}{\hbar}(H_0 - \mu\epsilon) + \partial_t\right)\Psi_i = 0 \tag{3.5}$$

for all times and spatial coordinates. We multiply Eq. (3.5) from the left with an arbitrary wave function Ψ_f^* and integrate. The functional is now

$$J = |\langle\Psi_i(T)|\Phi_f\rangle|^2 - \alpha \int_0^T |\varepsilon(t)|^2 \, dt - \int_0^T \langle\Psi_f|\left[\frac{i}{\hbar}(H_0 - \mu\epsilon) + \partial_t\right]|\Psi_i(t)\rangle \, dt, \quad (3.6)$$

where Ψ_f can be viewed as a Lagrange multiplier density, ensuring that Ψ_f satisfies the time-dependent Schrödinger equation at each point in space and time. In order to determine a stationary point of J, we do a functional derivative and set it to zero. Unfortunately, the differential equations obtained have coupled boundary conditions. Zhu *et al.* [39] have therefore multiplied the third term of Eq. (3.6) by $\langle\Psi_i(T)|\Phi_f\rangle$. Then they subtract the complex conjugate of this term. The new functional is therefore

$$J = J_1 + J_2 + J_3, \tag{3.7a}$$

$$J_1 = |\langle\Psi_i(T)|\Phi_f\rangle|^2, \tag{3.7b}$$

$$J_2 = -\alpha \int_0^T |\epsilon(t)|^2 \, dt, \tag{3.7c}$$

$$J_3 = -2\operatorname{Re}\left[\langle\Psi_i(T)|\Psi_f(T)\rangle \int_0^T \left\langle\Psi_f(t)|\left[\frac{i}{\hbar}(H - \mu\epsilon(t)) + \partial_t\right]|\Psi_i(t)\right\rangle \, dt\right]. \tag{3.7d}$$

Before we continue, a few remarks are in order: α can be replaced by an $\alpha(t)$ to impose time-dependent constraints on the laser shape, e.g. to force a cosine shaped envelope. The Lagrange multiplier Ψ_f can be regarded as a backward propagated wave function with $\Psi_f(T) = \Phi_f$ (see below). In J_3, the order of Ψ_i and Ψ_f in the prefactor is reversed compared with the integral, which cancels time-independent phases.

Calculating the derivative of the functional (for a detailed derivation, see [41]) and setting it to zero (i.e. extremum of J), the following equations are obtained

$$i\partial_t\Psi_i = \big(H_0 - \mu\epsilon(t)\big)\Psi_i(t), \quad \Psi_i(0) = \Phi_i(0), \tag{3.8}$$

$$i\partial_t\Psi_f = \big(H_0 - \mu\epsilon(t)\big)\Psi_f(t), \quad \Psi_i(T) = \Phi_f(T), \tag{3.9}$$

$$\epsilon(t) = -\frac{1}{\alpha}\operatorname{Im}\Big(\langle\Psi_i(t)|\Psi_f(t)\rangle\langle\Psi_f(t)|\mu|\Psi_i(t)\rangle\Big). \tag{3.10}$$

This coupled system of non-linear equations can now be solved iteratively [37]. We start with a guessed initial field $\epsilon^{(0)}(t)$ which can be arbitrary.[5]

---

[5] Using $\epsilon^{(0)} \equiv 0$ may lock the system in the initial state [42]. While using a constant field (i.e. a potential with the form of a wedge) seems to be a good starting point [private communication with Jan Werschnik].

3.2.1 Iteration algorithm

In the first step, Ψ_f, $\Psi_f(T) = \Phi_f$, is propagated backwards from $t = T$ to $t = 0$ using the guessed field. In the second step, $\Psi_f(t)$ is propagated from $t = 0$ to T using the same field $\epsilon^{(0)}$. Concurrently, the new field

$$\epsilon^{(1)}(t) = -\frac{1}{\alpha}\mathrm{Im}\Big(\langle\Psi_i(t)|\Psi_f(t)\rangle\langle\Psi_f(t)|\mu|\Psi_i(t)\rangle\Big) \tag{3.11}$$

is calculated and used for the propagation of Ψ_i. In the third step, Ψ_i is propagated backward from $t = T$ to $t = 0$ using $\epsilon^{(1)}$, the field is updated and used to propagate Ψ_f. In the fourth step, Ψ_f is propagated back with $\epsilon^{(1)}$, $\epsilon^{(2)}$ is calculated and used for propagating Ψ_i, and so on. Graphically,

$$\Psi_f^{(0)}(0) \quad \xleftarrow{\qquad\qquad \epsilon^{(0)} \qquad\qquad} \quad \Psi_f^{(0)}(T) := \Phi_f$$

$$\Psi_f^{(0)}(0) \quad \xrightarrow{\qquad\qquad \epsilon^{(0)} \qquad\qquad} \quad \Psi_f^{(0)}(T)$$

$$\Phi_i =: \Psi_i^{(1)}(0) \quad \xrightarrow{\quad \epsilon^1 := -\alpha^{-1}\mathrm{Im}\left(\langle\psi_i^{(1)}|\psi_f^{(0)}\rangle\langle\psi_f^{(0)}|\mu|\psi_i^{(1)}\rangle\right) \quad} \quad \Psi_i^{(1)}(T)$$

$$\Psi_i^{(1)}(0) \quad \xleftarrow{\qquad\qquad \epsilon^{(1)} \qquad\qquad} \quad \Psi_i^{(1)}(T)$$

$$\Psi_f^{(2)}(0) \quad \xleftarrow{\quad \epsilon^{(2)} := -\alpha^{-1}\mathrm{Im}\left(\langle\psi_i^{(1)}|\psi_f^{(2)}(T)\rangle\langle\psi_f^{(2)}|\mu|\psi_i^{(1)}(T)\rangle\right) \quad} \quad \Psi_f^{(2)}(T) := \Phi_f$$

$$\text{etc.}$$

Zhu *et al.* showed that this algorithm has the following convergence properties with regard to the functional J [39]: (i) The iteration sequence converges monotonically and quadratically in terms of the neighbouring field deviations. (ii) A larger deviation of the field between neighbouring iteration steps leads to faster convergence of the objective functional.

In fact, we could observe this behaviour in our calculations. In the first steps, the overlap and the functional increases a lot, while later iteration steps introduce only minor changes.

While we sticked to the above outlined algorithm, there are several modifications of the algorithm possible. One modification proposed by Zhu *et al.* [39] is to evaluate the first wave function bracket only at $t = 0$ and $t = T$,

$$\epsilon = -\frac{1}{\alpha}\mathrm{Im}\Big(\langle\Phi_i|\Psi_f(0)\rangle\langle\Psi_f(t)|\mu|\Psi_i(t)\rangle\Big), \quad \text{First, third, \dots step,}$$

$$\epsilon = -\frac{1}{\alpha}\mathrm{Im}\Big(\langle\Psi_i(T)|\Phi_f\rangle\langle\Psi_f(t)|\mu|\Psi_i(t)\rangle\Big), \quad \text{Second, fourth,\dots step.} \tag{3.12}$$

Zhu *et al.* expect that this algorithm has generally a faster convergence. Another possible modification is to revert the order of the propagations by first forward propagating Ψ_i,[6]. In order to optimize $\langle\Psi_i(T)|O|\Phi_f\rangle$, with O being a positive definite operator, the functional [40]

$$
\begin{aligned}
J =& \langle\Psi_i(T)|O|\Phi_f\rangle - \alpha \int_0^T \left|\epsilon(t)\right|^2 \mathrm{d}t \\
&- 2\,\mathrm{Re}\left(\int_0^T \left\langle X_f(t)\Big|\left[\frac{i}{\hbar}(H_0 - \mu\epsilon(t)) + \partial_t\right]\Big|\psi_i(t)\right\rangle \mathrm{d}t\right),
\end{aligned}
\tag{3.13}
$$

can be used, where $X_f(T) = O\Psi_i(T)$. However, in the following we restrict ourselves to the functional of Eq. (3.7).

3.3 Optimizing the HOMO–LUMO transition of LiF

We now apply the optimal control formalism, introduced in the last section, to a system which is as small and as realistic as possible. Lithium fluoride is well suited since it only contains two atoms and is rotationally invariant. This reduces the three dimensional problem to an effective two dimensional one, which we describe in cylindrical coordinates. To a certain extent, LiF also shows the hallmarks needed for transport since the HOMO[7] is located near the fluorine while the LUMO has an appreciable contribution of the density near the lithium atom.

The Kohn–Sham potential of LiF has been calculated with `octopus` [13] using pseudopotentials. The KS potential was then imported in optwo, a program which has been written specially for this thesis to do the optimal control of molecules with cylinderical symmetry. The potential exported by `octopus` lacks the non-local part of the pseudopotential, which may yield wrong eigenvalues and orbitals. In addition, in optwo we do not propagate the imported Kohn–Sham potential (it is therefore frozen in time). As further simplification, no other orbitals are propagated.

3.3.1 Calculation of $H\psi_i = \varepsilon_i\psi_i$

While we can simply calculate LiF with the `octopus` package, it cannot (yet) be used to do optimal control. Therefore, the Kohn–Sham potential of `octopus` is exported and the optimal control is done by an external program. In the following, we show what is needed to do optimal control using the imported KS potential.

---

[6] Initial results by Jan Werschnik show a slower convergence.

[7] HOMO stands for the highest occupied molecular orbital ('ground state') and LUMO for the lowest unoccupied molecular orbital ('first excited state').

HOMO, $E = -5.68$ eV   LUMO, $E = -1.86$ eV
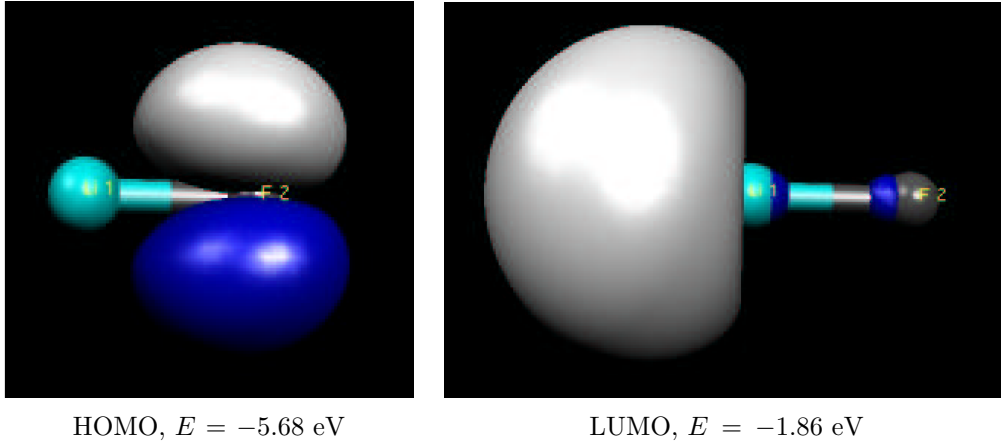
Fig. 3.1 Isosurfaces of the HOMO and LUMO of lithium fluoride. (Lithium is on the left, fluorine on the right.) The HOMO is doubly-degenerate and located near the fluorine (combining both HOMOs makes the HOMO φ independent in cylindrical coordinates) while the LUMO has some density located around the lithium atom. Note that the LUMO has still parts close to the fluorine which are only barely visible in this isosurface plot. [Gaussian calculations by courtesy of Angelica Zacarias.]

Orbital		Energy (Ha)	Energy (eV)	
1	HOMO−4	−24.12993	−656.6088	$m = 0$
2	HOMO−3	−1.85919	−50.5911	$m = 0$
3	HOMO−2	−0.88686	−24.1327	$m = 0$
4	HOMO−1	−0.21886	−5.9555	$m = 0$
5, 6	HOMO	−0.20891	−5.6847	$m = \pm 1$
7	LUMO	−0.06841	−1.8615	$m = 0$
8, 9	LUMO−1	0.01082	0.2944	$m = \pm 1$
10	LUMO−2	0.03950	1.0748	$m = 0$
11	LUMO−3	0.11062	3.0101	$m = 0$
12, 13	LUMO−4	0.13091	3.5622	$m = \pm 1$

Table 3.1 Molecular orbital eigenvalues of lithium fluoride. LiF has twelve electrons, four of which are inner core electrons. The orbitals with magnetic quantum number $|m| = 1$ are doubly degenerate. [Gaussian calculations by courtesy of Angelica Zacarias.]

First, we need to obtain the orbitals and eigenenergies. Since we use a KS potential, a single-particle Schrödinger equation has to be solved. The Hamiltonian has the form $H = T + V + V_{\text{ext}}$, where T denotes the kinetic part, V the KS potential and V_{ext} the potential induced by the external laser. For the calculation of the states, $V_{\text{ext}} = 0$. The kinetic energy operator can be written as

$$T = \frac{p^2}{2m_{\mathrm{e}}} = -\frac{\hbar^2}{2m_{\mathrm{e}}}\nabla^2 \stackrel{\mathrm{a.u.}}{=} -\frac{1}{2}\nabla^2. \tag{3.14}$$

In the remainder of this chapter, we use atomic units (cf. appendix D). Using Eq. (3.14) and cylindrical coordinates, the following Schrödinger equation needs to be solved

$$H\psi = \left(-\frac{1}{2}\nabla^2_{\mathrm{cyl}} + V(r,z,\phi)\right)\psi(r,z,\phi) = \varepsilon\psi(r,z,\phi). \tag{3.15}$$

In cylindrical coordinates, the Laplacian has the form [43]

$$\nabla^2_{\mathrm{cyl}} = \frac{1}{r}\partial_r(r\partial_r) + \frac{1}{r^2}\partial^2_\phi + \partial^2_z$$

$$= \partial^2_r + \frac{1}{r}\partial_r + \frac{1}{r^2}\partial^2_\phi + \partial^2_z. \tag{3.16}$$

Inserting Eq. (3.16),

$$H\psi = \left(-\frac{1}{2}\nabla^2_{\mathrm{cyl}} + V(r,z,\varphi)\right)$$

$$\left[-\frac{1}{2}\left(\partial^2_r + \frac{1}{r}\partial_r + \frac{1}{r^2}\partial^2_\varphi + \partial^2_z\right) + V(r,z,\varphi)\right]\psi(r,z,\varphi) = \varepsilon\psi(r,z,\varphi). \tag{3.17}$$

Since lithium fluoride is a molecule with cylinderical symmetry, i.e. the wave function is φ independent, we can replace $\psi(r,z,\varphi)$ by $\tilde{\psi}(r,z)\mathrm{e}^{im\varphi}$, $m \in \mathbb{Z}$. Multiplying Eq. (3.17) by $\mathrm{e}^{-im\varphi}$, we obtain as new Schrödinger equation

$$H\tilde{\psi}(r,z) = \left[-\frac{1}{2}\left(\partial^2_r + \frac{1}{r}\partial_r + \partial^2_z - \frac{m^2}{r^2}\right) + \tilde{V}(r,z)\right]\tilde{\psi}(r,z) = \varepsilon\tilde{\psi}(r,z). \tag{3.18}$$

Note that the eigenvalues of Eq. (3.17) and (3.18) are the same. By writing $\psi(r,z,\varphi)$ as $\tilde{\psi}(r,z)\mathrm{e}^{im\varphi}$, we can only do transitions were the magnetic quantum number m does not change, transitions with $\Delta m = \pm 1$ are thus not possible. This is because a linearly polarized laser can only do $\Delta m = 0$ transitions while a circularly polarized one is needed for $\Delta m = \pm 1$. By construction, our laser can only be polarized along the cylinder axis, i.e. along the axis of the molecule. We now set $\tilde{\psi}(r,z) =: \psi(r,z)$ and $\tilde{V}(r,z) =: V(r,z)$.

In order to discretize Eq. (3.18) properly, we need to look at the boundary conditions and therefore at the asymptotics. For bound states, $\langle\psi|\psi\rangle$ has to be finite (namely one) and therefore the wave function has to vanish for $|\boldsymbol{r}| \to \infty$, i.e. for $|z| \to \infty$ and $r \to \infty$. Using cylindrical coordinates, we have also to look at $r = 0$ (cf. [44]). As an ansatz, we use

$$\psi(r, z) = r^{\xi}\tilde{\psi}(r, z). \tag{3.19}$$

If we insert Eq. (3.19) in the Schrödinger equation, we obtain

$$
\begin{aligned}
Er^{\xi}\tilde{\psi}(r, z) = &-\frac{1}{2}\left(r^{\xi-2}\tilde{\psi}(r, z)\left(\xi^2 - m^2\right) + r^{\xi-1}\partial_r\tilde{\psi}(r, z)\left(1 + 2\xi\right)\right) \\
&+ r^{\xi}\left(-\frac{1}{2}\partial_r^2 - \frac{1}{2}\partial_z^2 + V(r, z)\right)\tilde{\psi}(r, z).
\end{aligned}
\tag{3.20}
$$

Since we use pseudopotentials, the potential is smooth and $V(r = 0, z)$ is finite. Therefore, we may Taylor-expand V in r around $r = 0$

$$V(r, z) = V(r, z)\big|_{r=0} + \partial_r V(r, z)\big|_{r=0}r + \frac{1}{2}\partial_r^2 V(r, z)\big|_{r=0}r^2 + O(r^3). \tag{3.21}$$

We also Taylor-expand the wave function $\tilde{\psi}$ in r around $r = 0$

$$\tilde{\psi}(r, z) = \tilde{\psi}(r, z)\big|_{r=0} + \partial_r\tilde{\psi}(r, z)\big|_{r=0}r + \frac{1}{2}\partial_r^2\tilde{\psi}(r, z)\big|_{r=0}r^2 + O(r^3). \tag{3.22}$$

We now insert Eq. (3.22) and (3.21) in the Schrödinger equation (3.20), neglect terms of higher order and collect the coefficients of the leading term, which is propotional to $r^{\xi-2}$. One can then deduce

$$\xi = |m|. \tag{3.23}$$

Reinserting this into Eq. (3.20), one obtains the boundary condition

$$\psi(r)\Big|_{r=0} = 0, \quad m \neq 0. \tag{3.24}$$

For $m = 0$, we need to look at the term proportional to $r^{\xi-1}$ and see then that $(\mathrm{d}\tilde{\psi}/\mathrm{d}r)|_{r=0} = 0$, therefore

$$\frac{\mathrm{d}\psi}{\mathrm{d}r}\Big|_{r=0} = 0, \quad m = 0. \tag{3.25}$$

With these two boundary conditions, Eq. (3.24) and (3.25), and the condition that ψ vanishes at infinity, the discretized Schrödinger equation will be solved.

3.3.2 Discretization

In order to solve the Schrödinger equation numerically in real-space, we have to discretize the Hamiltonian. The coordinates are written as r_i, $i = 1, \ldots, N_r$ and z_j, $j = 1, \ldots, N_z$. We use a two dimensional, uniform grid with a mesh width of $\Delta = |z_{j+1} - z_j| = |r_{i+1} - r_i|$ (FIG. 3.28). The wave function will be written as $\psi_{i,j} := \psi(r_i, z_j)$ and the potential as

$$V_{i,j} := V(r_i, z_j) + \frac{m^2}{2r_i^2}. \tag{3.26}$$

Since we do not want to calculate the kinetic part T of the Hamiltonian in momentum space, the derivatives in T have to be approximated.

$r_{\max}$ (N_r, N_z)

r

0

$-z_{\max}$ 0 $z_{\max}$

$(1,1)$ z
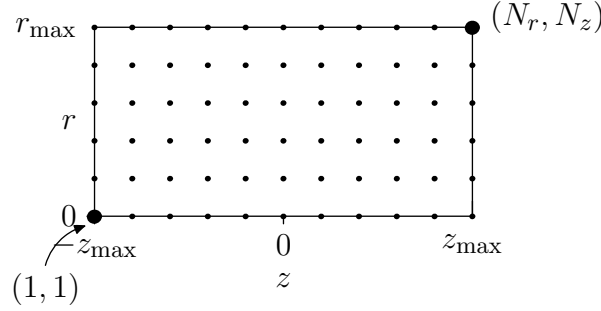
Fig. 3.2   Used coordinates

Using the three-point discretization formula (e. g. [45]), namely

$$\partial_r \psi_{i,j} = \frac{1}{2\Delta}(\psi_{i+1,j} - \psi_{i-1,j}) + O(\Delta^3), \tag{3.27a}$$

$$\partial_r^2 \psi_{i,j} = \frac{1}{\Delta^2}(\psi_{i+1,j} - 2\psi_{i,j} + \psi_{i-1,j}) + O(\Delta^4), \tag{3.27b}$$

$$\partial_z^2 \psi_{i,j} = \frac{1}{\Delta^2}(\psi_{i,j+1} - 2\psi_{i,j} + \psi_{i,j-1}) + O(\Delta^4), \tag{3.27c}$$

yields the discretized Schrödinger equation

$$H(i,j)\psi_{i,j} = \left(-\frac{1}{2}\left(\partial_r^2 + \frac{1}{r}\partial_r + \partial_z^2\right) + V_{ij}\right)\psi_{i,j} \tag{3.28}$$

$$\dot{=} -\frac{1}{2}\left(\frac{1}{a^2}(\psi_{i+1,j} + \psi_{i-1,j} + \psi_{i,j+1} + \psi_{i,j-1} - 4\psi_{i,j}) + \frac{1}{2a}\frac{1}{r}(\psi_{i+1,j} - \psi_{i-1,j})\right) + V_{i,j}\psi_{i,j}$$

$$= \qquad\qquad \left(-\frac{1}{2}\frac{1}{a^2}\right)\psi_{i,j-1}$$

$$+ \left(-\frac{1}{2}\left(\frac{1}{a^2} - \frac{1}{2a}\frac{1}{r}\right)\right)\psi_{i-1,j} \quad + \left(\frac{1}{2}\frac{4}{a^2} + V_{i,j}\right)\psi_{i,j} \quad + \left(-\frac{1}{2}\left(\frac{1}{a^2} + \frac{1}{2a}\frac{1}{r}\right)\right)\psi_{i+1,j}$$

$$+ \left(-\frac{1}{2}\frac{1}{a^2}\right)\psi_{i,j+1}.$$

There is a tricky point in this equation: The resulting matrix is not symmetric due to the different sign of $\psi_{i-1,j}$ and $\psi_{i+1,j}$ in the first derivative. Therefore, the eigenvalues may be complex. In our calculations the imaginary part was zero, though. However, one can symmetrize the matrix by substituting ψ by $\psi\sqrt{r}$ but this symmetization only works for the three-point formula (cf. [44]). In the following, we only look at the non-symmetric matrix using three- and five-point finite-differences.

Before we check the boundary conditions, we first construct a Hamilton matrix. In principle, the eigenvectors are matrices of the size $N_r \times N_z$, but since common eigensolvers expect a vector, we transform $\psi_{i,j}$ into a vector of the size $N = N_r N_z$. We set

$$\psi_l := \psi_{i,j} \quad \text{with } l(i,j) := N_z(i-1) + j. \tag{3.29}$$

The indices i and j can be regained from l using

$$i(l) = \lfloor (l-1)/N_z \rfloor + 1,$$
$$j(l) = (l-1) \bmod N_z + 1. \tag{3.30}$$

The resulting matrix has a band structure with tridiagonal entries and a sub-/super-diagonal N_z rows below/above the diagonal (FIG. 3.3). Since this is a sparse matrix it should not be stored fully.
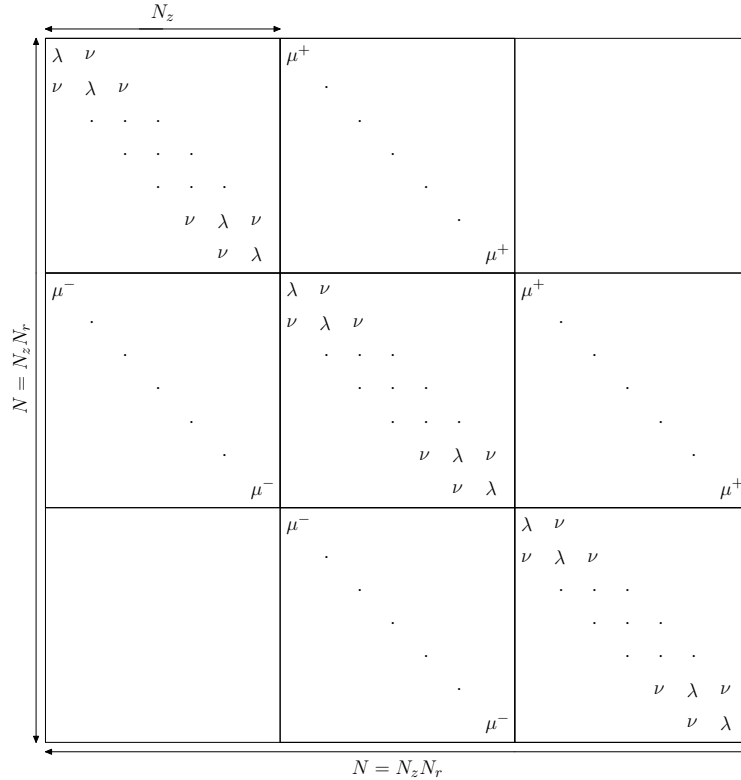
Fig. 3.3 Schematic Hamilton matrix using the three-point formula. In this figure, $\lambda = 2/\Delta^2 + V_{i,j}$, $\mu^\pm = -1/2(1/\Delta^2 \pm 1/2r_i\Delta)$ and $\nu = -1/2\Delta^2$.

We now need to check the boundary conditions. For $|z| \to \infty$ and $r \to \infty$ they are automatically fulfilled since the matrix has a finite size. Since points outside the

box are treated as zero, one has to to ensure that the box is big enough. We now look at $r \to 0$. The point r_1 couples (Eq. (3.28)) to the non-existing point at r_0. We introduce an offset for the radial coordinate, and start at $r_1 = \Delta r$ instead of at $r_1 = 0$ (i.e. $r_i = (i-1)\Delta + \Delta r$). We choose now $\Delta r = \Delta/2$ and evaluate $H\psi_{1,j}$. One observes then that the term with $\psi_{0,j}$ cancels. We therefore fulfil the boundary conditions.

3.3.3   The five-point discretization

The accuracy of the obtained eigenvalues can be be enhanced by using a higher order of finite-differences or going into Fourier space. But there is also a downside: The numerical effort increases and new errors due to the transformation or the larger matrices may occur. For the two-dimensional Harmonic oscillator in polar coordinates, the three-point formula shows errors up to about one per cent and the five-point up to 0.2 per mille [44]. In optwo both schemes are implemented, for the results shown, the five-point formula has been used.

The expressions of the five-point finite difference (cf. [44]) are

$$\partial_r \psi_{i,j} = \frac{1}{\Delta}\left(-\frac{1}{12}\psi_{i+2,j} + \frac{2}{3}\psi_{i+1,j} - \frac{2}{3}\psi_{i-1,j} + \frac{1}{12}\psi_{i-2,j}\right) + O(\Delta^5) \qquad (3.31)$$

for the first and

$$\partial_r^2 \psi_{i,j} = \frac{1}{\Delta^2}\left(-\frac{1}{12}\psi_{i+2,j} + \frac{4}{3}\psi_{i+1,j} - \frac{5}{2}\psi_{i,j} + \frac{4}{3}\psi_{i-1,j} - \frac{1}{12}\psi_{i-2,j}\right) + O(\Delta^6)$$
$$(3.32)$$

for the second derivative. Analogously for ∂_z^2. We now look at the boundary conditions. As before, $|\boldsymbol{r}| \to \infty$ poses no problem. We now insert the five-point formula (Eq. (3.32) and (3.32)) into the Schrödinger equation

$$E\psi_{i,j} = \left(\frac{1}{24\Delta^2} + \frac{1}{24r_i\Delta}\right)\psi_{i+2,j} + \left(-\frac{2}{3\Delta^2} - \frac{2}{3r_i\Delta}\right)\psi_{i+1,j}$$
$$+ \left(\frac{1}{24\Delta^2}\right)\psi_{i,j+2} + \left(-\frac{2}{3\Delta^2}\right)\psi_{i,j+1} + \left(\frac{5}{2\Delta^2} + V_{i,j} + \frac{m^2}{2r_i^2}\right)\psi_{i,j}$$
$$+ \left(-\frac{2}{3\Delta^2}\right)\psi_{i,j-1} + \left(\frac{1}{24\Delta^2}\right)\psi_{i,j-2}$$
$$+ \left(-\frac{2}{3\Delta^2} + \frac{2}{3r_i\Delta}\right)\psi_{i-1,j} + \left(\frac{1}{24\Delta^2} - \frac{1}{24r_i\Delta}\right)\psi_{i-2,j}. \qquad (3.33)$$

If one sets the offset Δr to the spacing Δ and evaluates Eq. (3.33) for r_1, the $\psi_{-1,j}$ term vanishes while $-1/6\Delta^2\,\psi_{0,j}$ remains. For $m \neq 0$ we need the boundary

condition $\psi_{0,j} = 0$ which is fulfilled due to the truncation of the matrix. (For $m = 0$ one can even construct a symmetric Hamilton matrix [44]). For $m = 0$ the first derivative of ψ at r_0 needs to vanish. As we show now, extra terms in the Hamilton matrix are needed. We start by writing the condition explicitly using Eq. (3.31)

$$0 \equiv \left. \frac{\partial \psi}{\partial r} \right|_{r=r_0} = \frac{1}{\Delta} \left(\frac{1}{12} \psi_{-2,j} - \frac{2}{3} \psi_{-1,j} + \frac{2}{3} \psi_{1,j} - \frac{1}{12} \psi_{2,j} \right)$$

$$\Leftrightarrow \psi_{-2,j} = 8\psi_{-1,j} - 8\psi_{1,j} + \psi_{2,j}. \tag{3.34}$$

Next we look for an expression for $\psi_{-1,j}$. We take the second derivative of $\psi_{0,j}$ using Eq. (3.34)

$$\left. \frac{\partial^2 \psi}{\partial r^2} \right|_{r=r_0} = \frac{1}{\Delta^2} \left(\frac{2}{3} \psi_{-1,j} - \frac{6}{5} \psi_{0,j} + 2\psi_{1,j} - \frac{1}{6} \psi_{2,j} \right). \tag{3.35}$$

and use it in the next step. We express $\psi_{1,j}$ using the Taylor expansion of ψ in r around r_0

$$\psi(r_1 = \Delta, z_j) = \psi_{0,j} + \left. \frac{\partial \psi(r, z_j)}{\partial r} \right|_{r=r_0} \Delta + \frac{1}{2} \left. \frac{\partial^2 \psi(r, z_j)}{\partial r^2} \right|_{r=r_0} \Delta^2$$

$$\Leftrightarrow \psi_{-1,j} = -\frac{6}{5} \psi_{0,j} + \frac{1}{4} \psi_{2,j}. \tag{3.36}$$

Now we can use $\psi_{-1,j}$ to express $\psi_{2,j}$ using the Taylor expansion

$$\psi(r_2 = 2\Delta, z_j) = \psi_{0,j} + \left. \frac{\partial \psi(r, z_j)}{\partial r} \right|_{r=r_0} 2\Delta + \frac{1}{2} \left. \frac{\partial^2 \psi(r, z_j)}{\partial r^2} \right|_{r=r_0} (2\Delta)^2$$

and obtain an expression for $\psi_{0,j}$

$$\psi_{0,j} = \frac{4}{3} \psi_{1,j} - \frac{1}{3} \psi_{2,j}. \tag{3.37}$$

If one inserts this in Eq. (3.33) for $\psi_{1,j}$ and $\psi_{2,j}$, we get a modified Hamiltonian for those points, namely

$$E\psi_{1,j} = \left(\frac{5}{2\Delta^2} - \frac{4}{9\Delta^2} + V_{1,j} + \frac{m^2}{2r_1^2} \right) \psi_{1,j} + \left(-\frac{2}{3\Delta^2} - \frac{2}{3r_1\Delta} + \frac{1}{9\Delta^2} \right) \psi_{2,j}$$

$$+ \left(\frac{1}{24\Delta^2} + \frac{1}{24r_1\Delta} \right) \psi_{3,j} + \left(-\frac{1}{24\Delta^2} \right) \psi_{1,j+2} + \left(\frac{2}{3\Delta^2} \right) \psi_{1,j+1}$$

$$+ \left(\frac{2}{3\Delta^2} \right) \psi_{1,j-1} + \left(-\frac{1}{24\Delta^2} \right) \psi_{1,j-2} \tag{3.38}$$

and

$$E\psi_{2,j} = \left(-\frac{2}{3\Delta^2} + \frac{2}{3r_2\Delta} + \frac{1}{36\Delta^2}\right)\psi_{1,j} + \left(-\frac{5}{2\Delta^2} - \frac{1}{144\Delta^2} + V_{2,j} + \frac{m^2}{2r_2^2}\right)\psi_{2,j}$$

$$+ \left(-\frac{2}{3\Delta^2} - \frac{2}{3r_2\Delta}\right)\psi_{3,j} + \left(\frac{1}{24\Delta^2} + \frac{1}{24r_2\Delta}\right)\psi_{3,j} + \left(-\frac{1}{24\Delta^2}\right)\psi_{2,j+2}$$

$$+ \left(\frac{2}{3\Delta^2}\right)\psi_{2,j+1} + \left(\frac{2}{3\Delta^2}\right)\psi_{2,j-1} + \left(-\frac{1}{24\Delta^2}\right)\psi_{2,j-2}, \tag{3.39}$$

respectively. (For $m = 0$ the Hamiltonian cannot be symmetrized using $\psi_{ij} = \tilde{\psi}_{ij}\sqrt{r_i}$ [44].)

3.3.4 Solving the eigenvalue problem

There exist several algorithms to solve eigenvalue problems of type encountered in the previous section [46–47]. Two of which are implemented in optwo. One is the `dgeev` routine which is part of LAPACK [48]. It expects a full matrix and is therefore slow and has a high memory consumption for larger number of points N. `dgeev` calculates always all N eigenvalues and, if requested, all eigenvectors.[8] The other solver which was used is `dneupd`. It is part of ARPACK [49]. `dneupd` implements the implicitly restarted Arnoldi iteration. The Arnoldi iteration saves time and memory by allowing to calculate only the n smallest or largest eigenvalues (and vectors). As used, it only needs $\psi^{(i+1)} = H\psi^{(i)}$ and is therefore quite memory efficient. Though, for unknown reasons, `dneupd` as used in optwo has convergence problems and the obtained eigenvalues are not close to the expected values. Therefore, for the results presented here, only the LAPACK routine has been used. Alternative algorithms for sparse matrices are conjugated gradient [50] and the Jacobi-Davidson algorithm [51].

The discretization and the eigensolver have been tested using a three-dimensional Harmonic oscillator whose potential is φ independent and whose analytic result is known. The results had an absolute error of up to about one per cent using the three-point formula and up to 0.2 per mille for the five-point formula. This is comparable with the MatLab calculations in [44].

3.3.5 Time propagation

Knowing only the eigenstates of the static system ($V_{\text{ext}} \equiv 0$) is not enough, we also need to know how the system evolves in time under the influence of a laser. We now need to find an explicit algorithm to calculate $\psi(r,t)$ knowing its initial state

---

[8] For symmetric matices LAPACK has routines for band matrices and one is able to calculate only the lowest N eigenvectors.

$\psi(r, t_0)$ at the time t_0. If the Hamiltonian does not depend explicitly on time, we can integrate the Schrödinger equation and obtain the unitary time evolution operator

$$U(t, t_0) = \exp(-\frac{\mathrm{i}}{\hbar} H\,(t - t_0)). \tag{3.40}$$

In the time-dependent case, we can deduce for infinitesimal time-steps $\mathrm{d}t$ that $U(t_0 + \mathrm{d}t, t_0) = (1 - \mathrm{i}/\hbar\, H\,\mathrm{d}t)$. We can now write $U(t, t_0)$ as product of infinitesimal time-steps and obtain

$$U(t, t_0) = \lim_{n\to\infty} \prod_{i=1}^{n} \exp\left(-\frac{\mathrm{i}}{\hbar} H\big(t_0 + i(t - t_0)/n\big)(t - t_0)/n\right). \tag{3.41}$$

If the Hamiltonian is time-independent then $H(t)$ commutes with $H(t')$ and the product of exponentials can be written as one exponential (as in Eq. (3.40)). For an explicitly time-dependent Hamiltonian, we have $[H(t), H(t')] \neq 0$ (for $t \neq t'$) and Eq. (3.41) can symbolically be written as

$$\psi(\boldsymbol{r}, t) = U(t, t_0)\psi(\boldsymbol{r}, t) = \hat{T} \int_{t_0}^{t} \exp\left(-\frac{\mathrm{i}}{\hbar} H(t')\,\mathrm{d}t'\right) \tag{3.42}$$

where $\hat{T}$ denotes the time-ordering operator.

A simple and crude approximation is to expand Eq. (3.40) for $H(t_0)$. Unfortunately, this is numerically not stable since it breaks the reversal symmetry of the Schrödinger equation [52], moreover such a time evolution operator is not unitary. The stability can be improved by enforcing the symmetry using

$$\psi(\boldsymbol{r}, t + \delta t/2) \approx \exp\left(-\frac{\mathrm{i}}{\hbar} H(t)\frac{\delta t}{2}\right) \psi(\boldsymbol{r}, t) \approx \exp\left(+\frac{\mathrm{i}}{\hbar} H(t + \delta t)\frac{\delta t}{2}\right) \psi(\boldsymbol{r}, t + \delta t). \tag{3.43}$$

A simple approach is to multiply Eq. (3.43) by $\exp\big(-\mathrm{i}/\hbar\,\delta t\, H(t + \delta t)\big)$ from the left, resulting in

$$\psi(\boldsymbol{r}, t + \delta t) \approx \exp\left(-\frac{\mathrm{i}}{\hbar} H(t + \delta t)\frac{\delta t}{2}\right) \exp\left(+\frac{\mathrm{i}}{\hbar} H(t)\frac{\delta t}{2}\right) \psi(\boldsymbol{r}, t). \tag{3.44}$$

The exponential functions of Eq. (3.44) can now be expanded. We used an expansion up to the fourth order (cf. [53]). The advantage of this method is that the algorithm is fast to implement and no matrix inversion is needed. This is the method which we used.

An alternative method is Crank–Nicholson. The starting point is again Eq. (3.43). Here, the exponential functions are expanded to the first order and multiplied by $\big(1 + \mathrm{i}/\hbar\,\delta t/2\, H(t + \delta t)\big)^{-1}$, symbolically written ($H$ is a matrix)

$$\psi(x, t + \delta t) \approx \frac{1 - \mathrm{i}/\hbar\, \delta t/2\, H(t)}{1 + \mathrm{i}/\hbar\, \delta t\, H(t + \delta t)} \psi(x, t). \tag{3.45}$$

Since the Crank–Nicholson algorithm requires a matrix inversion, it is not feasible for large systems. A stability analysis of Crank–Nicholson can be found in [54].

For most calculations, further approximations need to be done since at time t the Hamiltonian at time $t + \delta t$ is usually not known. Since we do not propagate the Kohn–Sham potential and the electric field $\epsilon(t)$ is known, we need not to predict $H(t + \delta t)$.

The used time-propagation and its implementation can be tested using the driven Harmonic oscillator since for this particular case an analytic solution exists [55]. At least if the time-steps are not to long, the result should match perfectly (tested using the sine function for the external field).

3.3.6 Absorbing boundaries

As soon as we use a strong laser, ionization occurs. That means that electron density moves towards the boundary of the box. In the real world, it does not come back. But in our system, the wave function is per construction zero at the boundary of the box, i. e. there is an infinite potential which confines the particles. Therefore, they are reflected and come back. One way to 'absorb' the density at the border is to multiply the wave function $\psi(\boldsymbol{r}, t)$ with a so called masking function $M(\boldsymbol{r})$ which has to be smooth, otherwise reflections occur. The masking function is typically defined (in one dimension) as

$$M(r) = \begin{cases} f(r), & r_{\mathrm{ab}} < |r| < r_{\mathrm{max}} \\ 1, & r < r_{\mathrm{ab}} \end{cases}, \tag{3.46}$$

where r_{max} is the extention of the box in r direction, $r_{\mathrm{max}} - r_{\mathrm{ab}}$ is the width of the absorbing boundaries and $f(r)$ is a smooth function with $f(r_{\mathrm{ab}}) = 1$. We used as masking function

$$f(r) = \left(\cos \frac{\pi\, (r - r_{\mathrm{ab}})}{2w} \right)^{1/4}, \quad w := r_{\mathrm{max}} - r_{\mathrm{ab}}, \tag{3.47}$$

which is depicted in FIG. 3.4. Another possibility is to add an imaginary potential which causes an exponential decay of the wave function (see e. g. [56]).

3.4 Application of the optimal control algorithm

As stated before, we want to find the optimal laser pulse to maximize the transition from the HOMO to the LUMO in lithium fluoride. We therefore calculate first
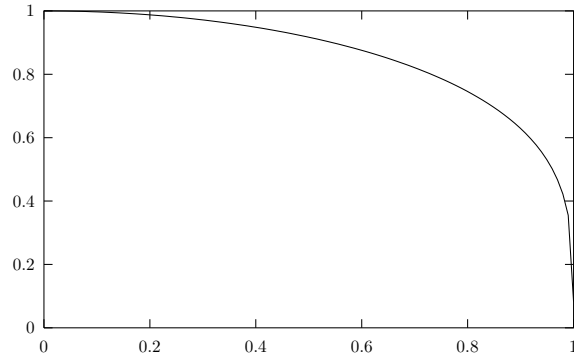
Fig. 3.4 Masking function $f(r) = \cos^{1/4}\left[(r - r_{ab})\pi/2w\right]$ with $w = 1$ and $r_{ab} = 0$.

the Kohn–Sham potential in `octopus` and then use it in optwo to re-create the eigenfunctions. Thereafter, the optimal control algorithm has been utilized with several parameters.

For the calculation of the Kohn–Sham potential in `octopus`, two pseudopotentials have been explored, the Hartwigsen–Goedecker–Hutter pseudopotential gave unsatisfactory results. With the Troullier–Martins potential, the calculated eigenvalues[9] (TABLE 3.2) match those of the all-electron calculation (TABLE 3.1). There is one peculiarity, though: The first eigenvalue of the pseudopotential calculation matches the second and not the third of the all-electron calculation, while consequently the third one is missing. A reason for this might be that the Troullier–Martins pseudopotential is not reliable in the inner regions. Furthermore the HOMO is non-degenerate in the pseudopotential and the HOMO−1 is doubly degenerate, while in the all-electron calculation this is reversed. Therefore we can indeed optimize the HOMO–LUMO transition since both have the same m quantum number.

Since laser induced transport is one possible application of the work, we looked at the charge transfer in lithium fluoride. We therefore calculated the electron density for each half of the cylinder, i. e.

$$n_i^l := 2\pi \int_{-\infty}^{0} \mathrm{d}z \int_{-\infty}^{\infty} \mathrm{d}r |\psi_i(r,z)|^2, \tag{3.48a}$$

$$n_i^r := 2\pi \int_{0}^{\infty} \mathrm{d}z \int_{-\infty}^{\infty} \mathrm{d}r |\psi_i(r,z)|^2, \tag{3.48b}$$

---

[9] Note that the eigenenergies of the Kohn–Sham system do not resemble those of the true system. Utilizing TDDFT one is able to calculate excitation energies. Since we do not propagate the Kohn–Sham potential, in optwo the excitation energies are the differences of the eigenenergies. For several systems this is a fair approximation.
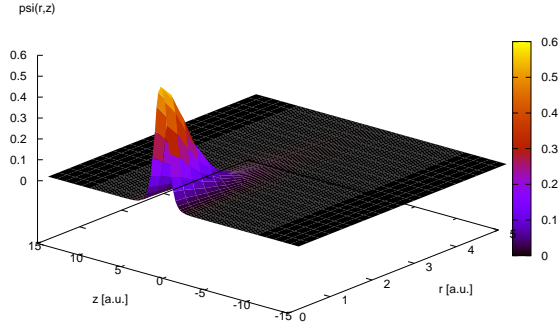
(*a*) HOMO−2 ($m = 0$), $E = -47.05$ eV
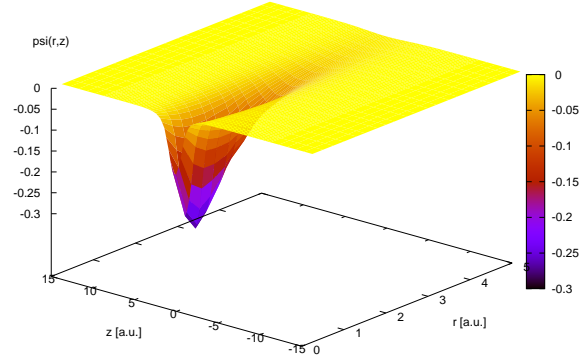
(*b*) HOMO−1 ($|m| = 1$), $E = -5.93$ eV
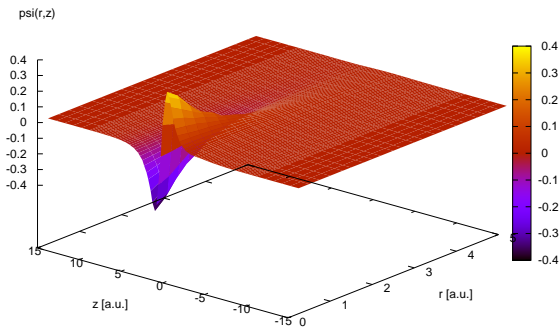
(*c*) HOMO ($m = 0$), $E = -5.67$ eV
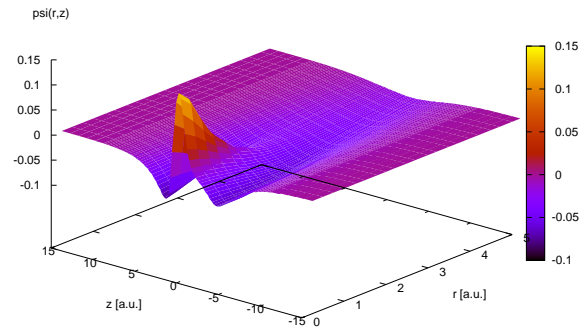
(*d*) LUMO ($m = 0$), $E = -1.77$ eV
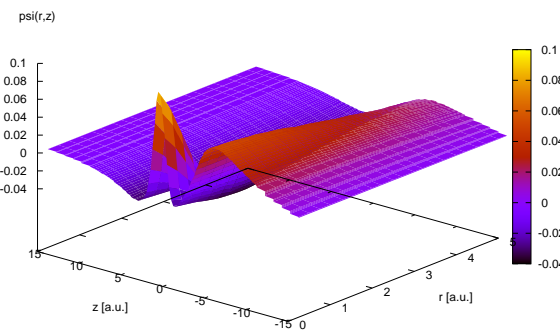
(*e*) LUMO−1 ($m = 0$), $E = -0.23$ eV
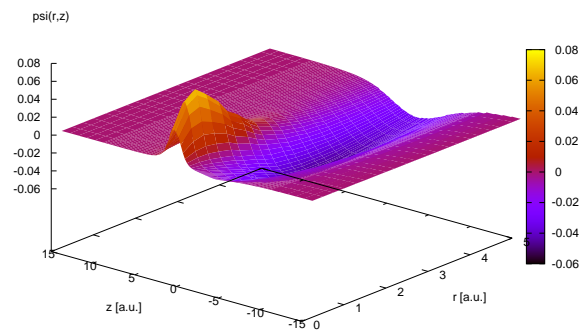
(*f*) LUMO−2 ($|m| = 1$), $E = -0.86$ eV

Fig. 3.5   Orbitals $\psi(r, z)$ as calculated with optwo using Troullier–Martins pseudopotentials. The eigenvalues shown are those of optwo. (*a*) shows an *s*-like wave function with finite value at $r = 0$, while in (*b*) the wave function is *p*-like and vanishes at $r = 0$. The plot has been cut off at $r = 5$ bohr to make the import features more visible.

		`octpus`	**optwo**			
Orbital		**Energy (Ha)**	**Energy (eV)**	**Energy (Ha)**	**Energy (eV)**	n_i^{F}
1	HOMO−2	−1.730969	−47.10206	−1.7291	−47.0510 $\quad m=0$	0.9933
2	HOMO−1	−0.216609	−5.89423			
3	HOMO−1	−0.216587	−5.89363	−0.2178	−5.9260 $\quad |m|=1$	0.9379
4	HOMO	−0.209679	−5.70566	−0.2085	−5.6733 $\quad m=0$	0.8156
5	LUMO	−0.064099	−1.74422	−0.0652	−1.7736 $\quad m=0$	0.7180
6	LUMO−1	0.010326	0.28098	0.0084	0.2279 $\quad m=0$	0.5711
7	LUMO−2	0.037067	1.00864			
8	LUMO−2	0.037067	1.00864	0.0317	0.8630 $\quad |m|=1$	0.8891
9	LUMO−3	0.064910	1.76629	0.0615	1.6730 $\quad m=0$	0.5697

Table 3.2 Eigenvalues obtained by `octopus` and optwo using a Troullier–Martins pseudopotential. Note that in `octopus` the HOMO−1 and in optwo the HOMO is degenerate. (The energy difference between HOMO and HOMO−1 is less than 1 eV.) m denotes the magnetic quantum number used for the optwo calculation and n_i^{F} how much density of that orbital is on the side of the cylinder were fluorine is.

where $n_i^{\mathrm{l}} + n_i^{\mathrm{r}} = n_i = \langle \psi_i | \psi_i \rangle = 1$. Instead of left/right we use the element name to denote either half of the cylinder: $n_i^{\mathrm{Li}} := n_i^{\mathrm{l}}$ and $n_i^{\mathrm{F}} := n_i^{\mathrm{r}}$. The results for the eigenstates are shown in TABLE 3.2. One sees that the charge is largely concentrated on the side of the fluorine.

Calculation settings: We used a cylindrical mesh with radius $r_{\mathrm{max}} = 8.25$ bohr = 4.37 Å, a cylinder length of two times $z_{\mathrm{max}} = 14.75$ bohr = 7.805 Å and a spacing of $\Delta = 0.25$ bohr = 0.13 Å. In optwo we have $N_r = 34$, $N_z = 119$ and $N = 4046$. The bondlength is $d(\mathrm{Li–F}) = 2.95$ bohr = 1.56 Å. We used a time-step of $\Delta t = 0.01$ a.u.$_{\mathrm{time}} = 2.4 \times 10^{-19}$ s and propagated for $T = 400$ a.u.$_{\mathrm{time}} = 9.7$ fs. The initial laser field was set to $\epsilon^{(0)} = 0.01\,\hbar/E_{\mathrm{h}} = 5.14$ GV m^{-1} or in terms of intensity $I_0 = 0.5\,c\varepsilon_0\,|\epsilon|^2 = 3.51 \times 10^{12}$ W cm^{-2}, integrated over time we obtain $E_{\mathrm{laser}} = 0.034$ J $\cdot$ cm^{-2}. A mask of the form $\cos^{1/4}$ has been used (for the width, see figure caption of each example). (Using a mask and propagating for fifty iterations takes about two days; one iteration denotes one forward and one backward propagation.)

First, we look at the results using a hard wall, i. e. no absorbing boundaries. Since especially the LUMO is only weakly bound and the laser has a high energy, one can expect a lot of ionization and, consequently, reflections which alter the spectrum of the optimized laser. The overlap and the laser energy are depicted in FIG. 3.6 for the penalty factors $\alpha = 0.1$, 1.0 and 2.0. With higher values of α, not only the energy of the laser is lower but the convergence is faster and the overlap approaches 100 per cent. This is a bit different from the harmonic oscillator where smaller α tend to give faster convergence (own tests, cf. also [57]). For $\alpha = 0.1$ the convergence is not
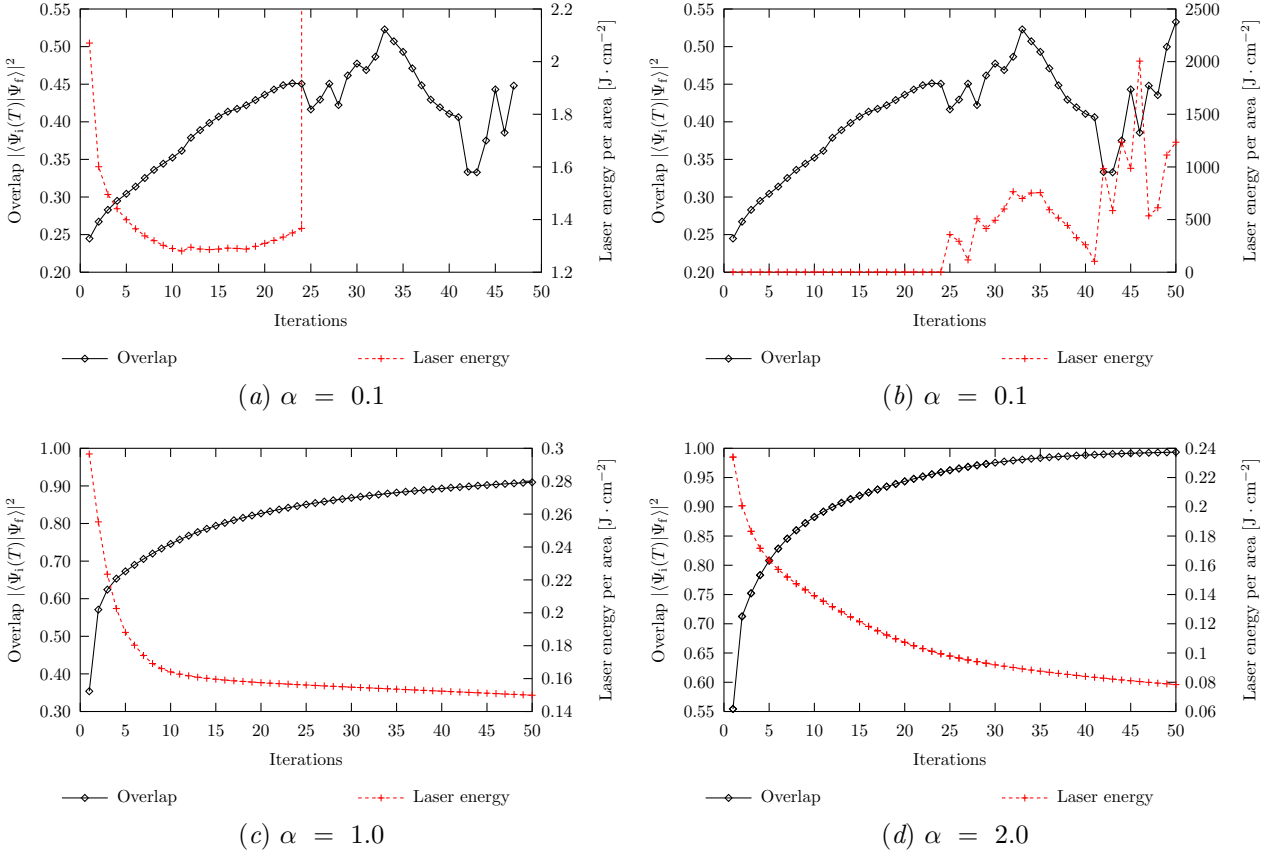
Fig. 3.6 Overlap and laser intensity for penalty factors $\alpha = 0.1$, 1.0 and 2.0 using a hard wall (no absorbing boundaries). (a, b) At the 25th iteration step using $\alpha = 0.1$ the laser energy shoots upwards. This is believed to be due to numerical inaccuracy in the time-propagation.

monotonic after the 25th iteration (FIG. 3.6a,b), indicating a numerical instability. Hence the results for $\alpha = 0.1$ are not reliable.

In order to remove the reflections, one can use absorbing boundaries. Typically they have a width of 10 % to 20 % of the box-size. Unfortunately, hardly any density was left using absorbing boundaries of 1.75 Å and a small α. In the worst case, the norm of $\psi_f(T)$ was only 10^{-7} (after a backward/forward cycle), while the norm of $\psi_i(T)$ (after forward propagation) was about fifty per cent. For different parameters, the loss could be reduced to 10 to 15 per cent for ψ_i and 45 per cent for ψ_f. Having the first case, the overlap and the energy zigzagged through the plot. In the second case, overlaps of over 70 % could be achived, while the overlap only oscillated smoothly. Interestingly, the laser energy had always the tendency to rise (or to slowly oscillate) rather than to fall. One possible attempt to improve the situation is to renormalize the laser field by the norm of the two wave functions,
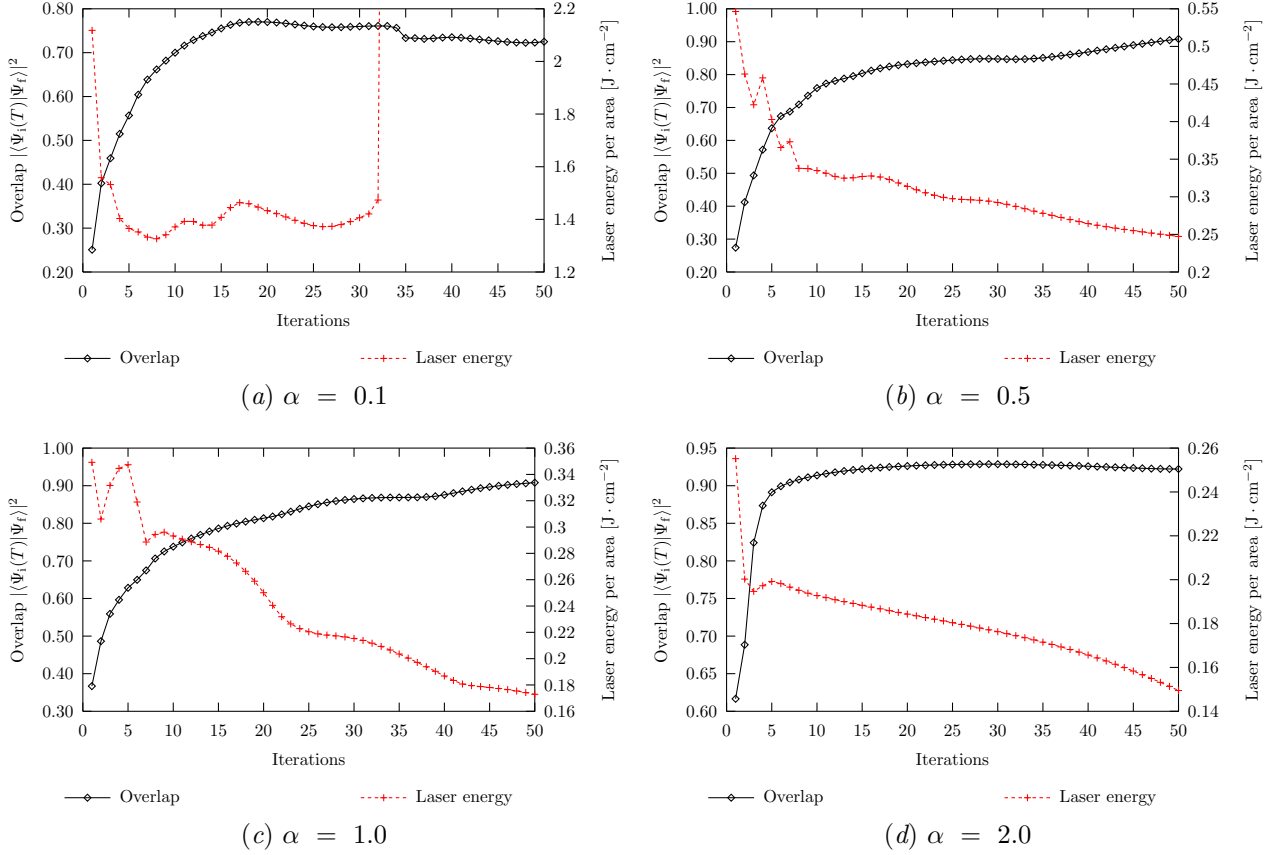
Fig. 3.7 Overlap and laser energy for penalty factors $\alpha = 0.1$, 0.5, 1.0 and 2.0 using absorbing boundaries with a width of 0.25 bohr $= 0.15$ Å. (*a*) At the 33rd step of the iteration, the surge up to $500\ \mathrm{W \cdot cm^{-2}}$ is presumably due to numerical inaccuracy in the time propagation. Norm of ψ_i and ψ_f at $t = T$: (*a*) 80–90 % for $\alpha = 0.1$, (*b*) 85–95 % for $\alpha = 0.5$, (*c*) 85–95 % for $\alpha = 0.5$ and (*d*) ≈ 95 % for $\alpha = 2.0$.

$$\epsilon = -\frac{1}{\alpha}\mathrm{Im}\frac{\langle\Psi_i|\Psi_f\rangle\langle\Psi_f|\mu|\Psi_f\rangle}{\langle\Psi_i|\Psi_i\rangle\langle\Psi_f|\Psi_f\rangle}. \tag{3.49}$$

This changes qualitatively the result since the laser energy now tends to fall as expected for the optimal control algorithm. Both, overlap and laser energy, are still slightly oscillating. In conclusion, the result using the renormalization is less promising: The overlap is slightly smaller then before and the laser energy is higher. The latter is probably the consequence of dividing the electric field by a number smaller than zero.

If we reduce the absorption to four to seven per cent, the algorithm starts to have the normal convergence behaviour. This can be seen in FIG. 3.7. In this example, we set the absorbing boundaries to the tiny value of 0.25 bohr $= 0.15$ Å, which means that only the edge points reduce the wave functions. We therefore can still expect

(a) Hard wall, $\alpha = 1.0$

(b) Absorbing boundaries, $\alpha = 1.0$

(c) Hard wall, $\alpha = 2.0$

(d) Absorbing boundaries, $\alpha = 2.0$
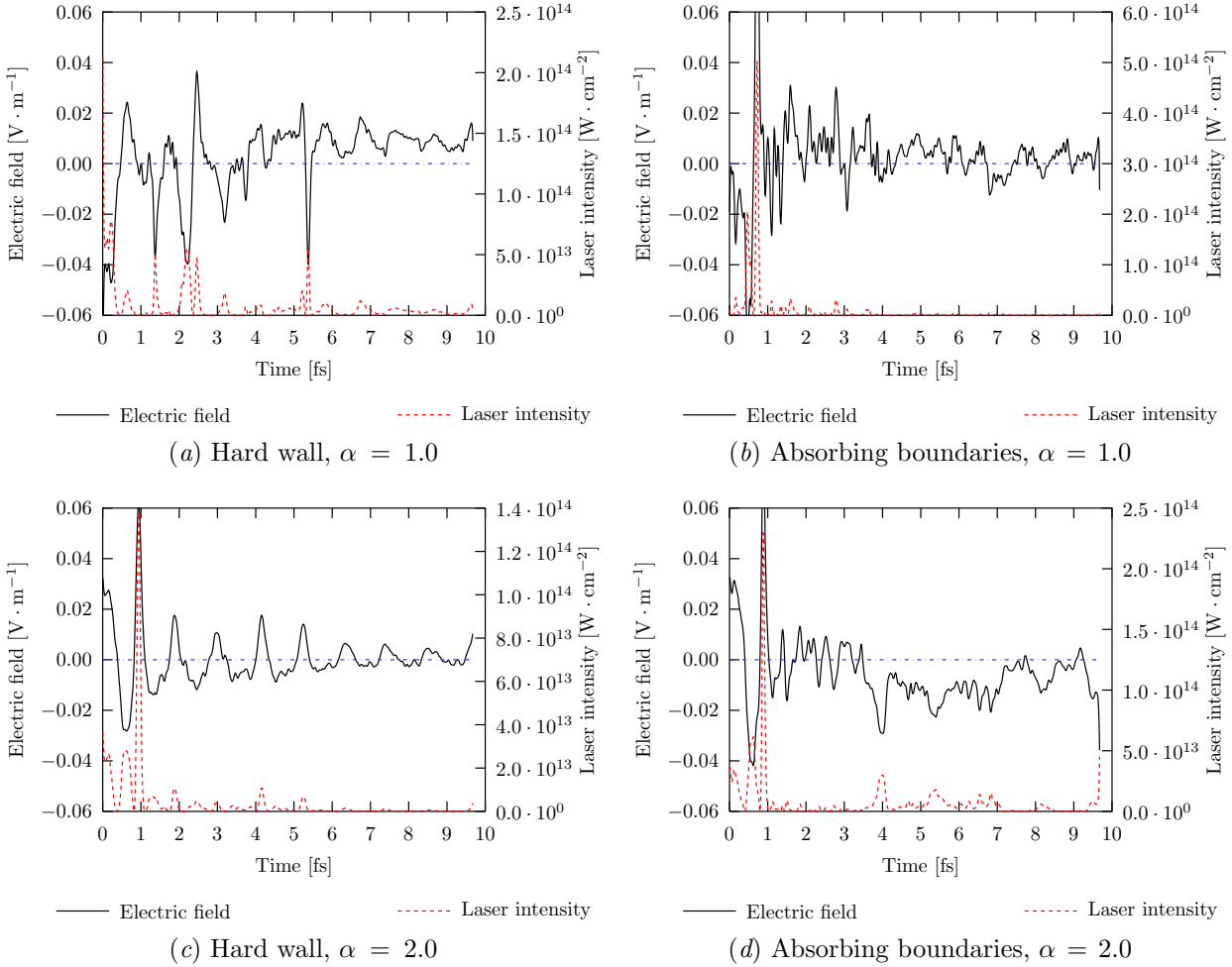
Fig. 3.8   Optimized laser for $\alpha = 2.0$ after 50 iteration steps. (a) Using hard walls. (b) Using 0.25 bohr = 0.15 Å absorbing boundaries.

that reflections occur. Note that we cannot easily increase the box by a substantial amount due to memory constraints.[10]

Comparing the resulting optimized laser pulses, one sees (FIG. 3.8) that for hard walls the laser is much smoother than for absorbing boundaries. Using $\alpha = 1$ the laser is rougher than for $\alpha = 2$. All lasers have a strong peak within the first femtosecond (for $\alpha = 1$ with hard walls this is less visible). Looking at the frequencies of the lasers FIG. 3.9, one sees a strong peak at the HOMO–LUMO transition energy of $\nu = 3.9\mathrm{eV}/h$, except for the $\alpha = 2$ case with absorbing boundaries which is a bit distorted. While $\alpha = 2$ with hard walls shows a direct and almost complete transition into the HOMO (FIG. 3.10c), the other examples in FIG. 3.10 show that

---

[10] Using 17.15 bohr instead of 14.75 bohr in the z direction caused `octopus` to die on memory allocation. The computer had 1 gibibyte of memory.

(a) Hard wall, $\alpha = 1.0$

(b) Absorbing boundaries, $\alpha = 1.0$

(c) Hard wall, $\alpha = 2.0$

(d) Absorbing boundaries, $\alpha = 2.0$
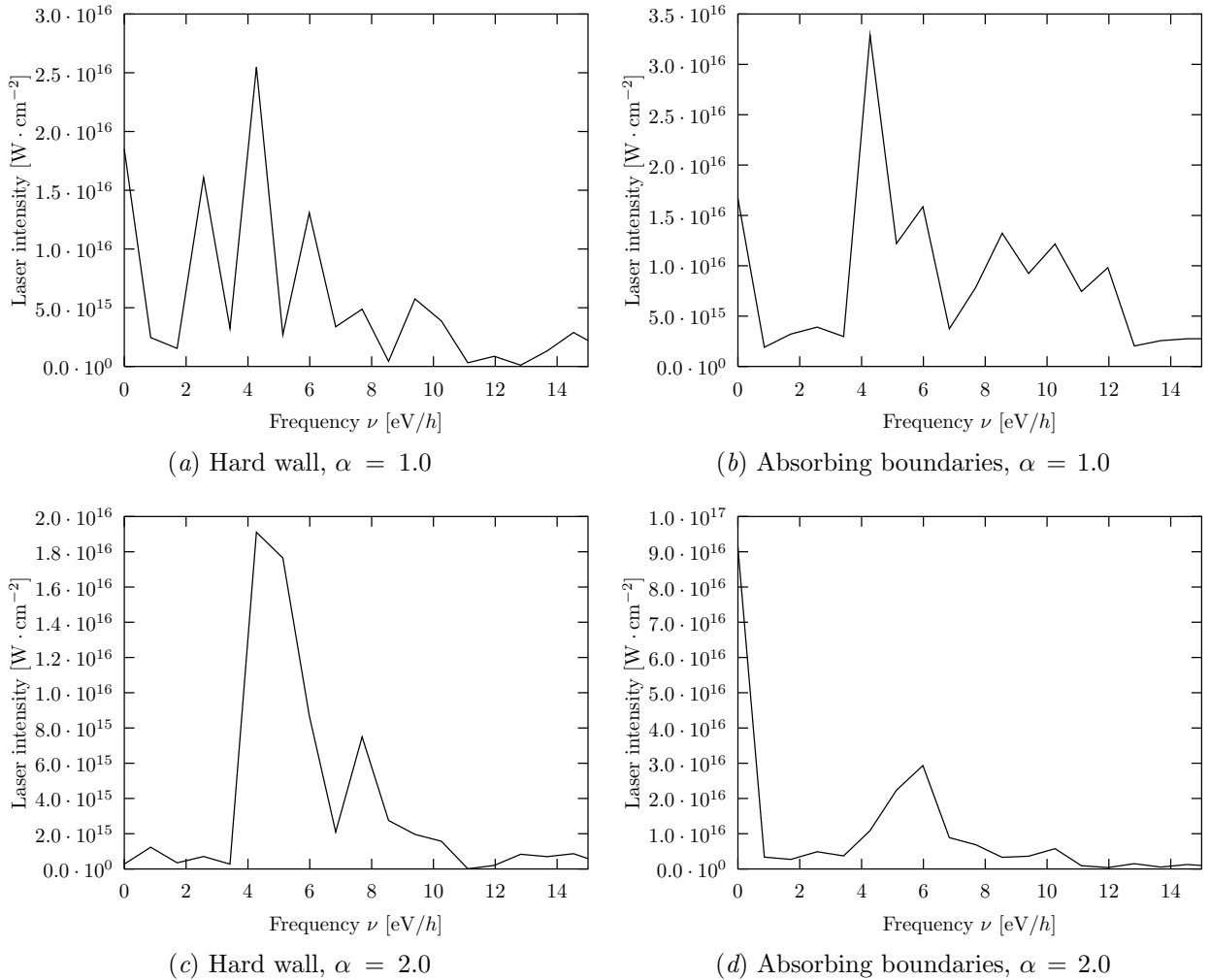
Fig. 3.9 Frequency spectra of the optimized laser for $\alpha = 1.0$ and 2.0 after 50 iteration steps. (a) Using hard walls. (b) Using 0.25 bohr = 0.15 Å absorbing boundaries. The transition energy of HOMO–LUMO is $\Delta E = 3.9$ eV.

intermediate states are populated (fortunately only those which are unoccupied). In case of absorbing boundaries, the sum of all occupation numbers is about ninety per cent. A comparison of the overlap and the laser energies in dependence on α can be found in TABLE 3.3.

One possible method to reduce the ionization and thus the absorption of electron density is to start with the forward propagation of Ψ_i instead of the backward propagation of Ψ_f. Since the same strong laser is applied for forward and backward propagation, the energetically higher state Ψ_f is much more prone to ionization. The reversed first iteration step might result in a better tailored laser and therefore a reduction of ionization already for the second step. Initial results show no significant improvement, though.

(a) Hard wall, $\alpha = 1.0$

(b) Absorbing boundaries, $\alpha = 1.0$

(c) Hard wall, $\alpha = 2.0$

(d) Absorbing boundaries, $\alpha = 2.0$
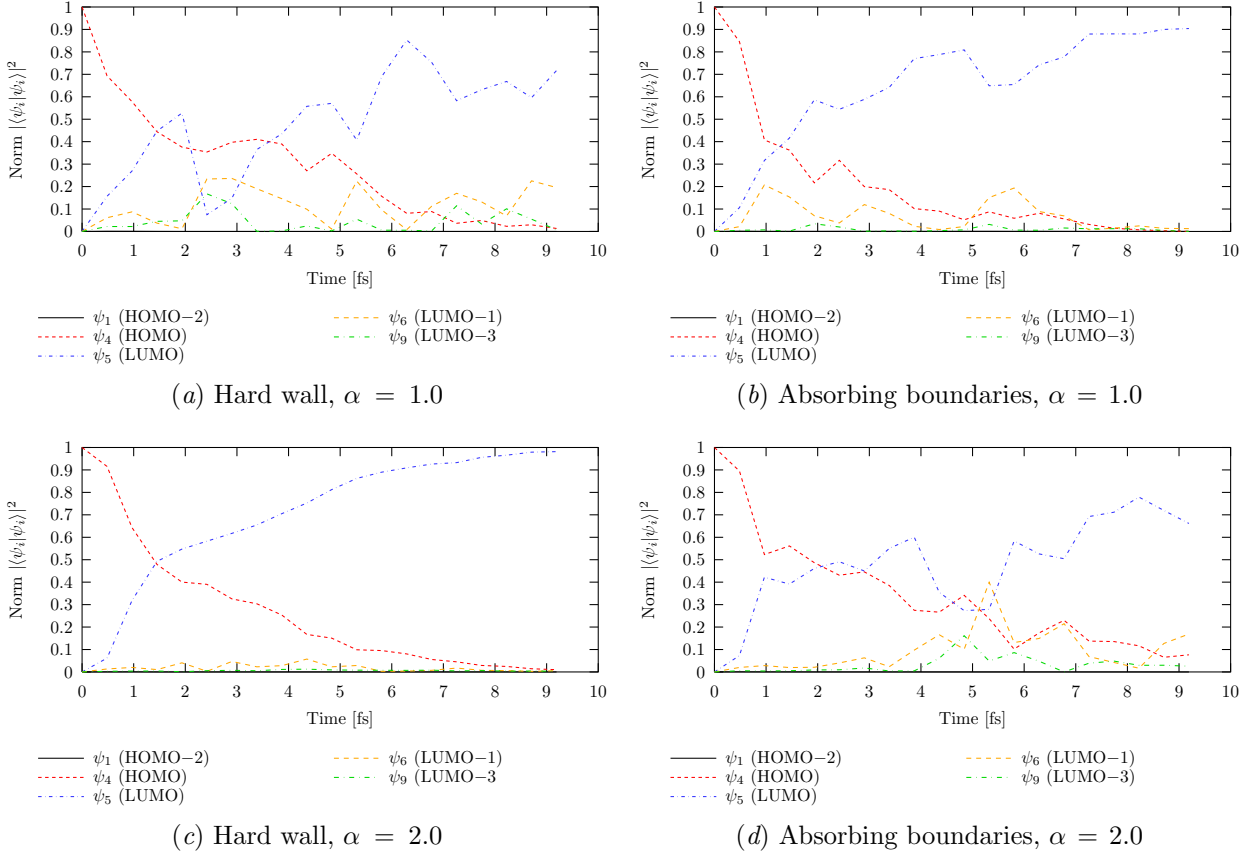
Fig. 3.10   Time evolution of the level population using the optimized laser with $\alpha = 1.0$ and 2.0 after 50 iteration steps. (a) Using hard walls. (b) Using 0.25 bohr = 0.15 Å absorbing boundaries. Orbitals with $m \neq 1$ omitted since they cannot be populated. Since we use absorbing boundaries in (a) and (d), the sum of those populations is less than one.

	Hard walls			**Absorbing boundaries**			
	E	$\int |\epsilon|^2 \mathrm{d}t$		E	$\int |\epsilon|^2 \mathrm{d}t$		Norm
α	$[J \cdot cm^{-2}]$	[a.u.]	Overlap	$[J \cdot cm^{-2}]$	[a.u.]	Overlap	$\langle \psi_\mathrm{i} | \psi_\mathrm{f} \rangle (T)$
0.1	1.309	987	0.925	1.433	1080	0.759	0.879
0.5				0.247	186.3	0.908	0.953
1.0	0.150	112.9	0.909	0.173	130.3	0.908	0.961
2.0	0.0784	59.1	0.993	0.149	112.6	0.922	0.975

Table 3.3   Overview about the overlap and the energy of the electric field for the different values of α with and without absorbing boundaries. The result is shown for the 50th iteration (for $\alpha = 0.1$, after 20 iteration due to the surge in the laser energy). The $\int |\epsilon|^2 \mathrm{d}t$ is measured in $\mathrm{a.u.}_\mathrm{el.field}^2 \mathrm{a.u.}_\mathrm{time} = \hbar^2 E_\mathrm{h}^2 / e^2 a_0^2$.

3.5   Conclusions

We have shown how a tailored laser can be used to optimize the population of a

51

final state. Using hard walls, one observes that larger penalty factors α ($\alpha \geq 2$) lead to higher overlaps, smaller laser intensities and faster convergence than lower ($\alpha \leq 1$). While this tendency is visible for $\alpha = 0.1$, the results for $\alpha = 0.1$ are not reliable due to numerical problems. For $\alpha = 2.0$ an almost complete transition could be achieved. Note that using a monochromatic laser of the transition energy also depopulates the final state and can therefore not produce such a high polulation. The resonance frequency is nevertheless a strong component in the spectrum.

In a real system, transitions between bound states and ionization are competing processes. For the calculation, we need to mimic ionization and prevent reflection by absorbing boundaries, otherwise the laser spectrum is not realistic. The optimal control algorithm tries to reduce the ionization in order to maximize the overlap. If a lot of ionization happens, a much smaller laser is tried in the next iteration. Nevertheless, convergency problems may occur when a large amount of density is absorbed.

In our calculations with slightly absorbing boundaries, the same behaviour with regard to α could be observed as with hard walls. Except for $\alpha = 0.1$ the convergence is monotonic (at least after the tenth iteration) and rather reliable. Using a too small box, density which, in the real world, would not be ionized is absorbed. This is presumably the case in the calculation. The only proper remedy of this numerical dilemma is to increase the size of the simulation box while simultaniously keeping a sizable absorption at the boundaries. This, however, turned out not to be possible on our present computer platforms due to memory constrains running `octopus`.

The artificial ionization can also be reduced by using a self-interaction-free functional such as the KLI (Krieger–Li–Iafrate) approximation. If the ionization is still to strong to prevent convergence, one could try to start with a hard wall and then turn on adiabatially the absorbing boundaries.

We did a spin-restricted calculation neglecting all but one orbital. The next logical step is to take the also other orbitals into account and, in addition, propagate the Kohn–Sham potential. In appendix B, we derive the expressions needed to calculate the new electric field, namely the overlap and the dipole moment using Slater wave functions. Of special interest is the spin-unrestricted calculation, where only one electron of an orbital is excited as it happens in nature. (If both are excited, autoionization occurs.) Such an excited state can only be written as the sum of two Slater determinants, requiring a generalization of the Kohn–Sham scheme.

I think it is a general rule that the originator of a new idea is not the most suitable person to develop it, because his fears of something going wrong are really too strong.

— Paul Dirac, 1902–84

4 Conclusion

In this thesis we have investigated the time evolution of chemical bonds and orbitals within the framework of time-dependent density-functional theory. Therefore we gave a short overview of the fundamentals of time-dependent DFT. We showed then how the electron localization function can be utilized to classify and visualize chemical bonds. Using its time-dependent generalization, which we derived, we were able to visualize the transition to anti-bonding orbitals and the stretching, breaking, and re-forming of chemical bonds. We further observed that ionization happens in localized blobs. While one can utilize the TDELF as a tool to obtain quantitative numbers, the main merit of the time-dependent electron localization function is that it creates meaningful pictures of complex reactions or structures in molecules and condensed matter which aid in understanding the physical phenomena behind.

We then looked at optimal control theory which can be used to prepare certain states in molecules or quantum dots. While this theory in its application to multi-electron systems is still in its infancy, it has advantages over genetic algorithm methods which are more prone to get locked in local minima or to experimental loop-back systems which require a huge apparatus. Until this method is fully competitive to those methods, some obstacles have to be overcome. One of the next steps will be the optimization of a multi-particle molecule in the time-dependent Kohn–Sham formalism, which can be excellently visualized using the ELF. Possible future applications encompass chemical reactions, photoisomerization, optical switches or quantum dots.

A TDELF auxiliary calculations

In order to save some space of lengthy but trivial calculations in the main part, the following auxiliary calculations have been moved into the appendix.

A.1 Simplification of C_σ

In this section, we use these conventions: The complex single-particle wave function and the single-particle density are written as

$$
\begin{aligned}
\phi_{i\sigma}(\boldsymbol{r},t) &:= \chi_{i\sigma}(\boldsymbol{r},t)\mathrm{e}^{\mathrm{i}\alpha_{i\sigma}(\boldsymbol{r},t)}, \\
n_{i\sigma}(\boldsymbol{r},t) &:= |\phi_{i\sigma}(\boldsymbol{r},t)|^2;
\end{aligned}
\tag{A.1}
$$

here χ and α are real functions. The wave functions can now be expressed in terms of the density and the phase α

$$
\phi_{i\sigma}(\boldsymbol{r},t) = n_{i\sigma}^{1/2}(\boldsymbol{r},t)\mathrm{e}^{\mathrm{i}\alpha(\boldsymbol{r},t)}.
\tag{A.2}
$$

The second term of C_σ in Eq. (2.34) of section 2.3.3 can be transformed to

$$
\begin{aligned}
&\frac{1}{2}\nabla_{r'}^2 \left.\frac{|n_\sigma(\boldsymbol{r}',\boldsymbol{r},t)|^2}{n_\sigma(\boldsymbol{r},t)}\right|_{r'=r} \\
&= \frac{1}{2}\frac{1}{n_\sigma(\boldsymbol{r},t)}\nabla_{r'}^2\big(n_\sigma^*(\boldsymbol{r}',\boldsymbol{r},t)n_\sigma(\boldsymbol{r}',\boldsymbol{r},t)\big)_{r'=r} \\
&= \frac{1}{2}\frac{\nabla_{r'}}{n_\sigma(\boldsymbol{r},t)}\Big(\big(\nabla_{r'}n_\sigma^*(\boldsymbol{r}',\boldsymbol{r},t)\big)n_\sigma(\boldsymbol{r}',\boldsymbol{r},t) + n_\sigma^*(\boldsymbol{r}',\boldsymbol{r},t)\big(\nabla_{r'}n_\sigma(\boldsymbol{r}',\boldsymbol{r},t)\big)\Big)_{r'=r} \\
&= \frac{1}{2}\frac{1}{n_\sigma(\boldsymbol{r},t)}\Big(\big(\nabla_{r'}^2 n_\sigma^*(\boldsymbol{r}',\boldsymbol{r},t)\big)n_\sigma(\boldsymbol{r}',\boldsymbol{r},t) + n_\sigma^*(\boldsymbol{r}',\boldsymbol{r},t)\big(\nabla_{r'}^2 n_\sigma(\boldsymbol{r}',\boldsymbol{r},t)\big) \\
&\quad + 2\big(\nabla_{r'}n_\sigma^*(\boldsymbol{r}',\boldsymbol{r},t)\big)\big(\nabla_{r'}n_\sigma(\boldsymbol{r}',\boldsymbol{r},t)\big)\Big)_{r'=r}.
\end{aligned}
\tag{A.3}
$$

We now calculate $\nabla_{r'}n$ and $\nabla_{r'}n^*$. In the following, n_σ is associated with the upper, n_σ^* with the lower sign of $\pm$ and $\mp$.

Appendix A: TDELF auxiliary calculations

$$\nabla_{r'} n_\sigma^{(*)}(\boldsymbol{r'}, \boldsymbol{r}, t) = \sum_{i=1}^{N_\sigma} \nabla_{\boldsymbol{r'}} \big(\phi_{i\sigma}^*(\boldsymbol{r'}, t)\phi_{i\sigma}(\boldsymbol{r}, t)\big)^{(*)}$$

$$= \sum_{i=1}^{N_\sigma} \nabla_{\boldsymbol{r'}} \big(n_{i\sigma}(\boldsymbol{r'}, t)\mathrm{e}^{\mp \mathrm{i}\alpha_{i\sigma}(\boldsymbol{r'}, t)}\big) n_{i\sigma}(\boldsymbol{r}, t)\mathrm{e}^{\pm \mathrm{i}\alpha_{i\sigma}(\boldsymbol{r'}, t)}$$

$$= \sum_{i=1}^{N_\sigma} n_{i\sigma}(\boldsymbol{r}, t)\mathrm{e}^{\pm \mathrm{i}\alpha_{i\sigma}(\boldsymbol{r'}, t)}$$

$$\times \left(\frac{1}{2}\frac{\nabla_{\boldsymbol{r'}} n_{i\sigma}(\boldsymbol{r}, t)}{n_{i\sigma}^{1/2}(\boldsymbol{r'}, t)}\mathrm{e}^{\mp \mathrm{i}\alpha_{i\sigma}(\boldsymbol{r'}, t)} \mp \mathrm{i}n_{i\sigma}^{1/2}(\boldsymbol{r'}, t)\mathrm{e}^{\mp \mathrm{i}\alpha_{i\sigma}(\boldsymbol{r'}, t)}\nabla_{\boldsymbol{r'}}\alpha_{i\sigma}(\boldsymbol{r'}, t) \right)$$

$$= \sum_{i=1}^{N_\sigma} \left(\frac{1}{2}\nabla n_{i\sigma}^{1/2}(\boldsymbol{r}, t) \mp \mathrm{i}n_{i\sigma}^{1/2}(\boldsymbol{r'}, t)\alpha_{i\sigma}(\boldsymbol{r'}, t) \right)$$

$$= \frac{1}{2}\nabla n_\sigma^{1/2}(\boldsymbol{r}, t) \mp \mathrm{i}N_\sigma \sum_{i=1}^{N_\sigma} n_{i\sigma}^{1/2}(\boldsymbol{r'}, t)\alpha_{i\sigma}(\boldsymbol{r'}, t) \tag{A.4}$$

Therefore, the second term of Eq. (A.3) is

$$\frac{2}{n_\sigma(\boldsymbol{r}, t)}\nabla_{\boldsymbol{r'}} n_\sigma^*(\boldsymbol{r'}, \boldsymbol{r}, t)\nabla_{\boldsymbol{r'}} n_\sigma(\boldsymbol{r'}, \boldsymbol{r}, t)$$

$$= \frac{2}{n_\sigma(\boldsymbol{r}, t)} \left(\frac{1}{4}(\nabla n_\sigma(\boldsymbol{r}, t))^2 + \left(\sum_{i=1}^{N_\sigma} \frac{n_{i\sigma}(\boldsymbol{r'}, t)\,\nabla\alpha_{i\sigma}(\boldsymbol{r'}, t)}{n_\sigma(\boldsymbol{r}, t)} \right)^2 \right)$$

$$= \frac{1}{2}\frac{(\nabla n_\sigma(\boldsymbol{r}, t))^2}{n_\sigma(\boldsymbol{r}, t)} + 2\frac{(j_\sigma(\boldsymbol{r}, t))^2}{n_\sigma(\boldsymbol{r}, t)}. \tag{A.5}$$

We now calculate the second derivative of n,

$$\nabla_{r'}^2 n_\sigma^{(*)}(\boldsymbol{r'}, \boldsymbol{r}, t)$$

$$= \sum_{i=1}^{N_\sigma} \nabla_{\boldsymbol{r'}} \left(\nabla_{\boldsymbol{r'}} \big(n_{i\sigma}^{1/2}(\boldsymbol{r'}, t)\mathrm{e}^{\mp \mathrm{i}\alpha(\boldsymbol{r'}, t)}\big) \right) n_{i\sigma}^{1/2}(\boldsymbol{r}, t)\mathrm{e}^{\pm \mathrm{i}\alpha(\boldsymbol{r}, t)}$$

$$= \sum_{i=1}^{N_\sigma} \nabla_{\boldsymbol{r'}} \left(\frac{1}{2}\frac{\nabla n_{i\sigma}(\boldsymbol{r}, t)}{n_{i\sigma}^{1/2}(\boldsymbol{r}, t)}\mathrm{e}^{\mp \mathrm{i}\alpha(\boldsymbol{r}, t)} \mp \mathrm{i}n_{i\sigma}^{1/2}(\boldsymbol{r}, t)\mathrm{e}^{\mp \mathrm{i}\alpha(\boldsymbol{r'}, t)}\nabla\alpha_{i\sigma}(\boldsymbol{r}, t) \right) n_{i\sigma}^{1/2}(\boldsymbol{r}, t)\mathrm{e}^{\pm \mathrm{i}\alpha(\boldsymbol{r}, t)}$$

$$= \sum_{i=1}^{N_\sigma} \left(n_{i\sigma}^{1/2}(\boldsymbol{r}, t)\mathrm{e}^{\pm \mathrm{i}\alpha(\boldsymbol{r}, t)} \right) \left(\frac{1}{2}\frac{\nabla^2 n_{i\sigma}(\boldsymbol{r}, t)}{n_{i\sigma}^{1/2}(\boldsymbol{r}, t)}\mathrm{e}^{\mp \mathrm{i}\alpha(\boldsymbol{r'}, t)} + \frac{1}{2}\left(-\frac{1}{2} \right)\frac{(\nabla n_{i\sigma}(\boldsymbol{r}, t))^2}{n_{i\sigma}^{1/2}(\boldsymbol{r}, t)}\mathrm{e}^{\mp \mathrm{i}\alpha(\boldsymbol{r'}, t)} \right.$$

$$\mp \mathrm{i}\frac{1}{2}\frac{\nabla n_{i\sigma}(\boldsymbol{r}, t)}{n_{i\sigma}^{1/2}(\boldsymbol{r}, t)}\mathrm{e}^{\mp \mathrm{i}\alpha(\boldsymbol{r'}, t)}\nabla\alpha_{i\sigma}(\boldsymbol{r}, t) \mp \mathrm{i}\frac{\nabla n_{i\sigma}(\boldsymbol{r}, t)}{n_{i\sigma}^{1/2}(\boldsymbol{r}, t)}\mathrm{e}^{\mp \mathrm{i}\alpha(\boldsymbol{r'}, t)}\nabla\alpha_{i\sigma}(\boldsymbol{r}, t)$$

$$\left. - n_{i\sigma}^{1/2}(\boldsymbol{r}, t)\mathrm{e}^{\mp \mathrm{i}\alpha(\boldsymbol{r'}, t)}\big(\nabla\alpha_{i\sigma}(\boldsymbol{r}, t)\big)^2 \mp \mathrm{i}n_{i\sigma}^{1/2}(\boldsymbol{r}, t)\mathrm{e}^{\mp \mathrm{i}\alpha(\boldsymbol{r'}, t)}\nabla^2\alpha_{i\sigma}(\boldsymbol{r}, t) \right)$$

$$
= \sum_{i=1}^{N_\sigma} \frac{1}{2} \nabla^2 n_{i\sigma}(\boldsymbol{r},t) - \frac{1}{4} \sum_{i=1}^{N_\sigma} \frac{\left(\nabla n_{i\sigma}(\boldsymbol{r},t)\right)^2}{n_{i\sigma}^{1/2}(\boldsymbol{r},t)} \mp \mathrm{i} \sum_{i=1}^{N_\sigma} \left(\nabla n_{i\sigma}(\boldsymbol{r},t) \nabla \alpha_{i\sigma}(\boldsymbol{r},t)\right)
$$

$$
- \sum_{i=1}^{N_\sigma} n_{i\sigma}(\boldsymbol{r},t) \left(\nabla \alpha_{i\sigma}(\boldsymbol{r},t)\right)^2 \tag{A.6}
$$

$$
= \frac{1}{2} \nabla^2 n_\sigma(\boldsymbol{r},t) - \frac{1}{4} \sum_{i=1}^{N_\sigma} \frac{\left(\nabla n_{i\sigma}(\boldsymbol{r},t)\right)^2}{n_{i\sigma}^{1/2}(\boldsymbol{r},t)} \mp \mathrm{i} \sum_{i=1}^{N_\sigma} \left(\nabla n_{i\sigma}(\boldsymbol{r},t) \nabla \alpha_{i\sigma}(\boldsymbol{r},t)\right) - \sum_{i=1}^{N_\sigma} \frac{\left(j_{i\sigma}(\boldsymbol{r},t)\right)^2}{n_{i\sigma}(\boldsymbol{r},t)}.
$$

For $\nabla_{r'}^2 n_\sigma^*(\boldsymbol{r}',\boldsymbol{r},t) + \nabla_{r'}^2 n_\sigma(\boldsymbol{r}',\boldsymbol{r},t)$ the imaginary parts cancel, the first term of Eq. (A.3) is thus

$$
\nabla_{r'}^2 n_\sigma^*(\boldsymbol{r}',\boldsymbol{r},t) + \nabla_{r'}^2 n_\sigma(\boldsymbol{r}',\boldsymbol{r},t) = \nabla^2 n_\sigma(\boldsymbol{r},t) - \frac{1}{2} \sum_{i=1}^{N_\sigma} \frac{\left(\nabla n_{i\sigma}(\boldsymbol{r},t)\right)^2}{n_{i\sigma}^{1/2}(\boldsymbol{r},t)} \tag{A.7}
$$

$$
- 2 \sum_{i=1}^{N_\sigma} \frac{\left(j_{i\sigma}(\boldsymbol{r},t)\right)^2}{n_{i\sigma}(\boldsymbol{r},t)}.
$$

A.2   Deriving the time-dependent ELF for a simplified, two-particle case

In this section, we derive the time-dependent electron localization function on a different route for a two-electron system with opposite spin. The kinetic energy of a non-interacting system

$$
T_{\mathrm{KS}} = \frac{\hbar^2}{2m} \sum_\sigma \int \mathrm{d}^3 r \sum_{i=1}^{N_\sigma} \phi_{i\sigma}^*(\boldsymbol{r},t) \left(-\nabla^2\right) \phi_{i\sigma}(\boldsymbol{r},t). \tag{A.8}
$$

Using Green's theorem (also known as Green's first identity) this can be changed to

$$
T_{\mathrm{KS}} = \frac{\hbar^2}{2m} \sum_\sigma \int \mathrm{d}^3 r \sum_{i=1}^{N_\sigma} \left(\nabla \phi_{i\sigma}^*(\boldsymbol{r},t)\right) \left(\nabla \phi_{i\sigma}(\boldsymbol{r},t)\right). \tag{A.9}
$$

We now define the kinetic energy density

$$
\tau_\sigma(\boldsymbol{r},t) = \sum_{i=1}^{N_\sigma} |\nabla \phi_{i\sigma}(\boldsymbol{r},t)|^2. \tag{A.10}
$$

Since we assume a two-electron system with opposite spin, $N_\sigma = 1$. Using the following definition for the wave function and density

$$
n_\sigma(\boldsymbol{r},t) = |\phi_\sigma(\boldsymbol{r},t)|^2, \quad \phi_\sigma(\boldsymbol{r},t) = \chi_\sigma(\boldsymbol{r}) \mathrm{e}^{\mathrm{i}\alpha_\sigma(\boldsymbol{r},t)}, \tag{A.11}
$$

where α and χ are real functions, the wave function can be written as

$$\phi_\sigma(\boldsymbol{r},t) = n_\sigma^{1/2}(\boldsymbol{r},t)\mathrm{e}^{\mathrm{i}\alpha_\sigma(\boldsymbol{r},t)}. \tag{A.12}$$

Now, we insert ϕ and n in the definition of C_σ Eq. (2.22) of section 2.3.1. Using

$$|\nabla\phi_\sigma(\boldsymbol{r},t)|^2 = \mathrm{e}^{-\mathrm{i}\alpha_\sigma(\boldsymbol{r},t)}\left(\frac{1}{2}\frac{\nabla n_\sigma(\boldsymbol{r},t)}{n_\sigma^{1/2}(\boldsymbol{r},t)}\right)\mathrm{e}^{\mathrm{i}\alpha_\sigma(\boldsymbol{r},t)}\left(\frac{1}{2}\frac{\nabla n_\sigma(\boldsymbol{r},t)}{n_\sigma^{1/2}(\boldsymbol{r},t)}\right)$$
$$= \frac{1}{4}\frac{\left(\nabla n_\sigma(\boldsymbol{r},t)\right)^2}{n_\sigma^{1/2}(\boldsymbol{r},t)} + n_\sigma(\boldsymbol{r},t)\left(\alpha_\sigma(\boldsymbol{r},t)\right)^2 = \frac{1}{4}\frac{\left(\nabla n_\sigma(\boldsymbol{r},t)\right)^2}{n_\sigma(\boldsymbol{r},t)} + \frac{j_\sigma^2(\boldsymbol{r},t)}{n_\sigma(\boldsymbol{r},t)}, \tag{A.13}$$

where $j_\sigma^2 = (\nabla\alpha)^2 n^2$ denotes the current density, one obtains

$$C_\sigma(\boldsymbol{r},t) = |\nabla\phi_\sigma(\boldsymbol{r},t)|^2 - \frac{1}{4}\frac{\left(\nabla n_\sigma(\boldsymbol{r},t)\right)^2}{n_\sigma(\boldsymbol{r},t)} - \frac{j_\sigma^2(\boldsymbol{r},t)}{n_\sigma(\boldsymbol{r},t)}. \tag{A.14}$$

This is conform with the result from the long derivation Eq. (2.37). Assuming real wave functions ($\alpha \equiv 0$ and thus $j \equiv 0$) we get again the result obtained by Becke and Edgecombe Eq. (2.6).

B Optimal control for many-particle systems

While the optimal control algorithm (Eq. (3.7)) allows the optimazation of many-particle systems, so far we have only looked at one-particle systems. The essential difference to the single-particle case is the way the overlap and the laser field are calculated. We derive now the necessary expressions to explicitly calculate the overlap, assuming that the wave functions are Slater determinants.

B.1 Calculation of the overlap $\langle \tilde{\Psi}|\Psi\rangle$

As in appendix C is shown, the overlap of two wave functions of this form

$$\Psi(x_1,\ldots,x_N) = \frac{1}{\sqrt{N!}} \begin{vmatrix} \psi_1(x_1) & \cdots & \psi_1(x_N) \\ \vdots & \ddots & \vdots \\ \psi_N(x_1) & \cdots & \psi_N(x_N) \end{vmatrix}, \quad x_i = (\boldsymbol{r}, \sigma_i), \tag{B.1}$$

is given by

$$\langle \tilde{\Psi}|\Psi\rangle = \det_{ij} \langle \tilde{\Psi}_i|\Psi_j\rangle = \sum_{\pi} \operatorname{sgn} \pi \prod_{i=1}^{N} \langle \tilde{\Psi}_i|\Psi_{\pi_i}\rangle. \tag{B.2}$$

The single-particle wave functions can be split into a spatial part $\phi_i^{\pm}$ and into a spin part $\chi_{\pm}$, i.e.

$$\begin{aligned} \psi_i^+(x) &= \phi_i^+(r)\chi_+(\sigma), \quad i = 1,\ldots,N_+, \\ \psi_i^-(x) &= \phi_i^-(r)\chi_-(\sigma), \quad i = 1,\ldots,N_-, \quad N = N_- + N_+. \end{aligned} \tag{B.3}$$

We can now define

$$\psi_i(x) := \begin{cases} \psi_i^+(x), & 1 \le i \le N_+ \\ \psi_{i-N_+}^-(x), & N_+ < i \le N \end{cases} \tag{B.4}$$

and obtain

$$\psi(x_1,\ldots,x_N) = \frac{1}{\sqrt{N!}} \begin{vmatrix} \psi_1(x_1) & \cdots & \psi_1(x_N) \\ \vdots & \ddots & \vdots \\ \psi_N(x_1) & \cdots & \psi_N(x_N) \end{vmatrix}$$

$$= \frac{1}{\sqrt{N!}} \begin{vmatrix} \psi_1^+(\boldsymbol{r}_1)\chi_+(\sigma_1) & \cdots & \psi_1^+(\boldsymbol{r}_N)\chi_+(\sigma_N) \\ \vdots & \ddots & \vdots \\ \psi_{N_+}^+(\boldsymbol{r}_1)\chi_+(\sigma_1) & \cdots & \psi_{N_+}^+(\boldsymbol{r}_N)\chi_+(\sigma_N) \\ \psi_1^-(\boldsymbol{r}_1)\chi_-(\sigma_1) & \cdots & \psi_1^-(\boldsymbol{r}_N)\chi_-(\sigma_N) \\ \vdots & \ddots & \vdots \\ \psi_{N_-}^-(\boldsymbol{r}_1)\chi_-(\sigma_1) & \cdots & \psi_{N_-}^-(\boldsymbol{r}_N)\chi_-(\sigma_N) \end{vmatrix} . \tag{B.5}$$

Using Eq. (B.5) the overlap can be calculated

$$\langle\tilde{\Psi}|\Psi\rangle = \det{}_{ij}\,\langle\tilde{\psi}_i|\psi_j\rangle$$

$$= \begin{vmatrix} \langle\tilde{\psi}_1^+|\psi_1^+\rangle & \cdots & \langle\tilde{\psi}_1^+|\psi_{N_+}\rangle & \langle\tilde{\psi}_1^+|\psi_1^-\rangle & \cdots & \langle\tilde{\psi}_1^+|\psi_{N_-}^-\rangle \\ \vdots & \ddots & \vdots & \vdots & \ddots & \vdots \\ \langle\tilde{\psi}_{N_+}^+|\psi_1^+\rangle & \cdots & \langle\tilde{\psi}_{N_+}^+|\psi_{N_+}\rangle & \langle\tilde{\psi}_{N_+}^+|\psi_1^-\rangle & \cdots & \langle\tilde{\psi}_{N_+}^+|\psi_{N_-}^-\rangle \\ \langle\tilde{\psi}_1^-|\psi_1^+\rangle & \cdots & \langle\tilde{\psi}_1^-|\psi_{N_+}\rangle & \langle\tilde{\psi}_1^-|\psi_1^-\rangle & \cdots & \langle\tilde{\psi}_1^-|\psi_{N_-}^-\rangle \\ \vdots & \ddots & \vdots & \vdots & \ddots & \vdots \\ \langle\tilde{\psi}_{N_-}^-|\psi_1^+\rangle & \cdots & \langle\tilde{\psi}_{N_-}^-|\psi_{N_+}\rangle & \langle\tilde{\psi}_{N_-}^-|\psi_1^-\rangle & \cdots & \langle\tilde{\psi}_{N_-}^-|\psi_{N_-}^-\rangle \end{vmatrix}$$

$$=: \begin{vmatrix} \Phi_{++} & \Phi_{+-} \\ \Phi_{-+} & \Phi_{--} \end{vmatrix} , \tag{B.6}$$

where $\langle\tilde{\psi}_i^{\tilde{\sigma}}|\psi_j^\sigma\rangle = \langle\phi_i^{\tilde{\sigma}}|\phi_j^\sigma\rangle\langle\tilde{\chi}_{\tilde{\sigma}}|\chi_\sigma\rangle$. Assuming no spin flip, i.e. $\tilde{\chi}_\pm \equiv \chi_\pm$, we can make use of the orthonormality of χ and obtain thus the following sparse matrix

$$\langle\tilde{\Psi}|\Psi\rangle = \begin{vmatrix} \Phi_{++} & 0 \\ 0 & \Phi_{--} \end{vmatrix} = \det\langle\varphi_i^+|\varphi_j^+\rangle \, \det\langle\varphi_i^-|\varphi_j^-\rangle. \tag{B.7}$$

And if further $N_+ = N_- = N/2$ and $\phi_i^+ \equiv \phi_i^-$, $i = 1,\ldots,N/2$ (e.g. in spin-restricted calculations), this simplifies to

$$\langle\tilde{\psi}|\psi\rangle = \left(\det\langle\varphi_i^+|\varphi_j^+\rangle\right)^2. \tag{B.8}$$

B.2 Calculation of the dipole moment $\langle\tilde{\psi}|\hat{\boldsymbol{X}}|\psi\rangle$

The electric dipole moment is $\boldsymbol{p} = \langle\Psi|\left(\sum_i q\hat{\boldsymbol{r}}_i\right)|\Psi\rangle$ and since $q = e \overset{\text{a.u.}}{=} 1$ we have to calculate

$$\sum_{i=1}^{N} \langle \tilde{\Psi} | \hat{\boldsymbol{r}}_i | \Psi \rangle, \quad \Psi = \tilde{\Psi}. \tag{B.9}$$

The used algorithm for optimal control requires that $\psi = \tilde{\psi}$ cannot be assumed; strictly speaking Eq. (B.9) is then no longer an electric dipole moment, but we will use the term nevertheless. The wave function shall have the form Eq. (B.1). We define now

$$\hat{\boldsymbol{X}} := \sum_{i=1}^{N} \hat{x}_i, \quad \hat{x}_i := \hat{r}_i. \tag{B.10}$$

Plugging the Slater determinant into Eq. (B.9), the explicitly written equation is

$$\langle \tilde{\psi} | \hat{\boldsymbol{X}} | \psi \rangle = \frac{1}{N!} \int \mathrm{d}^3(\boldsymbol{r}_1, \ldots, \boldsymbol{r}_N) \sum_{\{\sigma_l\}} \sum_{i=1}^{N}$$
$$\times \begin{vmatrix} \tilde{\psi}_1^*(x_1) & \cdots & \tilde{\psi}_1^*(x_N) \\ \vdots & \ddots & \vdots \\ \tilde{\psi}_N^*(x_1) & \cdots & \tilde{\psi}_N^*(x_N) \end{vmatrix} \hat{x}_i \begin{vmatrix} \psi_1(x_1) & \cdots & \psi_1(x_N) \\ \vdots & \ddots & \vdots \\ \psi_N(x_1) & \cdots & \psi_N(x_N) \end{vmatrix}. \tag{B.11}$$

This can be simplified since

$$\int \mathrm{d}^3(\boldsymbol{r}_1, \ldots, \boldsymbol{r}_N) \sum_{\{\sigma_l\}} \begin{vmatrix} \tilde{\psi}_1^*(x_1) & \tilde{\psi}_2^*(x_1) & \cdots \\ \tilde{\psi}_1^*(x_2) & \tilde{\psi}_2^*(x_2) & \cdots \\ \vdots & \vdots & \ddots \end{vmatrix} \hat{x}_2 \begin{vmatrix} \psi_1(x_1) & \psi_2(x_1) & \cdots \\ \psi_1(x_2) & \psi_2(x_2) & \cdots \\ \vdots & \vdots & \ddots \end{vmatrix}$$
$$= \int \mathrm{d}^3(\boldsymbol{r}_1, \ldots, \boldsymbol{r}_N) \sum_{\{\sigma_l\}} \begin{vmatrix} \tilde{\psi}_1^*(x_2) & \tilde{\psi}_2^*(x_2) & \cdots \\ \tilde{\psi}_1^*(x_1) & \tilde{\psi}_2^*(x_1) & \cdots \\ \vdots & \vdots & \ddots \end{vmatrix} \hat{x}_2 \begin{vmatrix} \psi_1(x_2) & \psi_2(x_2) & \cdots \\ \psi_1(x_1) & \psi_2(x_1) & \cdots \\ \vdots & \vdots & \ddots \end{vmatrix}$$
$$= \int \mathrm{d}^3(\boldsymbol{r}_1, \ldots, \boldsymbol{r}_N) \sum_{\{\sigma_l\}} \begin{vmatrix} \tilde{\psi}_1^*(x_1) & \tilde{\psi}_2^*(x_1) & \cdots \\ \tilde{\psi}_1^*(x_2) & \tilde{\psi}_2^*(x_2) & \cdots \\ \vdots & \vdots & \ddots \end{vmatrix} \hat{x}_1 \begin{vmatrix} \psi_1(x_1) & \psi_2(x_1) & \cdots \\ \psi_1(x_2) & \psi_2(x_2) & \cdots \\ \vdots & \vdots & \ddots \end{vmatrix}. \tag{B.12}$$

In the last step we have renamed $x_2 \to x_1$ and $x_1 \to x_2$. We now arbitrarily choose $\hat{x}_i := \hat{x}_1$, $i = 2, \ldots, N$, and obtain

$$\langle \tilde{\psi} | \hat{\boldsymbol{X}} | \psi \rangle = \frac{N}{N!} \int \mathrm{d}^3 (\boldsymbol{r}_1, \ldots, \boldsymbol{r}_N) \sum_{\{\sigma_l\}}$$

$$\times \begin{vmatrix} \tilde{\psi}_1^*(x_1) & \cdots & \tilde{\psi}_1^*(x_N) \\ \vdots & \ddots & \vdots \\ \tilde{\psi}_N^*(x_1) & \cdots & \tilde{\psi}_N^*(x_N) \end{vmatrix} \hat{x}_1 \begin{vmatrix} \psi_1(x_1) & \cdots & \psi_1(x_N) \\ \vdots & \ddots & \vdots \\ \psi_N(x_1) & \cdots & \psi_N(x_N) \end{vmatrix}, \quad \text{(B.13)}$$

which we now expand with respect to the first row ($= x_1$). M_{ij} denotes the minor, i.e. the determinant where row i and column j have been cancelled.

$$\langle \tilde{\psi} | \hat{\boldsymbol{X}} | \psi \rangle = \frac{N}{N!} \int \mathrm{d}^3 (\boldsymbol{r}_1, \ldots, r_N) \sum_{\{\sigma_l\}} \left(\sum_{i=1}^N (-1)^{1+i} \tilde{\psi}_i^*(x_1) \tilde{M}_{1i}^*(x_2, \ldots, x_N) \right) \hat{x}_1$$

$$\times \left(\sum_{j=1}^N (-1)^{1+j} \psi_j(x_1) M_{1j}(x_2, \ldots, x_N) \right)$$

$$= \frac{1}{(N-1)!} \int \mathrm{d}^3 \{ \boldsymbol{r}_l \} \sum_{\{\sigma_l\}} \left(\sum_{i,j=1}^N (-1)^{i+j} \right.$$

$$\times \langle \tilde{\psi}_i(x_1) | \hat{x}_1 | \psi_j(x_1) \rangle \tilde{M}_{1i}^*(x_2, \ldots, x_N) M_{1j}(x_2, \ldots, x_N) \Big)$$

$$= \sum_{ij}^N (-1)^{i+j} \langle \psi_i(x_1) | \hat{x}_1 | \psi_j(x_1) \rangle \frac{1}{(N-1)!} \int \mathrm{d}^3 (\boldsymbol{r}_2, \ldots, \boldsymbol{r}_N)$$

$$\times \sum_{(\sigma_2, \ldots, \sigma_N)} \tilde{M}_{1i}^*(x_2, \ldots, x_N) M_{1j}(x_2, \ldots, x_N). \quad \text{(B.14)}$$

Knowing that

$$\langle \tilde{\psi} | \psi \rangle = \frac{1}{N!} \int \mathrm{d}^3 (\boldsymbol{r}_1 \ldots, \boldsymbol{r}_N) \sum_{(\sigma_1, \ldots, \sigma_N)} \det{}_{ij} \tilde{\psi}_i^*(x_j) \cdot \det{}_{ij} \psi_i(x_j) = \det{}_{ij} \langle \tilde{\psi}_i | \psi_j \rangle, \tag{B.15}$$

we can write the integral in Eq. (B.14) as

$$\frac{1}{(N-1)!} \int \mathrm{d}^3 (\boldsymbol{r}_2, \ldots, \boldsymbol{r}_N) \sum_{(\sigma_2, \ldots, \sigma_N)} \tilde{M}_{1i}^*(x_2, \ldots, x_N) M_{1j}(x_2, \ldots, x_N)$$

$$= \big(\det{}_{lm} \langle \tilde{\psi}_l | \psi_m \rangle \big)_{ij}$$

$$:= \det{}_{l'm'} \langle \tilde{\psi}_{l'} | \psi_{m'} \rangle, \quad l', m' = 1, \ldots, N, \text{ and } l' \neq i, \ m' \neq j. \tag{B.16}$$

Here $\left(\det_{lm} \langle \tilde{\psi}_l | \psi_m \rangle \right)_{ij}$ denotes the determinant in which row i and column j are deleted; therefore is $M_{1j}(x_2, \ldots, x_N) = \left(\det_{lm} \psi_l(x_m) \right)_{1j}$. We finally obtain

$$\langle \tilde{\psi} | \hat{X} | \psi \rangle = \sum_{i,j=1}^{N} (-1)^{i+j} \langle \tilde{\psi}_i | \hat{x}_1 | \psi_j \rangle \left(\det_{lm} \langle \tilde{\psi}_l | \psi_m \rangle \right)_{ij}. \tag{B.17}$$

We define analogously to the overlap calculation

$$\left(\det_{lm} \langle \tilde{\psi}_l | \psi_m \rangle \right)_{ij} =: \left(\begin{vmatrix} \Phi'_{++} & \Phi'_{+-} \\ \Phi'_{-+} & \Phi'_{--} \end{vmatrix} \right)_{ij}; \tag{B.18}$$

this can be simplified for $\tilde{\chi}_i \equiv \chi_i$, where $\psi_i(\boldsymbol{r}, \sigma) = \varphi_i(\boldsymbol{r}) \chi_i(\sigma)$. Assuming again that no spin flip occurs, i.e. $\Phi'_{-+} = \Phi'_{+-} = 0$, the reduced determinant has these properties

$$\left(\det_{lm} \langle \tilde{\psi}_l | \psi_m \rangle \right)_{ij} = \left(\begin{vmatrix} \Phi'_{++} & 0 \\ 0 & \Phi'_{--} \end{vmatrix} \right)_{ij} = \begin{cases} \det \Phi_{++} \, M_{ij}^{++}, & i, j \in \{1, \ldots, N_+\} \\ \det \Phi_{--} \, M_{ij}^{--}, & i, j \in \{1, \ldots, N_+\} \\ 0, & \text{otherwise} \end{cases} . \tag{B.19}$$

Hence

$$\langle \tilde{\psi} | \hat{\boldsymbol{X}} | \psi \rangle = \sum_{i,j=1}^{N_+} (-1)^{i+j} \langle \tilde{\varphi}_i | \hat{\boldsymbol{x_1}} | \varphi_j \rangle M_{ij}^{++} \det \Phi_{--}$$

$$+ \sum_{i,j=1}^{N_-} (-1)^{i+j} \langle \tilde{\varphi}_i | \hat{\boldsymbol{x_1}} | \varphi_j \rangle M_{ij}^{--} \det \Phi_{++}. \tag{B.20}$$

In the spin-restricted case, we have $N_- = N_+ = N/2$ and $\varphi_i \equiv \varphi_i^+$ and consequently $\Phi_{++} = \Phi_{--}$, thus

$$\left(\det_{lm} \langle \tilde{\psi}_l | \psi_m \rangle \right)_{ij} = \det \Phi \left(\det \Phi \right)_{ij}. \tag{B.21}$$

The spin-restricted electric dipole moment is thus given by

$$\langle \tilde{\psi} | \hat{\boldsymbol{X}} | \psi \rangle = 2 \sum_{i,j=1}^{N/2} (-1)^{i+j} \langle \tilde{\varphi}_i | \hat{x}_1 | \varphi_j \rangle \det \Phi \left(\det \Phi \right)_{ij} \tag{B.22}$$

$$= 2 \left(\sum_{i,j=1}^{N/2} \langle \tilde{\psi}_i | \hat{x}_1 | \psi_j \rangle \det_{l,m} \langle \tilde{\psi}_l | \psi_m \rangle \right) \det_{l,m} \langle \tilde{\psi}_l | \psi_m \rangle, \quad l, m = 1, \ldots, N/2.$$

Appendix B: Optimal control for many-particle systems

C Proof for the overlap of two Slater wave functions

We now show that for two wave functions Ψ and $\tilde{\Psi}$ which can be written as Slater determinants of single-particle wave functions ψ_i and $\tilde{\psi}_i$,

$$\Psi(x_1,\ldots,x_N) = \frac{1}{\sqrt{N!}} \begin{vmatrix} \psi_1(x_1) & \cdots & \psi_1(x_N) \\ \vdots & \ddots & \vdots \\ \psi_N(x_1) & \cdots & \psi_N(x_N) \end{vmatrix} =: \frac{1}{\sqrt{N!}} \det_{ij} \psi_i(x_j), \qquad (C.1)$$

this identity holds true

$$\langle \tilde{\Psi} | \Psi \rangle = \det_{ij} \langle \tilde{\psi}_i | \psi_j \rangle. \qquad (C.2)$$

In the following we calculate spin-restricted, i.e. $x = \boldsymbol{r}$, which saves us the sum over the spins; the full, spin-unrestricted calculation is analogous.

$$\begin{aligned}
\langle \tilde{\Psi} | \Psi \rangle &= \frac{1}{N!} \int \mathrm{d}^3\{x_l\}\, \tilde{\psi}^*(x_1,\ldots,x_N)\psi(x_1,\ldots,x_N) \\
&= \frac{1}{N!} \int \mathrm{d}^3\{x_l\} \begin{vmatrix} \tilde{\psi}_1^*(x_1) & \cdots & \tilde{\psi}_1^*(x_N) \\ \vdots & \ddots & \vdots \\ \tilde{\psi}_N^*(x_1) & \cdots & \tilde{\psi}_N^*(x_N) \end{vmatrix} \begin{vmatrix} \psi_1(x_1) & \cdots & \psi_1(x_N) \\ \vdots & \ddots & \vdots \\ \psi_N(x_1) & \cdots & \psi_N(x_N) \end{vmatrix} \\
&= \frac{1}{N!} \int \mathrm{d}^3\{x_l\} \left(\sum_\pi \mathrm{sgn}\,\pi \prod_i \tilde{\psi}_i^*(x_{\pi_i}) \right) \left(\sum_\mu \mathrm{sgn}\,\mu \prod_i \psi_i(x_{\mu_i}) \right) \\
&= \frac{1}{N!} \int \mathrm{d}^3\{x_l\} \sum_{\pi,\mu} \mathrm{sgn}\,\pi\,\mathrm{sgn}\,\mu \left(\prod_i \tilde{\psi}_i^*(x_{\pi_i}) \right) \left(\prod_j \psi_j(x_{\mu_j}) \right) \\
&= \frac{1}{N!} \int \mathrm{d}^3\{x_l\} \sum_{\pi,\mu} \mathrm{sgn}\,\pi\,\mathrm{sgn}\,\mu \prod_i \tilde{\psi}_i^*(x_{\pi_i})\psi_i(x_{\mu_i}) \\
&= \frac{1}{N!} \int \mathrm{d}^3\{x_l\} \sum_{\pi,\mu} \mathrm{sgn}\,\pi\,\mathrm{sgn}\,\mu \prod_i \tilde{\psi}_{\pi_i}^*(x_i)\psi_{\mu_i}(x_i) \\
&= \frac{1}{N!} \sum_{\pi,\mu} \mathrm{sgn}\,\pi\,\mathrm{sgn}\,\mu \prod_i \int \mathrm{d}^3 x_i\, \tilde{\psi}_{\pi_i}^*(x_i)\psi_{\mu_i}(x_i). \qquad (C.3)
\end{aligned}$$

The last integral is independent of the variable x_i. Thus we can replace x_i by x and obtain

Appendix C: Proof for the overlap of two Slater wave functions

$$\langle \tilde{\Psi} | \Psi \rangle = \frac{1}{N!} \sum_{\pi,\mu} \operatorname{sgn} \pi \operatorname{sgn} \mu \prod_i \langle \tilde{\psi}^*_{\pi_i} | \psi_i \rangle. \qquad (C.4)$$

Since the terms of the product commute, they can be ordered in a way that $\mu_i \equiv i$. Then $\operatorname{sgn} \mu \equiv 1$ and this yields the final result

$$\langle \tilde{\Psi} | \Psi \rangle = \sum_{\pi} \operatorname{sgn} \pi \prod_i \langle \tilde{\psi}_{\pi_i} | \psi_i \rangle \underbrace{\sum_{\mu} 1}_{N!}$$

$$= \det_{ij} \langle \tilde{\psi}_i | \psi_j \rangle. \qquad (C.5)$$

D Atomic, 'convenient' and SI Units

In atomic and molecular physics several unit systems are used, each having its advantages and disadvantages:

— The International System of Units, universally abbreviated SI (from the French *Le Système International d'Unités*). This system covers all areas of physics, it widely used and standardized (ISO 1000, DIN 1301) and is the only legal unit in the EU (ECC directives 80/181 and 89/617).

  But SI units have two disadvantages: The numbers for typical observables of atoms are usually tiny and one has to carry a lot of constants through the calculation.

— For 'convenient units' a different frame of reference for some units is used. This is done in order to get numbers which can be expressed without exponentials.

— The atomic units simplify the equations by setting several units to one; for atoms the numbers are usually also usable without exponentials. The drawback is that converting these units into SI is not trivial since one has to replace several ones by constants.

There exist several primers about SI units, for instance at the Bureau International des Poids et Mesures (`http://www.bipm.org/`) or at the physics page of the NIST [58].

D.1 Atomic Units

When using atomic units (a. u.), the Planck constant is 2π ($\hbar = 1$) and those constants are one: electron mass ($m_\mathrm{e} = 1$; atomic unit of mass), elementary charge ($e = 1$; atomic unit of charge) and the Bohr radius ($1 = a_0 = 4\pi\varepsilon_0\hbar^2/m_\mathrm{e}e^2$; atomic unit of length). Therefore the electric constant has to be $\varepsilon_0 = 1/4\pi$ and since $\alpha = e^2/4\pi\varepsilon_0\hbar c \approx 1/137$, the vacuum speed of light is $c = 1/\alpha$. The energy is measured in hartree ($E_\mathrm{H} = e^2/4\pi\varepsilon_0 a_0 = \alpha^2 m_\mathrm{e}c^2 = 1$) and the atomic unit of time is $\hbar/E_\mathrm{H} = 1$.

D.2 'Convenient units'

This is not a official system of units since the problem defines what is convenient. The advantage is that one can use all SI units and replace only a few by a different frame of reference; typically these are length and energy. The length is then measured in Ångströms (1 Å = 10^{-10} m) and the energy in electron volts (1 eV = 1 e J/C). One may also choose to measure the mass in electron volts using this relation: $E = mc^2 \Rightarrow m = E/c^2$.

D.3 Comparison and conversion

Here we give a short overview, for further conversion factors, see next section and reference [58].

	SI units	convenient units	atomic units
Length	Metre: 1 m	Ångström: 1 Å = 10^{-10} m	Bohr radius: 1 bohr = 1 a_0
Time	Second: 1 s	–	a. u. of time: 1 a. u.$_{\text{time}}$ = 1 $\hbar/E_{\text{h}}$
Mass	Kilogram: 1 kg	–	a. u. of mass: 1 a.u.$_{\text{mass}}$ = 1 m_{e}
Charge	Coulomb: 1 C	–	a. u. of mass: 1 a.u.$_{\text{charge}}$ = 1 e
Energy	Joule: 1 J	Electron volt: 1 eV = 1 e J/C	Hartree: 1 hartree = 1 $e^2/4\pi\varepsilon_0 a_0$

D.4 Constants

Taken from the 'NIST Reference on Constants, Units, and Uncertainty' [58].

- **Speed of light in vacuum:** $c \equiv c_0 = 299\,792\,458$ m s^{-1} (exact)
- **Electric constant:** $\varepsilon_0 = 1/\mu_0 c^2 = 8.854\,187\,817\ldots \times 10^{-}12$ F m^{-1} (exact)
- **Magnetic constant:** $\mu_0 = 4\pi \times 10^{-7}$ N A^{-2} = 12.566 370 614... N A^{-2} (exact)
- **Planck constant:**
  $h = 6.626\,068\,76(52) \cdot 10^{-34}$ J s = $4.135\,667\,27(16) \cdot 10^{-15}$ eV s
  $\hbar = h/2\pi = 1.054\,571\,596(82) \times 10^{-34}$ J s = $6.582\,118\,89(26) \times 10^{-16}$ eV s
- **Elementary charge:** $e = 1.602\,176\,462(63) \times 10^{-19}$ C
- **Electron mass:** $m_{\text{e}} = 9.109\,381\,88(72) \times 10^{-31}$ kg
- **Proton mass:** $m_{\text{p}} = 1.672\,621\,58(13) \times 10^{-27}$ kg
- **Proton-electron mass ratio:** $m_{\text{p}}/m_{\text{e}} = 1\,836.152\,6675(39)$
- **Fine-structure constant:**
  $\alpha = e^2/4\pi\varepsilon_0\hbar c = 7.297\,352\,533(27) \times 10^{-3}$
  $\alpha^{-1} = 137.035\,999\,76(50)$

Non-SI units excepted for use with the SI

– **Electron volt:** $1 \text{ eV} = 1 \ e \text{ J/C} = 1.602\,176\,462(63) \times 10^{-19}$ J

Atomic units

– **a. u. of charge: elementary charge:** $e = 1.602\,176\,462(63) \times 10^{-19}$ C
– **a. u. of mass: electron mass:** $m_\text{e} = 9.109\,381\,88(72) \times 10^{-31}$ kg
– **a. u. of action: reduced Planck constant:** $\hbar = h/2\pi = 1.054\,571\,596(82) \times 10^{-34}$
– **a. u. unit of length: Bohr radius (bohr):** $a_0 = 0.529\,177\,2083(19) \times 10^{-10}\,m$
– **a. u. of energy, Hartree energy (hartree, Ha):** $E_\text{h} = e^2/4\pi\varepsilon_0 a_0 = 2R_\infty = \alpha^2 m_e c^2 = 4.359\,743\,81(34) \times 10^{-18}$ J

– **a. u. of time:** $\hbar/E_\text{h} = 2.418\,884\,326\,500(18) \times 10^{-17}$ s
– **a. u. of force:** $E_\text{h}/a_0 = 8.238\,721\,81(64) \times 10^{-8}$ N
– **a. u. of velocity:** $a_0 E_\text{h}/\hbar = \alpha c = 2.187\,691\,2529(80) \times 10^{6}$ m s^{-1}
– **a. u. of momentum:** $\hbar/a_0 = 1.992\,851\,51.16) \times 10^{24}$ kg m s^{-1}
– **a. u. of current:** $e E_\text{h}/\hbar = 6.623\,617\,53(26) \times 10^{-3}$ A
– **a. u. of charge density:** $e/a_0^3 = 1.081\,202\,285(43) \times 10^{12}$ C m^{-3}

– **a. u. of electric potential:** $E_\text{h}/e = 27.211\,3834(11)$ V
– **a. u. of electric field:** $E_\text{h}/ea_0 = 5.142\,206\,24(20) \times 10^{11}$ V m^{-1}
– **a. u. of electric field gradient:** $E_\text{h}/ea_0^2 = 9.717\,361\,53(39) \times 10^{21}$ V m^{-2}
– **a. u. of electric dipole moment:** $ea_0 = 8.478\,352\,67(33) \times 10^{-30}$ C m
– **a. u. of electric quadrupole moment:** $ea_0^2 = 4.486\,551\,00(18) \times 10^{-40}$ C m^2
– **a. u. of electric polarizability:** $e^2 a_0^2/E_\text{h} = 1.648\,777\,251(18) \times 10^{-41}$ C^2 m^2 J^{-1}

Appendix D: Atomic, 'convenient' and SI Units

Abbreviations and Acronyms

a. u.   Atomic unit

DFT   Density functional theory

ELF   Electron localization function

gs   Ground state

HF   Hartree–Fock

HOMO   Highest occupied molecular orbital

KS   Kohn–Sham

LUMO   Lowest unoccupied molecular orbital

OCT   Optimal Control Theory

`octopus`   This is not (yet) an acronym but refers to the animal (Optimal Control, . . . , Universal Solution).

TD   Time dependent

Used symbols

Symbols of common physical constants can be found in section D.4.

$\partial_x^n = \frac{\partial^n}{\partial x^n}$	n-th partial derivation in x
$\frac{\mathrm{d}^n}{\mathrm{d}x^n}$	n-th total derivation in x
α	a weight factor
$\mathbb{C}$	the set of complex numbers
Δ	mesh width
ε	the eigenenergy of a wave function
ε_i	the eigenenergy of the i-th wave function
$\epsilon, \epsilon(t)$	the electric field, assumed to be constant in space
$\int \mathrm{d}^3(\boldsymbol{r}_1, \ldots, \boldsymbol{r}_N)$	short for $\int \mathrm{d}^3 r_1 \int \mathrm{d}^3 r_2 \cdots \int \mathrm{d}^3 r_N$
$H = T + V$	the Hamiltonian of a system
i, j	usually running variables in sums
i	imaginary unit, $\mathrm{i}^2 = -1$
J	a functional
N	the number of the particles of the system
$\mathbb{N}$	the set of natural numbers: $\{1, 2, 3, \ldots\}$
$\mathbb{N}_0$	the set of natural numbers and zero: $\{0, 1, 2, 3, \ldots\}$
n	density or density matrix
π, μ	in sums: a permutation; π_i and μ_i are the i-th items of the tuple π and μ
Ψ	an N-particle wave function
ψ, ϕ	a single-particle wave function
ψ_i, ϕ_i	the i-th single-particle wave function, the i-th orbital
σ	the spin, here restricted to $\sigma \in \{-\frac{1}{2}, \frac{1}{2}\}$
$\boldsymbol{r}$	a spatial coordinate, usually in three dimensions
$\mathbb{R}$	the set of real numbers
sgn	signum (or sign) of a permutation
T	the kinetic energy part of a Hamiltonian
$\hat{T}$	Time-order operator
V	a potential
V_{ext}	an external potential
W	interaction, e. g. Coulomb interaction between electrons
x	a coordinate, comprises the spatial and the spin part
$\propto$	proportional

$\dot{\propto}$	proportional in leading order
$\dot{=}$	equivalent in leading order
A^{T}	A transposed
A^*	A complex conjugated
$A^\dagger$	A adjoint
$\lceil \cdot \rceil$	round to the nearest higher integer ('ceiling')
$\lfloor \cdot \rfloor$	round to the nearest lower integer ('floor')
$O(\cdot)$	this Landau symbol is defined as $f = O(\phi) :\Leftrightarrow |f(x)| < A\phi(x)$ for a constant A and all x
$o(\cdot)$	this Landau symbol is defined as $f = o(\phi) :\Leftrightarrow f/\phi \to 0$

I don't mind your thinking slowly: I mind your publishing faster than you think.   — Wolfgang Pauli, 1900–58

References

[1] W. Kohn, Review of Modern Physics **71**, 1253 (1999).

[2] J. P. Perdew and S. Kurth, in *Density functionals: theory and applications*, Vol. 500 of *Lecture notes in physics* , edited by D. P. Joubert (Springer, Heidelberg, 1998). Available from http://www.physik.fu-berlin.de/~kurth/publ.html.

[3] K. Burke and friends, *The ABC of DFT* . (2003). http://dft.rutgers.edu/kieron /beta.

[4] P. L. Taylor and O. Heinonen, *A Quantum Appoach to Condensed Matter Physics* (Cambridge University Press, Cambridge, 2002), chapter 5.

[5] E. K. U. Gross, J. F. Dobson, and M. Petersilka, in *Density Functional Theory II: Relativistic and Time Dependent Extensions*, Vol. 181 of *Topics in Current Chemistry* , edited by R. F. Nalewajski (Springer, Heidelberg, 1996), p. 81.

[6] P. Hohenberg and W. Kohn, Physical Review **136**, B864 (1964).

[7] W. Kohn and L. J. Sham, Physical Review **140**, A1133 (1965).

[8] C.-O. Almbladh and U. von Barth, Physical Review B **31**, 3231 (1985).

[9] D. M. Ceperley and B. J. Alder, Physical Review Letters **45**, 566 (1980).

[10] E. Runge and E. K. U. Gross, Physical Review Letters **52**, 997 (1984).

[11] F. Nogueira, A. Castro, and M. A. L. Marques, in *A Primer in Density Functional Theory*, Vol. 620 of *Lecture Notes in Physics* , edited by C. Fiolhais, F. Nogueira, and M. A. L. Marques (Springer-Verlag, Berlin, 2003), p. 220.

[12] W. E. Pickett, Computer Physics reports **9**, 115 (1989).

[13] M. A. L. Marques, A. Castro, G. F. Bertsch, and A. Rubio, Computer Physics Communications **151**, 60 (2002). http://www.tddft.org/programs/octopus/.

[14] C. Hartwigsen, S. Goedecker, and J. Hutter, Physical Review B **58**, 3641 (1998).

[15] N. Troullier and J. L. Martins, Physical Review B **43**, 1993 (1991).

[16] J. Daintith, editor, *A Dictionary of Chemistry* Oxford Paperback Reference. (Oxford Paperbacks, Oxford, 2000).

[17] G. N. Lewis, Journal of the American Chemical Society **38**, 762 (1916).

[18] R. F. W. Bader and H. Essén, The Journal of Chemical Physics **80**, 1943 (1984).

[19] A. D. Becke and K. E. Edgecombe, The Journal of Chemical Physics **92**, 5397 (1990).

[20] R. F. W. Bader, S. Johnson, and T.-H. Tang, Journal of Physical Chemistry **100**, 15398 (1996).

[21] F. W. Wagner, editor, *Electron Localization Function (ELF) – Chemical Bonding Analysis in Real Space*, http://www.cpfs.mpg.de/ELF/.

[22] D. B. Chesnut, Journal of Physical Chemistry A **104**, 11644 (2000).

References

[23] A. Savin, R. Nesper, S. Wengert, and T. F. Fässler, Angewandte Chemie Int. Ed. Engl. **36**, 1808 (1997).

[24] J. K. Burdett and T. A. McCormick, Journal of Physical Chemistry A **102**, 6366 (1998).

[25] V. Tsirelson and A. Stash, Chemical Physics Letters **351**, 142 (2002).

[26] T. Burnus, M. A. L. Marques, and E. K. U. Gross. Submitted.

[27] Z. Chang, A. Rundquist, H. Wang, M. M. Murnane, and H. C. Kapteyn, Physical Review Letters **79**, 2967 (1997).

[28] C. Spielmann *et al.*, Science **278**, 661 (1997).

[29] M. Drescher *et al.*, Nature **419**, 803 (2002).

[30] B. Silvi and A. Savin, Nature **371**, 683 (1994).

[31] A. D. Becke, International Journal of Quantum Chemistry **23**, 1915 (1983).

[32] E. K. U. Gross, *Electron localization function*, Coffee Seminar, Thursday [April] 18, 2002.

[33] D. R. Lide, editor, *CRC Handbook of Chemistry and Physics* (CRC Press, Boca Raton, FL, 2001), 82th ed.

[34] J. P. Perdew and A. Zunger, Physical Review B **23**, 5048 (1981).

[35] O. Sugino and Y. Miyamoto, Physical Review B **59**, 2579 (1999).

[36] M. Shapiro and P. Brumer, *Principles of the Quantum Control of Molecular Processes*. (Wiley, New York. Chichester., 2003).

[37] R. S. Judson and H. Rabitz, Physical Review Letters **68**, 1500 (1992).

[38] A. Assion *et al.*, Science **282**, 919 (1998).

[39] W. Zhu, J. Botina, and H. Rabitz, The Journal of Chemical Physics **108**, 1953 (1998).

[40] W. Zhu and H. Rabitz, The Journal of Chemical Physics **109**, 385 (1998).

[41] K. Sundermann, Ph.D. thesis, Freie Universität Berlin, (1998). http://www.diss.fu-berlin.de/1998/15/

[42]

[43] W. Weisstein, *Cylindrical coordinates*, http://mathworld.wolfram.com/CylindricalCoordinates.html.

[44] S. Kurth, *Real-space discretization of the schrödinger equation for cylindrically symmetric potentials: Problems and partial solutions* (unpublished, 2003).

[45] H. R. Schwarz, *Numerische Mathematik* (B. G. Teubner, Stuttgart, 1997), chapter 10.

[46] G. H. Golub and C. F. Van Loan, editors, *Matrix computation* (North Oxford Academic Publishing, Oxford, 1983).

[47] G. H. Golub and H. A. van der Vorst, Journal of Computational and Applied Mathematics **123**, 35 (2000).

[48] E. Anderson *et al.*, *LAPACK Users' Guide*. (Society for Industrial and Applied Mathematics, Philadelphia, PA, 1999), 3rd ed. http://www.netlib.org/lapack/.

[49] R. B. Lehoucq, D. C. Sorensen, and C. Yang, *ARPACK User's Guide: Solution of Large Scale Eigenvalue Problems by Implicitely Restarted Arnoldi Methods*. (Society for Industrial and Applied Mathematics, Philadelphia, 1998). The software and this guide are available from Netlib at http://www.netlib.org /scalapack/index.html.

[50] T. Kalkreuter and H. Simma, Computer Physics Communications **93**, 33 (1996).

[51] G. L. G. Sleijpen and H. A. Van der Vorst, SIAM Review **42**, 267 (2000).

[52] C. Leforestier *et al.*, Journal of Computational Physics **94**, 59 (1991).

[53] J. Giansiracusa, *Comparison of methods for numerical time-integration of the schrödinger equation* (2002). http://www.phys.washington.edu/~bertsch/num3. ps

[54] K. Kime, *Control of electronic materials* (2002). Crank Nicolson with stability ananlysis.

[55] B. Hamprecht, *Exact solutions of the time dependent Schroedinger equation in one space dimension* (unpublished, 1997). eprint: quant-ph/0211040.

[56] A. N. Hussain and G. Roberts, Physical Review A **63**, 012703 (2000).

[57] J. Werschnik, *Optimal control: How-to and some results*, Coffee Seminar, January 20, 2003.

[58] Taylor and Mohr, *NIST reference on constants, units, and uncertainty*, http: //physics.nist.gov/cuu/index.html.